To the Graduate Council:

I am submitting herewith a thesis written by Rajivkumar K. Kapadia entitled "Segmented Active Constrained Layer Damping Treatments." I have examined the final copy of this thesis for form and content and recommend that it be accepted in partial fulfillment of the requirements for the degree of Master of Science, with a major in Mechanical Engineering.

Grzegorz Kawiecki, Major Professor

We have read this thesis
and recommend its acceptance:

Accepted for the Council:

Associate Vice Chancellor and
Dean of The Graduate School

SEGMENTED ACTIVE CONSTRAINED LAYER

DAMPING TREATMENTS

A Thesis

presented for the

Master of Science

Degree

The University of Tennessee, Knoxville

Rajivkumar Kapadia

August 1996

ACKNOWLEDGMENTS

I would like to thank Dr. Grzegorz Kawiecki for his patience, invaluable guidance and encouragement throughout the course of this research. I would also like to thank my committee members, Dr. Frank Speckhart and Dr. William Hamel, for their comments on my research work. I am also very thankful to the Department of Energy for funding this research. I am grateful to the everybody in the fabrication shop and the electrician Mr. Dennis Higdon of the Mechanical and Aerospace Engineering Department for their time and suggestions. I would also like to appreciate the help of the department secretaries, Marva and Betty, for helping me with the departmental paper work.

I am indebted to my parents, Dr. K. N. Kapadia and Mrs. P. K. Kapadia, and my brother and sister, for their love and support, which made me pursue my higher education. I would also like to thank a personal friend Mr. Vipin Bhagat and his family for their care and encouragement throughout my graduate studies.

ABSTRACT

Active vibration control of flexible robotic arms is important for improving their overall accuracy and efficiency. The objective of this research is to demonstrate the feasibility of applying the concept of Active Constrained Layer Damping treatment to reduce the level of vibration in flexible robotic arms. The active damping treatment under consideration consists of a viscoelastic layer sandwiched between two piezoelectric layers. Shear deformation of the viscoelastic layer causes energy loss and thus vibration damping.

Analytical and numerical approaches to obtain the equation of motion for a beam treated with active constrained layer damping treatment will be presented. Experimental results for slender beams partially treated with active constrained layer damping treatment are demonstrated. Slender beams are used because this research is focused on controlling vibrations of flexible robotic manipulator arms with low natural frequencies. Comparison is made between the performance of active and passive treatments. Also, the effect of constraining layer segmentation is analyzed. The presented results demonstrate excellent performance of segmented active constrained layer treatments for low frequency vibration attenuation.

TABLE OF CONTENTS

LIST OF TABLES

LIST OF FIGURES

NOMENCLATURE

A cross-sectional area

b width of a beam

B_0 characteristic length in single layer = $(h_1 h_2 E_2 / G)^{1/2}$

C capacitance of the piezoelectric sensor

d distance between neutral axis of the sandwiched beam and the interface between the sensor and the viscoelastic layer = $h_2 + h_1/2 + D$

d_{31} piezoelectric strain coefficient

D distance between neutral axis of the beam sensor layer and the interface between the beam/sensor layer and the viscoelastic layer = $(E_3 h_3^2 + 2 E_4 h_3 h_4 + E_4 h_4^2)/[2 (E_3 h_3 + E_4 h_4)]$

D_t intermediate constant $= (E_1 h_1 + E_3 h_3 + E_4 h_4) / b$

E modulus of elasticity

$E_1 I_1$ flexural rigidity of a piezoelectric actuator

$E_2 I_2$ flexural rigidity of a viscoelastic layer

$E_3 I_3$ flexural rigidity of a piezoelectric sensor

$E_4 I_4$ flexural rigidity of a plain untreated beam

$E_e h_e$ equivalent flexural stiffness per unit width = $(E_3 h_3 + E_4 h_4)$

g intermediate constant = $G/h_2 [(E_1 h_1 + E_e h_e)/ (E_1 h_1 E_e h_e)]$

g_{31} piezoelectric voltage coefficient

G complex shear modulus of the viscoelastic layer

G'	storage shear modulus
G''	loss shear modulus
h	thickness
i	$=(-1)^{1/2}$
I	moment of inertia
k	intermediate constant = $(\rho_4\,\omega^2 / E_4)^{1/2}$
k_{31}	electromechanical coupling coefficient
k_{3t}	dielectric constant
K_d	derivative control gain
K_p	proportional control gain
l	nondimensionalized length
L	length
m	mass density of treated beam/unit length and unit width
m_4	mass density per unit length of plain beam
$[N_i(\xi)]$	shape functions
t	time
u	longitudinal displacement
V_c	voltage fed back to the constraining layer
V_s	voltage induced by the sensor layer
W_s	strain energy per radian
w	transverse deflection

Y intermediate constant $= d^2 / D_t [(E_1 h_1 E_e h_e) / (E_1 h_1 + E_e h_e)]$

α_i constants

ε_b bending strain

ε_e extensional strain

ε_p piezoelectric actuator strain

ε_s piezoelectric sensor strain

γ shear strain in the viscoelastic layer

$\{\Delta_i\}$ nodal displacement vector

Subscripts

1 beam layer

2 piezoelectric sensor

3 viscoelastic layer

4 piezoelectric actuator

i,j,k indices

CHAPTER 1

INTRODUCTION

High vibration amplitudes and low damping ratios may cause low positioning accuracy of telerobotic manipulators and fatigue failures. One of the most successful methods of improving structural damping characteristics is a passive constrained layer approach. A typical passive constrained layer treatment consists of a viscoelastic layer surface bonded to a structure and a stiff, usually metal, film bonded to the free surface of the viscoelastic layer. Studies aimed at flexural vibration control of beams using a variety of damping treatment configurations are described in References 1, 5, 6, 7 and 8.

The purpose of this study is to investigate the feasibility of increasing the damping ratio of a flexible robotic manipulator using a novel approach called Active Constrained Layer Damping (ACLD) method. That approach is based on the traditional Passive Constrained Layer Damping (PCLD) method as described in References 2 and 3. As mentioned earlier, a passive constrained layer treatment consists of a viscoelastic layer sandwiched between the base structure and a stiff constraining layer. The energy dissipation property of the polymeric viscoelastic material improves the structural damping. A typical active damping treatment consists of a viscoelastic layer sandwiched between a piezoelectric actuator layer and a piezoelectric sensor layer that is bonded to the beam. Piezoelectric material, when excited by an actuation voltage to induce strain, is referred to as a piezoelectric actuator. When the piezoelectric material is mechanically strained to induce voltage across it, it is referred to as a piezoelectric sensor. When the beam is excited by an external source, the sensor layer bonded to the beam generates a signal. In the simplest implementation the sensor signal, with a reversed polarity, is fed back through an amplifier to the active constraining layer. The strain induced in the active layer increases the magnitude of a shear deformation in the viscoelastic layer much above the level that can be reached using a passive constraining layer. Since the shear deformation causes an energy loss in the form of heat, the damping ratios for such a structure is higher.

The effectiveness of passive constrained layer treatments for damping low frequency vibrations can be significantly improved by constraining layer segmentation. Studies concentrated on the advantages of passive constrained viscoelastic layer treatment segmentation are presented in References 4, 5, 6, 7, and 8. The present research establishes the feasibility of that concept extension to active constrained layer treatments. Experimental results presented show that the amount of energy dissipated by an active constrained layer treatment increases by constraining layer segmentation. Also the analytical and numerical models presented can be used to optimize the damping treatments for different configurations. Such a surface damping treatment has a high energy dissipation to weight ratio as compared to conventional constrained layer damping treatments. The research done has devised a new effective method of structural vibration attenuation. Important commercial applications of such treatments can be found, among others, in the car and aircraft industry where weight is a important factor.

CHAPTER 2

LITERATURE REVIEW

Passive constrained layer damping has been used extensively for structural vibration damping. Active damping treatment is a recent approach and proves to be very effective for damping structural vibrations. Representative studies published in the field of passive and active constrained layer viscoelastic damping will be outlined in the following literature review.

2.1 Application of passive constrained layer damping treatment to vibration attenuation

Viscoelastic sandwich structures have been considered by many researchers over the last forty years. Special attention has been devoted to the vibrations of three-layer sandwich beams damped by a viscoelastic layer as shown in Figure 2.1.

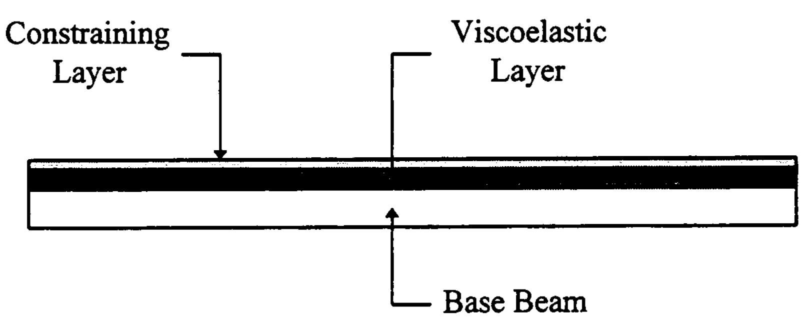

Figure 2.1: Schematic of the passive constrained layer damping treatment

Kerwin[15,16] explained the concept of a passive constrained layer damping treatment and supported it with an experimental evidence of its inherent advantages. Passive constraining layer treatments are attractive mainly because of low weight and high effectiveness. The most common application of passive constrained layer damping tapes is the enhancement of structural damping in aircraft structures. Parfitt and Lambeth[5] showed that the improvement in the energy dissipation in a constrained viscoelastic layer is large when compared with unconstrained viscoelastic layer. They showed that the application of a constraining layer increases the shear in the viscoelastic layer which is responsible for the energy loss. Mead and Markus derived the widely used sixth order equation of motion for the three-layer sandwich beam with a passive constraining layer treatment (see Equation (2.1)) in terms of transverse displacements.

$$\frac{\partial^6 w}{\partial x^6} - g(1+Y)\frac{\partial^4 w}{\partial x^4} + \frac{m}{D_t}\left(\frac{\partial^4 w}{\partial x^2 \partial t^2} - g\frac{\partial^2 w}{\partial t^2}\right) = \frac{1}{D_t}\left(\frac{\partial^2 q}{\partial x^2} - gq\right) \tag{2.1}$$

Experimental results presented in Reference 1 for a passive constrained layer damping treatments show good agreement with a solution obtained using Equation (2.1).

Parfitt and Lambeth[5,6] have outlined a procedure for determining optimal parameters of a damping tape. The modal energy loss coefficient is used to optimize the damping treatment parameters such as the segment length of the constraining layer length or the thickness of the viscoelastic layer. Plunkett and Lee[4] have derived the loss coefficient equation (see Equation (2.2)) for a sandwich structure. They devised a formulation for getting an optimal segment length of the passive constraining layer for a given structure. Experimental results in their paper show the variation of the energy loss coefficient as the constraining layer segment length changes. Equation (2.2), as given in Reference 4, shows the dependence of the loss coefficient on the nondimensionalized length l of the system. The nondimensionalized length l is a function of the constraining layer thickness, viscoelastic layer thickness, modulus of elasticity of the constraining layer, shear modulus of the viscoelastic layer and the length of the constraining layer. The energy loss coefficient is maximum for the nondimensionalized length l=3.28.

$$\eta_l = 4\pi\frac{1}{l}\left[\frac{\sinh(A)\sin(\theta/2)-\sin(B)\cos(\theta/2)}{\cosh(A)+\cos(B)}\right] \tag{2.2}$$

where,

$A = l\cos(\theta/2)$

$B = l\sin(\theta/2)$

$\theta =$ Loss angle of the viscoelastic material

$l = L/B_0 = 3.28$ for maximum loss

Figure 2.2 show the variation of loss coefficient for any beam as a function of a change of the nondimensionalized length l. The energy loss is maximum at $l = 3.28$.

Reference 11 describes a finite element technique to model a sandwich beam structure. The presented model is based on the Hamilton's principle and a displacement based finite element approach is used.

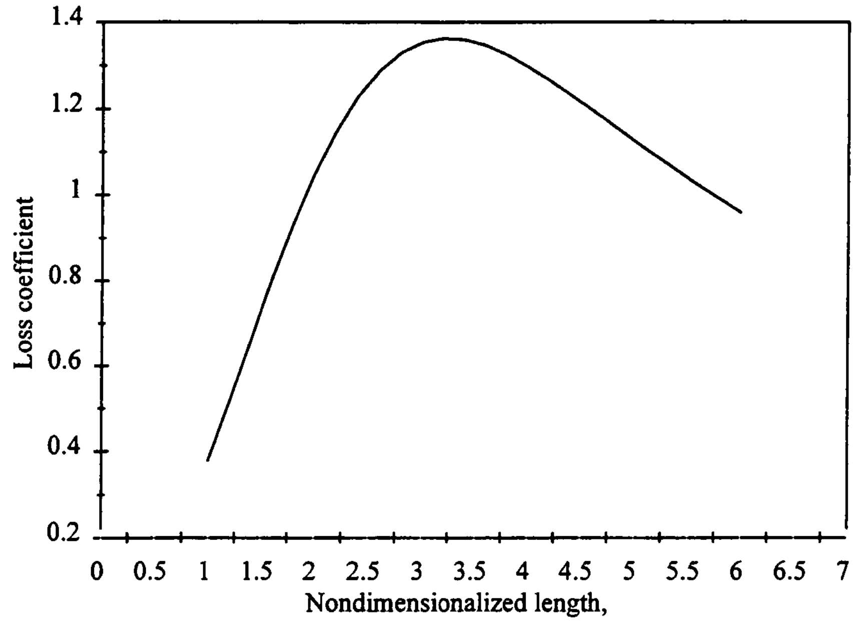

Figure 2.2 : Loss coefficient vs. nondimensionalized length

2.2 Piezoelectric materials and their application in active constrained layer damping treatments to vibration attenuation

References dealing with the development of smart structures are presented. Also, previous work on the development of active damping treatments is outlined.

2.2.1 Piezoelectric materials as a part of the technology leading to the development of smart structures

Piezoelectric materials are among the most critical components in the development of smart structures. Smart structures are those that incorporate actuators and sensors that are highly integrated into the structure and have structural functionality. For example, a mechanically intelligent structure can alter both its mechanical states (position, velocity) and its mechanical characteristics (stiffness, damping). Table 2.1 lists some materials used in smart structures development. The piezoelectric materials used in the present research are PZT G-1195 and PVDF.

Table 2.1 Listing of smart materials characteristics

Material	Actuation Mechanism	ε_{max} [a] μstrain
PZT G1195	Piezoceramic	350
PVDF	Piezofilm	10
PMN	Electrostrictor	500
Terfenol	Magnetostrictor	580
Nitinol	Shape alloy	8500

[a] For a sheet of an actuator bonded to an aluminum beam ($t_s/t_a = 10$) in bending

Also, much effort is directed towards applying piezoelectric elements alone, without any viscoelastic material, in commercial smart adaptive structures. The field is fast evolving with Smart Ski[10] listed as the first large scale consumer product to benefit from the use of piezoelectric materials. Research is also done in developing new piezoelectric strain actuators for large displacements. However, the effectiveness of piezoceramic materials is low when they are bonded directly to such large stiff structures as robotic arms.

2.2.2 Application of active constrained layer damping treatments to vibration attenuation

The use of piezoelectric material as the constraining layer in damping treatment is a recent approach extending the passive constraining layer damping concept. The use of active damping treatments was first mentioned by Baz and Ro[2, 3]. They extended the sixth order differential equation developed by Mead and Markus[1] to model an active constrained layer treatment. They also derived a finite element model to predict the performance of the active damping treatment[12]. This model was based on Hamilton's principle and the displacement based finite element formulation was used. However, very little experimental work has been done in the field of active constrained layer damping treatment. To the best of my knowledge, no commercial application of this concept has been developed yet.

CHAPTER 3

BASIC CONCEPT

The mechanism of constrained layer damping is explained. Advantages of an active constraining layer concept over a passive constraining layer method are addressed. The mechanisms of energy dissipation in segmented passive and active constraining layers is explained. The goal is to develop treatments that can produce large shear in the viscoelastic layer and thus improve the damping properties of the structure.

3.1 Flexural vibration damping using passive constrained layer treatment

Viscoelastic damping is exhibited strongly in many polymeric and glassy materials. By proper tailoring, polymeric materials can be manufactured to exhibit a variety of damping, strength, durability, creep resistance, thermal stability and other desirable properties over a selected temperature and frequency ranges. A variety of viscoelastic materials are listed with their properties in Reference 19. Proper selection of a viscoelastic material is very important to get best damping characteristics of a damping treatment.

The passive constrained layer damping treatment consists of a viscoelastic layer sandwiched between the basic structure and a thin stiff constraining layer. Figure 3.1 shows a treated beam with all three layers.

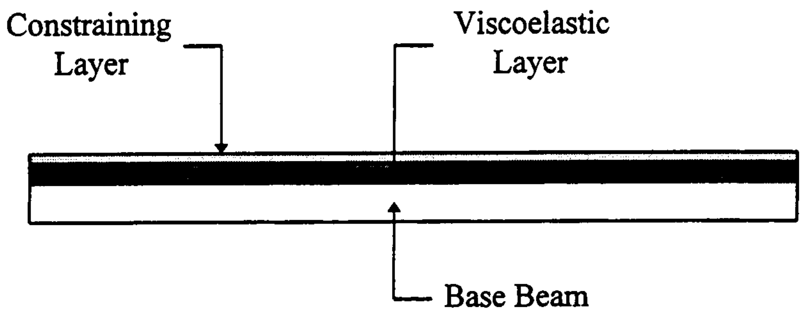

Figure 3.1 : Schematic of the passive constrained layer damping treatment

Figures 3.2 (a) shows a beam deflected from its neutral position. The beam and the constraining layer, because of the high modulus of elasticity resists extension producing shear stress in the viscoelastic layer. Figure 3.2 (b) compares the shear strain produced in the viscoelastic layer in the presence and absence of a constraining layer.

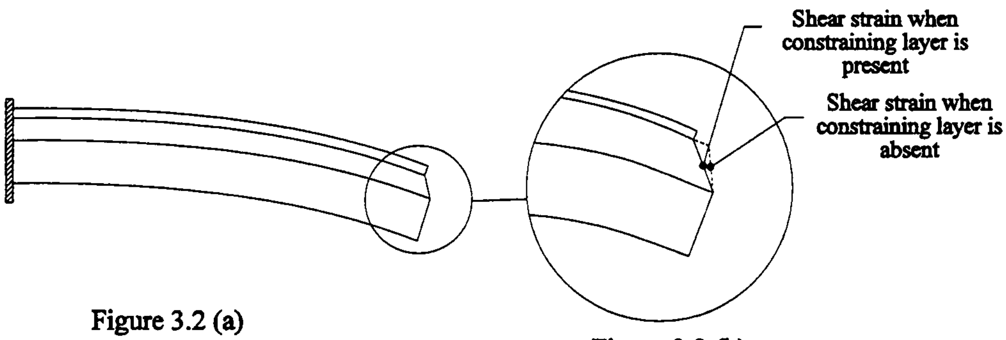

Figure 3.2 (a)

Figure 3.2 (b)

Figure 3.2 : Shear strain for a passive constrained layer damping treatment
(a) Beam with a passive constrained layer treatment in deflected position (b) Amplified view of the shear strain produced in the viscoelastic layer

In the case of a free viscoelastic layer (no constraining layer) shear strain is not significant since even the free surface of the viscoelastic material undergoes deflections comparable to beam deflections. When the viscoelastic layer is constrained by a stiff layer, shear strain magnitude is increased. Since most of the energy dissipation is caused by shear, constrained viscoelastic layers are, therefore, capable of producing higher damping than unconstrained treatments.

3.2 Flexural vibration damping using active constrained layer treatment

The active constrained layer damping treatment is based on the same principle as the passive constrained layer damping treatment. However, in active constrained layer damping treatment the viscoelastic layer is sandwiched between a beam/sensor layer and a constraining actuator layer. A piezoelectric sensor layer is placed on the beam. The constraining layer is made of a piezoelectric film or a piezoelectric plate that works as an actuator. The treatment thus consists of three layers as shown in Figure 3.3 forming a smart constrained layer damping treatment with built in sensing and actuation capabilities.

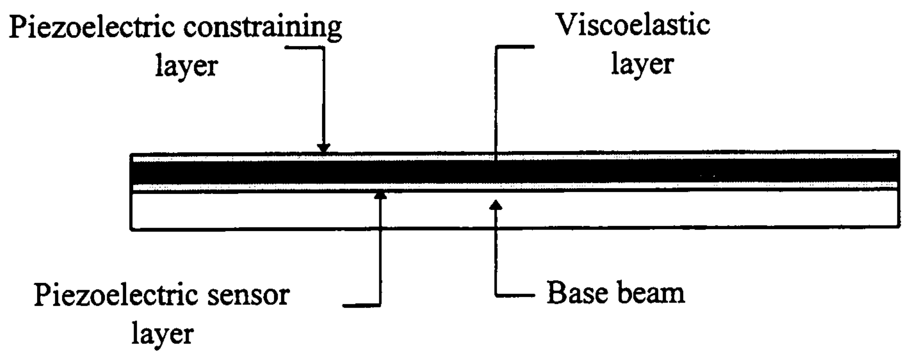

Figure 3.3 : Schematic of an active constrained layer damping treatment

When beam is excited strain is produced at the surface of the beam. The piezoelectric sensor, bonded to the surface, is strained producing a charge because of a piezoelectric effect. A signal from the sensor layer is then fed to an amplifier. The amplified signal is fed back with a reversed polarity to the piezoelectric constraining layer. The piezoelectric actuator is thus strained because of a piezoelectric effect in the opposite direction to that of the sensor. At a typical position during a cycle of flexural vibration shown in Figure 3.4(a), the sensor layer is extended. Since the feedback signal to the constraining piezoelectric layer has a reversed polarity, the constraining layer reduces its length. Thus, as seen in Figure 3.4(b), the shear strain γ_a in the viscoelastic layer is higher compared to the shear strain γ_p developed due to the conventional passive constraining layer. Furthermore, the contraction of the piezoelectric constraining layer produces a bending moment which tends to bring the beam back to its equilibrium position. Therefore, because of this dual effect, the energy dissipation in the active damping approach is much larger and the vibrations are damped more effectively when compared to a passive treatment.

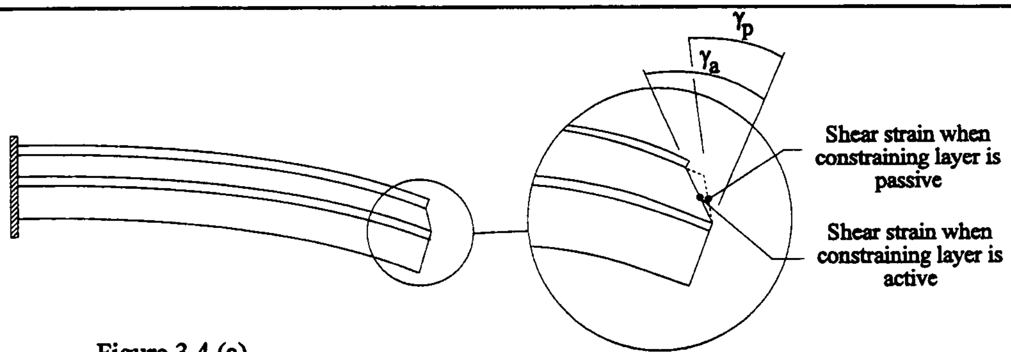

Figure 3.4 (a)

Figure 3.4 (b)

Figure 3.4 : Shear strain for an active constrained layer damping treatment
(a) Beam with an active constrained layer treatment in a deflected position (b) Amplified view of the shear strain produced in the viscoelastic layer

As described earlier it is apparent that the effectiveness of the smart treatment depends on the type of feedback to the active constraining layer. Both proportional and derivative control laws have been shown to be effective in providing an excellent performance of the treatment. Proper manipulation of the sensor signal will render better damping characteristics. In general, an active constrained layer damping treatment is a weight effective, reliable and simple vibration damping method. Its additional, and very important, characteristic is the fail safe feature. The treatment retains a portion of its vibration damping ability even in case of power failure.

3.3 Effects of constraining layer segmentation

It has been shown, for passive constrained layer treatments, that the energy dissipation in the viscoelastic layer can be increased for low frequency vibrations by segmenting the constraining layer. The amount of energy dissipated in a viscoelastic layer depends on the magnitude of shear strain in that layer. The effectiveness of a shear damping treatment depends mainly on geometrical and material parameters. These are, among others, viscoelastic layer thickness, constraining layer thickness, elastic and shear properties of the treatment and the constraining layer segment length[4,5,6,19]. The expression derived by Plunkett and Lee[4] for an energy loss corresponding to a differential element of a segment of the constraining layer can be written as

$$d(\Delta W) = \pi h_2 G''\gamma^2 = \pi h_2 G'' \frac{\varepsilon_0^2}{h_2^2} B_0^2 \left| \frac{\sinh(x / B_0)}{\cosh(L_1 / 2B_0)} \right|^2 \qquad (3.1)$$

It is customary in dealing with linearized behavior of dynamic systems to describe the properties of viscoelastic materials as complex quantities. The viscoelastic material here is characterized by a complex shear modulus G = G' + iG''. The component G' is called storage shear modulus while the component G'' is known as a loss shear modulus. The complex properties can will be explained using an example.

Consider a rubber ball falling from a certain height, as shown in Figure 3.5.

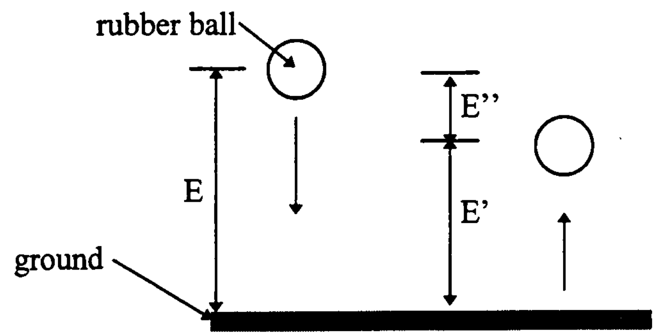

Figure 3.5 : Real and complex part of elastic modulus of a rubber ball

After the ball hits the ground, it bounces back to a certain height. Now, let the material of the ball have a complex elastic modulus, E = E' + iE''. The loss in height is proportional to the complex part E'' of the shear modulus, while the height gained is proportional to the real part E'. On the second bounce, some height will be lost again and the bouncing of the ball will eventually die out.

The loss shear modulus G'' is used to evaluate the energy loss. The energy loss per unit strain ε_0 along a segment, as predicted by Equation (3.1), is shown in Figure 3.6 for three different passive segment lengths. The following treatment parameters were assumed : $h_1 = 0.052$ mm, $h_2 = 0.508$ mm, $L = 50/n$ mm (where n denotes the number of segments), $E_1 = 2.25 \times 10^9$ Pa and $G = (3.5934 + 5.2464\, i) \times 10^5$ Pa. We can note that the amount of dissipated energy depends strongly on the length of a segment. Clearly, comparing the area under the curves, the treatment with the constraining layer divided into two segments performs much better than the other two.

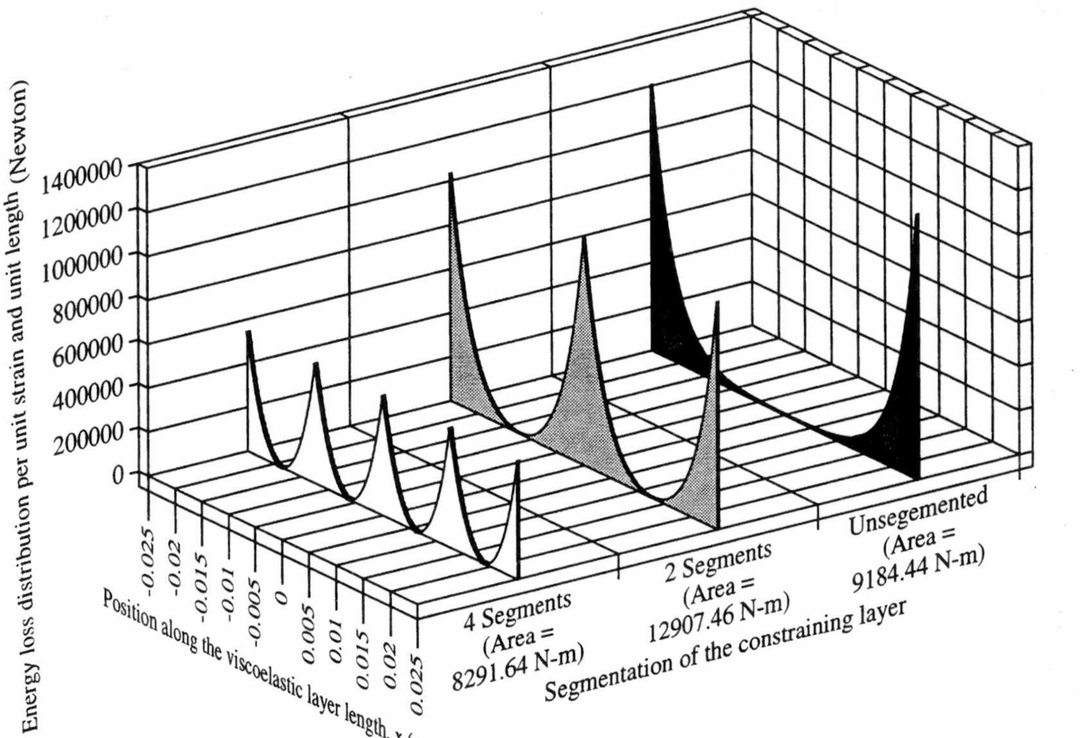

Figure 3.6 : Shear energy loss distribution over the length of the viscoelastic layer for different constraining layer segmentation

The present work was based on an assumption that since the mechanism of damping is the same for passive and active cases, the segmentation of an active constraining layer should improve the active constrained layer performance, similarly as it improves a passive layer performance. Analytical and experimental results presented later show that there is an optimal constraining layer segment length for which the damping ratio is maximum. Evidently, for passive and active treatments the optimal lengths are different. But since the mechanism of damping is the same in either case, an optimal segmentation will give higher damping ratios.

CHAPTER 4

ANALYTICAL FORMULATION

Analytical models are presented to predict the response of a beam with active constrained layer damping treatment. The sixth order differential equation of motion derived by Baz and Ro[2] is examined. The equation is used to predict the steady state response of a beam for base excitation boundary condition. The loss coefficient is evaluated using the energy approach presented by Plunkett and Lee[4]. That model is used to derive an optimal segment length for passive constrained layer treatment on a actual specimen.

4.1 The equation of motion

Mead and Markus[1] presented an analytical model for a passive constrained layer damping treatment on a beam with arbitrary boundary conditions. They derived a sixth-order differential equation of motion, in terms of transverse displacement, for a passive constrained layer treatment. That model was extended by Baz and Ro[2] to analyze steady state vibrations of a beam with the active constrained layer treatment and subjected to a harmonic tip force. A modified version of that model is used here to represent a beam with active constrained layer damping treatment undergoing steady state vibrations due to a base excitation. Herewith presented are some highlights of that analytical model.

The model is based on the following assumptions.

a) Shear strain in the piezoelectric sensor/actuator layers and in the beam is negligible.

b) Longitudinal stresses in the viscoelastic layer are negligible.

c) The transverse displacements of all points on any cross-section of the sandwiched structure are considered equal.

d) The piezoelectric sensor/actuator layers and the beam are assumed to be elastic and dissipate no energy, while the sandwiched layer is assumed to be linearly viscoelastic.

e) The piezoelectric sensor and the beam are considered to be perfectly bonded together so that they can be reduced to a single equivalent structure.

4.1.1 The analytical model

The schematic of a beam is shown in Figure 4.1. The mathematical modeling is done by dividing the partially treated beam into three sections.

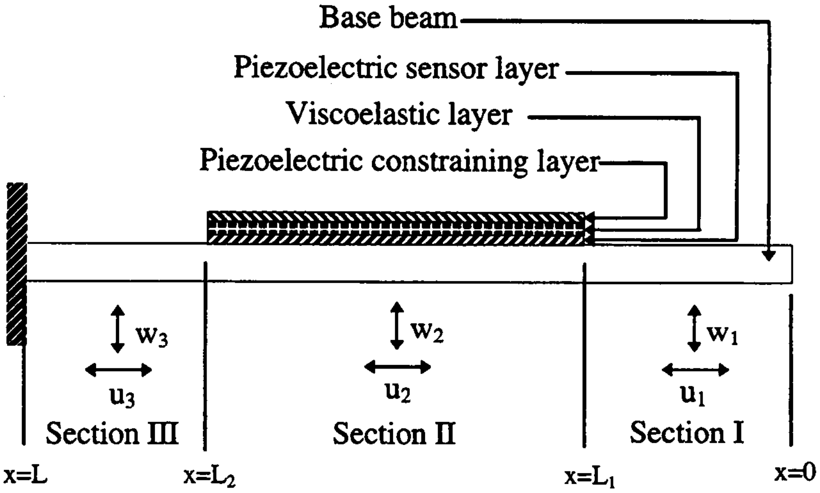

Figure 4.1 : Schematic layout of the beam and various sections defined for the beam

Section I and Section III are modeled as Euler-Bernoulli beams. Section II is modeled as a three layer beam with the displacements and internal loading shown in Figure 4.2.

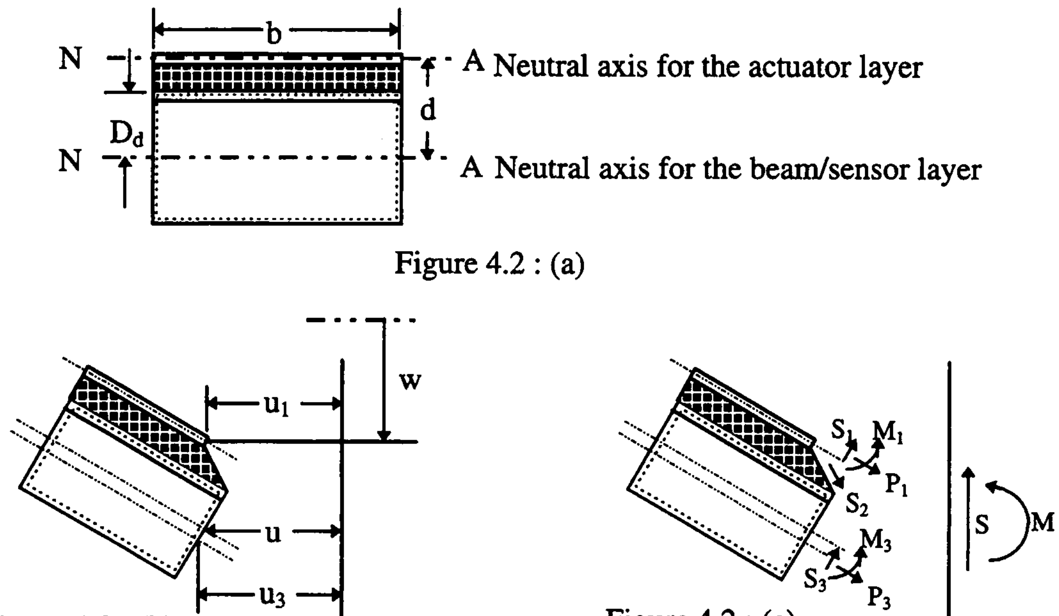

Figure 4.2 : (a)

Figure 4.2 : (b)

Figure 4.2 : (c)

Figure 4.2 : Deflections, forces and moments on a treated section of a beam (a) Schematic of a section of the treated beam, (b) Deflections of the treated beam, (c) Forces and moments on the deflected beam

The equations are derived considering the equilibrium conditions at any instant. The equation of motion for different sections of the partially treated beam, shown in Figure 4.1, are

$$E_4 I_4 \frac{\partial^4 w_1}{\partial x^4} = -m_4 \frac{\partial^2 w_1}{\partial t^2}, \qquad 0 \le x \le L_1 \qquad (4.1)$$

$$\frac{\partial^6 w_2}{\partial x^6} - g(1+Y)\frac{\partial^4 w_2}{\partial x^4} + \frac{m}{D_t}\frac{\partial^4 w_2}{\partial x^2 \partial t^2} = \frac{mg}{D_t}\frac{\partial^2 w_2}{\partial t^2}, \qquad L_1 \le x \le L_2 \qquad (4.2)$$

$$E_4 I_4 \frac{\partial^4 w_3}{\partial x^4} = -m_4 \frac{\partial^2 w_3}{\partial t^2}, \qquad L_2 \le x \le L \tag{4.3}$$

Equations (4.1) and (4.3) are the classical Euler-Bernoulli beam equations. Equation (4.2) is a sixth order equation describing the dynamics of the beam portion with active constrained layer treatment.

4.1.2 The boundary and compatibility conditions

The system of Equations (4.1), (4.2) and (4.3) can be solved by separation of variables using boundary conditions shown in Figure 4.3.

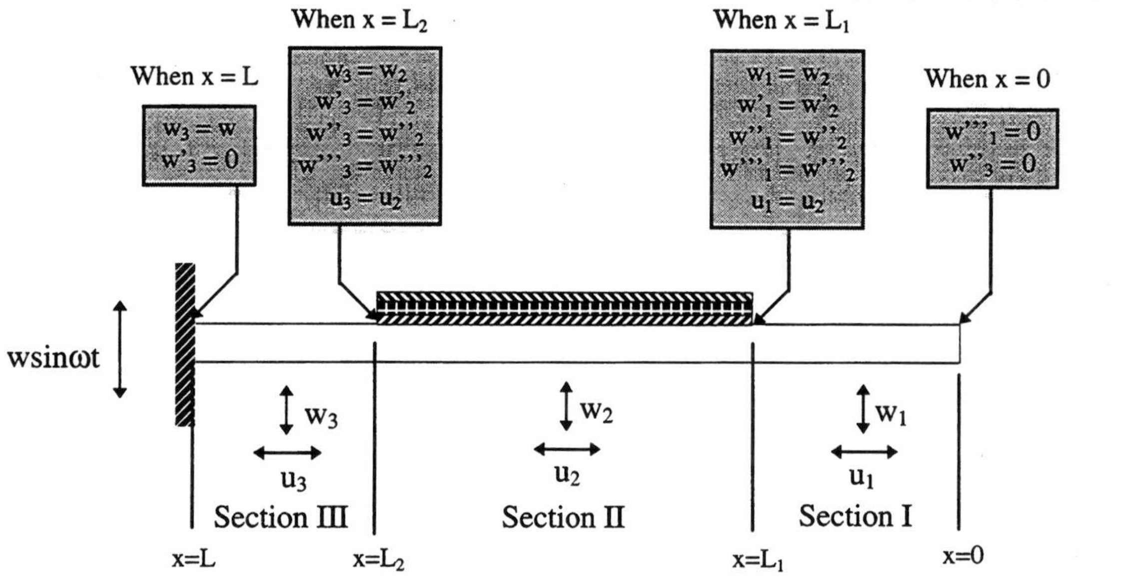

Figure 4.3 : Boundary and compatibility conditions for a beam with active constrained layer damping treatment

The boundary conditions and the compatibility conditions are explicitly listed below along with appropriate explanations.

a) Boundary conditions :

Corresponding to Figure 4.3 the boundary conditions are listed below.

i) At the free end (x = 0) the shear force is equal to zero for no externally applied load

$$\left.\frac{d^3w_1}{dx^3}\right)_{x=0} = 0 \tag{4.4}$$

ii) The moment is zero at the free end (x = 0) since no external moment is applied.

$$\left.\frac{d^2w_1}{dx^2}\right)_{x=0} = 0 \tag{4.5}$$

iii) The beam is subjected to a sinusoidal transverse deflection, $w_f = w \sin\omega t$, at the fixed end (x = L).

$$w_3)_{x=L} = w \tag{4.6}$$

iv) The slope at the fixed end (x = L) is zero.

$$\left.\frac{dw_3}{dx}\right)_{x=L} = 0 \tag{4.7}$$

b) Compatibility conditions :

The compatibility at the interfaces of the treated beam and the plain sections of the beam require altogether eight equations to match transverse compatibility and two equations to match longitudinal compatibility. Corresponding to Figure 4.3 the ten compatibility conditions are listed below.

i) Transverse deflections at $x = L_1$ are the same.

$$w_1)_{x=L1} = w_2)_{x=L1} \tag{4.8}$$

ii) Slopes of the beam at $x = L_1$ are the same.

$$\left.\frac{dw_1}{dx}\right)_{x=L_1} = \left.\frac{dw_2}{dx}\right)_{x=L_1} \tag{4.9}$$

iii) Induced bending moments in the beam at $x = L_1$ are the same.

$$\left.\frac{d^2w_1}{dx^2}\right)_{x=L_1} = \left.\frac{d^2w_2}{dx^2}\right)_{x=L_1} \tag{4.10}$$

iv) Induced shear forces in the beam at $x = L_1$ are the same.

$$\left.\frac{d^3w_1}{dx^3}\right)_{x=L_1} = \left.\frac{d^3w_2}{dx^3}\right)_{x=L_1} \tag{4.11}$$

v) Longitudinal deflections of the beam at $x = L_1$ are the same.

$$u_1\big)_{x=L_1} = u_2\big)_{x=L_1}$$

The above equation can be reduced to give the following condition in terms of the transverse deflections (Baz and Ro[3]).

$$\begin{aligned}\left(\frac{1}{k}\right)\cot(kL_1)\left[\frac{1}{g}\frac{d^4w_2}{dx^4} - Y\frac{d^2w_2}{dx^2} - \frac{m\omega^2}{D_t g}w_2 - \frac{Y}{d}\varepsilon_p\right]_{x=L_1} &= \\ -\left[\frac{1}{g^2}\frac{d^5w_2}{dx^5} - \frac{Y}{g}\frac{d^3w_2}{dx^3} - \left(Y + \frac{m\omega^2}{D_t g}\right)\frac{dw_2}{dx} - \frac{Y}{d}x\varepsilon_p\right]_{x=L_1}&\end{aligned} \tag{4.12}$$

vi) Transverse deflections at $x = L_2$ are the same.

$$w_2)_{x=L2} = w_3)_{x=L2} \tag{4.13}$$

vii) Slopes of the beam at $x = L_2$ are the same.

$$\left.\frac{dw_2}{dx}\right)_{x=L_2} = \left.\frac{dw_3}{dx}\right)_{x=L_2} \tag{4.14}$$

viii)Induced bending moments in the beam at $x = L_2$ are the same.

$$\left.\frac{d^2w_2}{dx^2}\right)_{x=L_2} = \left.\frac{d^2w_3}{dx^2}\right)_{x=L_2} \tag{4.15}$$

ix) Induced shear forces in the beam at $x = L_2$ are the same.

$$\left.\frac{d^3w_2}{dx^3}\right)_{x=L_2} = \left.\frac{d^3w_3}{dx^3}\right)_{x=L_2} \tag{4.16}$$

x) Longitudinal deflections of the beam at $x = L_2$ are the same.

$$\left.u_2\right)_{x=L_2} = \left.u_3\right)_{x=L_2}$$

The above equation can be reduced to give the following condition in terms of the transverse deflections (Baz and Ro[3]).

$$\begin{gathered}\left(\frac{1}{k}\right)\cot\left(k\left(L_2 - L\right)\right)\left[\frac{1}{g}\frac{d^4w_2}{dx^4} - Y\frac{d^2w_2}{dx^2} - \frac{m\omega^2}{D_t g}w_2 - \frac{Y}{d}\varepsilon_p\right]_{x=L_2} = \\ \left[\frac{1}{g^2}\frac{d^5w_2}{dx^5} - \frac{Y}{g}\frac{d^3w_2}{dx^3} - \left(Y + \frac{m\omega^2}{D_t g}\right)\frac{dw_2}{dx} - \frac{Y}{d}x\varepsilon_p\right]_{x=L_2}\end{gathered} \tag{4.17}$$

4.1.3 The piezoelectric control forces

The strain-voltage relations for the piezoelectric material when it acts as a sensor and an actuator are given in Appendix I. The effect of the piezoelectric strain is reflected in the compatibility conditions as can be seen in Equations (4.12) to (4.17).

The piezoelectric actuator strain ε_p depends on the feedback voltage V_c from the piezoelectric sensor. The control feedback voltage V_c can be manipulated using proportional and derivative control laws.

$$V_c = -K_p V_s - K_d \frac{dV_s}{dt} \tag{4.18}$$

K_p and K_d are the proportional and derivative control gains and V_s is the sensor voltage. The negative sign indicates the reverse polarity feedback to the active constraining layer.

A Mathematica program written by Chenyi Hu[25] was modified to solve Equations (4.1) to (4.3) simultaneously along with the boundary conditions shown in Figure 4.2 and listed in the previous section. The listing of the code is given in Appendix II. Typical results obtained for a beam (later designated as PF31, see chapter 6) are shown in Figure 4.4.

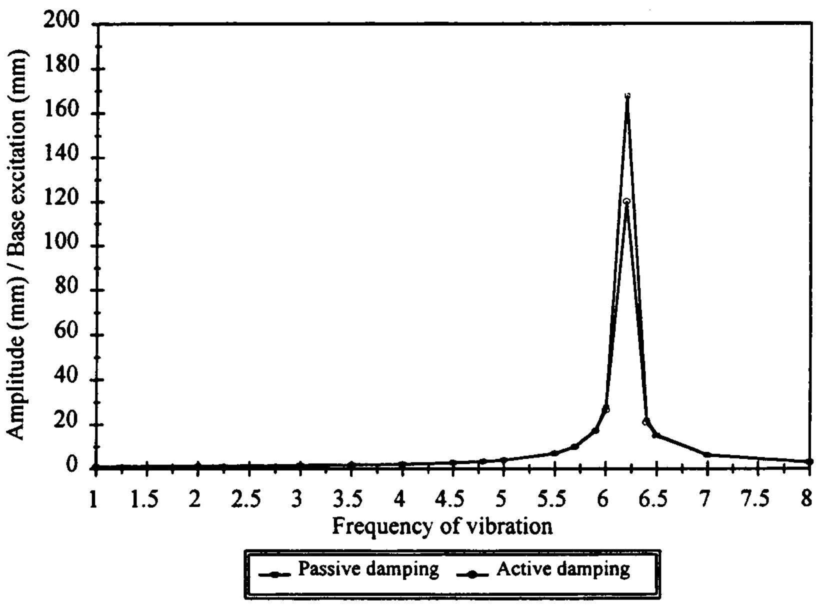

Figure 4.4 : Analytical predictions of the frequency response for specimen PF31

4.2 Loss coefficient for a constrained viscoelastic layer damping treatment

The model is based on the modal strain energy approach. As mentioned earlier the model predicts the energy loss due to shear in the viscoelastic layer.

The following assumptions are used in this analysis.

a) The thickness of the constraining layer and viscoelastic layer are small compared to the beam thickness.

b) The viscoelastic material is assumed to behave linearly and is characterized by a complex shear modulus.

c) The constraining layer and beam are assumed to dissipate no energy.

d) Uniform shear is assumed.

e) The elastic modulus of the viscoelastic layer is assumed to be small when compared to the moduli of the beam and constraining layer.

The damping of mechanical vibrations can be expressed in a nondimensional form by a loss coefficient η_s which is the ratio of the energy dissipated per vibration cycle to the maximum modal strain energy of the system.

$$\eta_s = \frac{\text{Energy dissipated per cycle}}{\text{Maximum modal strain energy of the system}} = \frac{\Delta W_s}{2\pi W_s} \tag{4.19}$$

The viscoelastic material is assumed to have a complex shear modulus. The energy loss in the viscoelastic material is the complex part of the shear strain energy in the viscoelastic layer. The loss coefficient[4] for each segment of the constraining layer is

$$\eta_l = 4\pi \frac{1}{l}\left[\frac{\sinh(A)\sin(\theta/2) - \sin(B)\cos(\theta/2)}{\cosh(A) + \cos(B)}\right] \tag{4.20}$$

where,

$A = l\cos(\theta/2)$

$B = l\sin(\theta/2)$

θ = loss angle of the viscoelastic material

$l = L/B_0 = 3.28$ for maximum loss

A typical graph showing the nondimensionalized length l versus loss coefficient η_s for a specimen later designated as PF4# (# = 1,2,3,4) (see chapter 6) is shown in Figure 4.5.

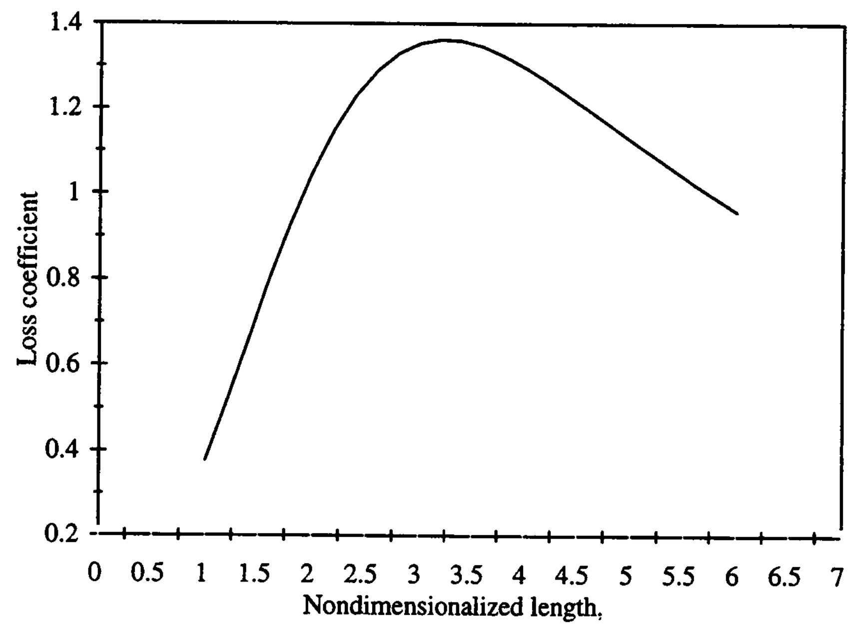

Figure 4.5 : Loss coefficient vs. nondimensionalized length for specimens PF4#

The optimal segment length (corresponding to a maximum η_s) for passive constrained layer treatment is obtained when $l = 3.28$. Since the mechanism of energy loss for an active treatment is the same, a similar character of segment length - energy dissipation relationship is expected. A listing of a Mathematica program producing the energy loss values, shear distribution and optimal segment length is given in Appendix III.

CHAPTER 5

FINITE ELEMENT MODEL

This chapter describes the finite element formulation for the analysis of an active constrained layer damping treatment. Geometrically complex structures are difficult to handle using analytical technique presented before. The finite element analysis allows to avoid the difficulties experienced in laying down the compatibility conditions for a segmented constraining layer treatment in the analytical model used to derive the equation of motion.

5.1 Formulation of the finite element model

The presented finite element model is an extension of the work of Baz and Ro[12]. This model can handle various boundary conditions. It takes into account the behavior of distributed piezoelectric sensor and distributed piezoelectric actuator. The presented model can handle both proportional and derivative control laws. An added feature of the model is the capability to handle constraining layer segmentation.

The presented model is based on the following assumptions.

a) Shear strains in the piezoelectric sensor/actuator layers and in the beam are negligible.

b) The transverse displacements of all points on any cross-section of the sandwiched structure are considered equal.

c) The piezoelectric sensor/actuator layers and the base beam are assumed to be elastic and to dissipate no energy, while the sandwiched layer is assumed to be linearly viscoelastic.

d) The piezoelectric sensor and the base beam are considered to be perfectly bonded together such that they can be reduced to a single equivalent layer.

5.2 Basic kinematic relationships

Strains in the various layers of the treatment of the beam are needed to derive the energies associated with each layer. Necessary strain expressions were derieved using the geometry shown in Figure 5.1.

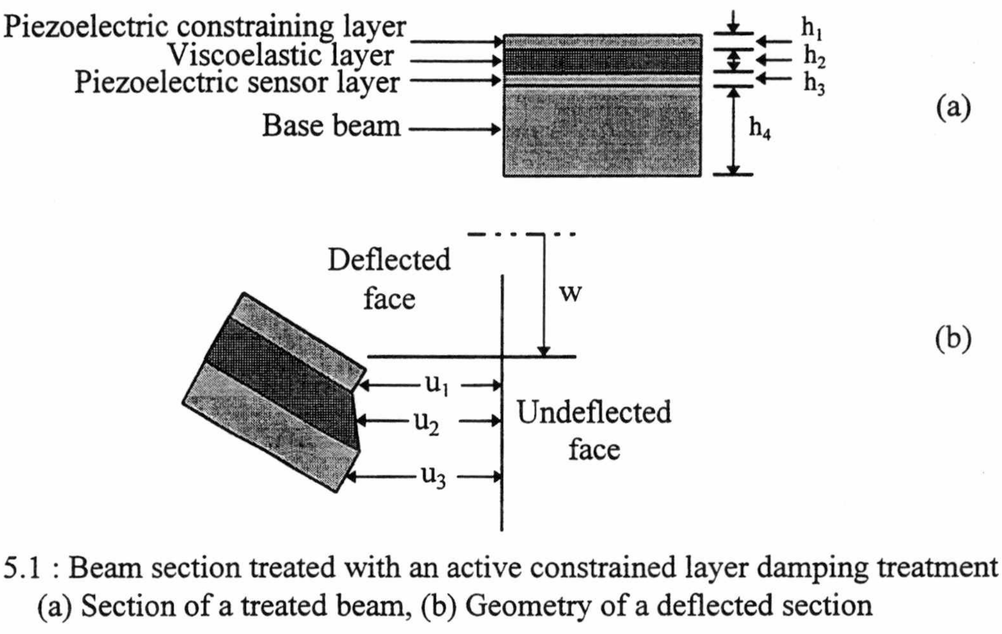

Figure 5.1 : Beam section treated with an active constrained layer damping treatment (a) Section of a treated beam, (b) Geometry of a deflected section

5.2.1 Strain induced in the beam/sensor layer

Strains induced in the beam are due to bending and extension of the beam/sensor. The strain due to bending can be expressed as

$$\varepsilon_b = \frac{\partial w}{\partial x} \tag{5.1}$$

The strain induced in the beam/sensor layer due to the extension can be expressed as

$$\varepsilon_e = \frac{\partial u_3}{\partial x} \tag{5.2}$$

5.2.2 Strain induced in the constraining layer

Strains induced in the constraining layer are due to bending and extension of the constraining layer. The piezo induced strain is needed as a longitudinal force and bending moments. They will be included in the force vector derived later. The strain due to bending is again expressed as

$$\varepsilon_b = \frac{\partial w}{\partial x} \tag{5.3}$$

The strain induced due to the extension of the constraining layer can be expressed as

$$\varepsilon_e = \frac{\partial u_1}{\partial x} \tag{5.4}$$

5.2.3 Strain induced in the viscoelastic layer

Strains induced in the viscoelastic layer are attributed to the bending, extension and shear of the viscoelastic layer. The strain due to bending is again expressed as

$$\varepsilon_b = \frac{\partial w}{\partial x} \tag{5.5}$$

The strain induced due to the extension of the viscoelastic layer can be expressed as

$$\varepsilon_e = \frac{\partial u_2}{\partial x} \tag{5.6}$$

From the geometry of the beam we can write,

$$u_2 = \frac{1}{2}\left[(u_1 + u_3) + (h_1 - h_3 - h_4)\frac{\partial w}{\partial x}\right] \tag{5.7}$$

Thus the extensional strain in the viscoelastic layer can be expressed as

$$\varepsilon_e = \frac{1}{2}\left[\left(\frac{\partial u_1}{\partial x} + \frac{\partial u_3}{\partial x}\right) + (h_1 - h_3 - h_4)\frac{\partial^2 w}{\partial x^2}\right] \tag{5.8}$$

The shear strain in the viscoelastic layer can be obtained from Figure 5.1 as

$$\gamma = \frac{\partial w}{\partial x} + \frac{\partial u_2}{\partial z} = \frac{d}{h_2}\left(\frac{\partial w}{\partial x}\right) + \frac{(u_1 - u_3)}{h_2} \tag{5.9}$$

where,

$$d = h_2 + h_1/2 + D$$

and $$\frac{\partial u_2}{\partial z} = \frac{h_1 + h_3}{2h_2}\frac{\partial w}{\partial x} + \frac{u_1 - u_3}{h_2}$$

5.3 Shape functions

The shape functions are derived assuming isoparametric finite elements. The modeling is done using a displacement based finite element method. The longitudinal displacement of the beam and the constraining layer are assumed to be linearly distributed over the length of the beam. Thus the following expressions are assumed.

$$u_1 = \alpha_1 x + \alpha_2 \tag{5.10}$$

$$u_2 = \alpha_3 x + \alpha_4 \tag{5.11}$$

The distribution of transverse displacement of the element is approximated by a cubic expression.

$$w = \alpha_5 x^3 + \alpha_6 x^2 + \alpha_7 x + \alpha_8 \tag{5.12}$$

The constants α_1, α_2, α_3, α_4, α_5, α_6, α_7 and α_8 can be obtained in terms of the eight nodal degrees of freedom of the element as shown in Figure 5.2.

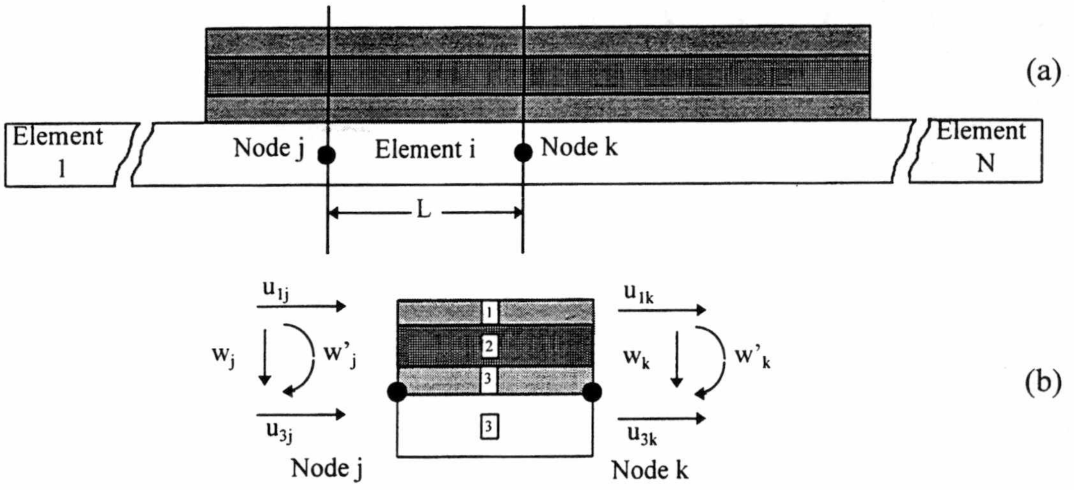

Figure 5.2 : Finite elements used to model a partially treated beam (a) Finite element model of a beam treated with active constrained layer treatment, (b) Degrees of freedom associated with a element with active constrained layer damping treatment

The formulation of the finite element model becomes easy if a local coordinate system is used. Thus the degrees of freedom are expressed in a local ξ coordinate system as

$$u_1 = a_1 \xi + a_2 \tag{5.13}$$

$$u_2 = a_3 \xi + a_4 \tag{5.14}$$

$$w = a_5\xi^3 + a_6\xi^2 + a_7\xi + a_8 \tag{5.15}$$

where $\xi = \dfrac{x}{L/2}$, a_1, a_2, a_3, a_4, a_5, a_6, a_7 and a_8 are constants

The Jacobian associated with the coordinate transformation is

$$J = \left[\frac{L}{2}\right] \tag{5.16}$$

and thus det(J) = L/2

Therefore, the vector of displacement in matrix form is,

$$\begin{Bmatrix} u_1 \\ u_3 \\ w \\ w' \end{Bmatrix} = \underbrace{\begin{bmatrix} \xi & 1 & 0 & 0 & 0 & 0 & 0 & 0 \\ 0 & 0 & \xi & 1 & 0 & 0 & 0 & 0 \\ 0 & 0 & 0 & 0 & \xi^3 & \xi^2 & \xi & 1 \\ 0 & 0 & 0 & 0 & 3\xi^2 & 2\xi & 1 & 0 \end{bmatrix}}_{\{[f(\xi)]\}} \begin{Bmatrix} a_1 \\ a_2 \\ a_3 \\ a_4 \\ a_5 \\ a_6 \\ a_7 \\ a_8 \end{Bmatrix} \tag{5.17}$$

where $$\{[f(\xi)]\} = \begin{bmatrix} \xi & 1 & 0 & 0 & 0 & 0 & 0 & 0 \\ 0 & 0 & \xi & 1 & 0 & 0 & 0 & 0 \\ 0 & 0 & 0 & 0 & \xi^3 & \xi^2 & \xi & 1 \\ 0 & 0 & 0 & 0 & 3\xi^2 & 2\xi & 1 & 0 \end{bmatrix} = \begin{Bmatrix} [f_1(\xi)] \\ [f_2(\xi)] \\ [f_3(\xi)] \\ [f_4(\xi)] \end{Bmatrix}$$

The nodal displacements for an element can be obtained from the above equation and is as under for node j and node k of an element i shown in Figure 5.2.

$$
\{\Delta_i\} = \begin{Bmatrix} u_{1j} \\ u_{3j} \\ w_j \\ w'_j \\ u_{1k} \\ u_{3k} \\ w_k \\ w'_k \end{Bmatrix} = \underbrace{\begin{bmatrix} -1 & 1 & 0 & 0 & 0 & 0 & 0 & 0 \\ 0 & 0 & -1 & 1 & 0 & 0 & 0 & 0 \\ 0 & 0 & 0 & 0 & -1 & 1 & -1 & 1 \\ 0 & 0 & 0 & 0 & 6/L & -4/L & 2/L & 0 \\ 1 & 1 & 0 & 0 & 0 & 0 & 0 & 0 \\ 0 & 0 & 1 & 1 & 0 & 0 & 0 & 0 \\ 0 & 0 & 0 & 0 & 1 & 1 & 1 & 1 \\ 0 & 0 & 0 & 0 & 6/L & 4/L & 2/L & 0 \end{bmatrix}}_{[A]_e} \underbrace{\begin{Bmatrix} a_1 \\ a_2 \\ a_3 \\ a_4 \\ a_5 \\ a_6 \\ a_7 \\ a_8 \end{Bmatrix}}_{\{a\}} \quad (5.18)
$$

$$
\therefore \{\Delta_i\} = [A]_e \{a\}
$$

$$
\text{or} \qquad \{a\} = [A]_e^{-1} \{\Delta_i\} \quad (5.19)
$$

Now from equations (5.17) to (5.19)

$$
\begin{Bmatrix} u_1 \\ u_3 \\ w \\ w' \end{Bmatrix} = \{[f(\xi)]\}\{a\} = \{[f(\xi)]\}[A]_e^{-1}\{\Delta_i\} = \{[N(\xi)]\}\{\Delta_i\} \quad (5.20)
$$

where,

$$
\{[N(\xi)]\} = \{[f(\xi)]\}[A]_e^{-1} = \begin{Bmatrix} [N_1(\xi)] \\ [N_2(\xi)] \\ [N_3(\xi)] \\ [N_4(\xi)] \end{Bmatrix}
$$

$$
= \begin{bmatrix} \frac{1-\xi}{2} & 0 & 0 & 0 & \frac{1+\xi}{2} & 0 & 0 & 0 \\ 0 & \frac{1-\xi}{2} & 0 & 0 & 0 & \frac{1+\xi}{2} & 0 & 0 \\ 0 & 0 & \frac{\xi^3-3\xi+2}{4} & \frac{L(\xi^3-\xi^2-\xi+1)}{8} & 0 & 0 & \frac{-\xi^3+3\xi+2}{4} & \frac{L(\xi^3+\xi^2-\xi-1)}{8} \\ 0 & 0 & \frac{3\xi^2-3}{4} & \frac{L(3\xi^2-2\xi-1)}{8} & 0 & 0 & \frac{3\xi^2-3}{4} & \frac{L(3\xi^2+2\xi-1)}{8} \end{bmatrix}
$$

(5.21)

Functions $[N_1(\xi)]$, $[N_2(\xi)]$, $[N_3(\xi)]$ and $[N_4(\xi)]$ in Equation (5.21) are the mapping as well as the shape functions for the element representing the four degrees of freedom.

5.4 Energy expressions in terms of the shape functions

The energy expressions associated with the various layers of the active constrained layer treatment are listed below. Appendix IV outlines the derivations of the energy functions used for the viscoelastic layer. Derivation of other energy functions can be found in Reference 20.

5.4.1 Strain energies for various layers

Strain energy expressions for various layers follow.

a) Constraining layer

Strain energy in the constraining layer is generated by extension and bending of the layer. The strain energy due to extension is

$$U_{e1} = \frac{1}{2} E_1 A_1 \{\Delta_i\}^T \left[\int_{-1}^{1} [N_1'(\xi)]^T [N_1'(\xi)] \det(J) d\xi \right] \{\Delta_i\} \tag{5.22}$$

The strain energy due to bending is

$$U_{b1} = \frac{1}{2} E_1 I_1 \{\Delta_i\}^T \left[\int_{-1}^{1} [N_3''(\xi)]^T [N_3''(\xi)] \det(J) d\xi \right] \{\Delta_i\} \tag{5.23}$$

b) Viscoelastic layer

Strain energies are generated by extension, bending and shear deformation of the viscoelastic layer. The strain energy due to extension is

$$U_{e2} = \frac{1}{2}E_2A_2\{\Delta_i\}^T\left[\int_{-1}^{1}[N_5(\xi)]^T[N_5(\xi)]\det(J)d\xi\right]\{\Delta_i\} \tag{5.24}$$

where $[N_5(\xi)]$ is an interpolating function equal to

$$\frac{1}{2}\left([N_1'(\xi)]+[N_2'(\xi)]+\left(\frac{h_1-h_3-h_4}{2}\right)[N_3''(\xi)]\right)$$

The strain energy due to bending is

$$U_{b2} = \frac{1}{2}E_2I_2\{\Delta_i\}^T\left[\int_{-1}^{1}[N_6(\xi)]^T[N_6(\xi)]\det(J)d\xi\right]\{\Delta_i\} \tag{5.25}$$

where $[N_6(\xi)]$ is again an interpolating function and is equal to

$$\frac{1}{h_2}\left([N_1'(\xi)]-[N_2'(\xi)]+\left(\frac{h_1+h_3+h_4}{2}\right)[N_3''(\xi)]\right) \tag{5.26}$$

The strain energy due to shear can be expressed

$$U_{s2} = \frac{1}{2}G_2A_2\{\Delta_i\}^T\left[\int_{-1}^{1}[N_7(\xi)]^T[N_7(\xi)]\det(J)d\xi\right]\{\Delta_i\} \tag{5.27}$$

where $[N_7(\xi)]$ is again an interpolating function and is equal to

$$\frac{1}{h_2^2}\left([N_1(\xi)]-[N_2(\xi)]+d[N_3'(\xi)]\right)$$

c) Sensor/beam layer

The strain energies are due to extension and bending of the sensor/beam layer. The strain energy due to extension is

$$U_{e3} = \frac{1}{2} E_e A_e \{\Delta_i\}^T \left[\int_{-1}^{1} [N_2'(\xi)]^T [N_2'(\xi)] \det(J) d\xi \right] \{\Delta_i\} \tag{5.28}$$

The strain energy due to bending is

$$U_{b3} = \frac{1}{2} E_e I_e \{\Delta_i\}^T \left[\int_{-1}^{1} [N_3''(\xi)]^T [N_3''(\xi)] \det(J) d\xi \right] \{\Delta_i\} \tag{5.29}$$

All of the above mentioned energies, equations (5.22) to (5.29), can be combined to give

$$U = U_{e1} + U_{b1} + U_{e2} + U_{b2} + U_{s2} + U_{e3} + U_{b3} = \frac{1}{2} \{\Delta_i\}^T [K_i] \{\Delta_i\} \tag{5.30}$$

where $[K_i]$ is the equivalent stiffness matrix of the ith element.

5.4.2 Kinetic energies for various layers

The kinetic energy for various layers is given below.

a) Constraining layer

$$\begin{aligned} T_1 &= \frac{1}{2} \rho_1 A_1 \int_{-1}^{1} \left(\dot{w}^2 + \dot{u}_1^2 \right) \det(J) d\xi \\ &= \frac{1}{2} \rho_1 A_1 \{\dot{\Delta}_i\}^T \left[\int_{-1}^{1} \left([N_3(\xi)]^T [N_3(\xi)] + [N_1(\xi)]^T [N_1(\xi)] \det(J) d\xi \right) \right] \{\dot{\Delta}_i\} \end{aligned} \tag{5.31}$$

b) Viscoelastic layer

$$
\begin{aligned}
T_2 &= \frac{1}{2}\rho_2 A_2 \int_{-1}^{1} \left(\dot{w}^2 + \dot{u}_2^2\right) \det(J)d\xi \\
&= \frac{1}{2}\rho_2 A_2 \{\dot{\Delta}_i\}^T \left[\int_{-1}^{1} \left([N_3(\xi)]^T [N_3(\xi)] + [N_8(\xi)]^T [N_8(\xi)] \det(J)d\xi \right) \right] \{\dot{\Delta}_i\}
\end{aligned} \tag{5.32}
$$

where the interpolation function $[N_8(\xi)]$ is equal to

$$
\frac{1}{2}\left([N_1(\xi)] + [N_2(\xi)] + (h_1 - h_3 - h_4)[N_3'(\xi)]\right)
$$

c) Sensor/beam layer

$$
\begin{aligned}
T_3 &= \frac{1}{2}\rho_e A_e \int_{-1}^{1} \left(\dot{w}^2 + \dot{u}_3^2\right) \det(J)d\xi \\
&= \frac{1}{2}\rho_e A_e \{\dot{\Delta}_i\}^T \left[\int_{-1}^{1} \left([N_3(\xi)]^T [N_3(\xi)] + [N_2(\xi)]^T [N_2(\xi)] \det(J)d\xi \right) \right] \{\dot{\Delta}_i\}
\end{aligned} \tag{5.33}
$$

All of the above mentioned kinetic energies, equations (5.31) to (5.33), can be summed to give

$$
T = T_1 + T_2 + T_3 = \frac{1}{2}\{\dot{\Delta}_i\}^T [M_i]\{\dot{\Delta}_i\} \tag{5.34}
$$

where $[M_i]$ is the equivalent mass matrix for the ith element

5.5 Mass and stiffness matrices library

Different integrals listed as equations (5.22) to (5.34) need to be integrated once since all the shape functions are functions of ξ only. The results of those integrations are listed in Appendix V along with the Mathematica program used to do the integrations. Three types of elements used in the finite element analysis of a segmented active constrained layer damping treatment are shown in Figure 5.3. Stiffness and mass matrices are obtained for all of the elements used. This is done by taking into consideration only the energy associated with the layers present in the element.

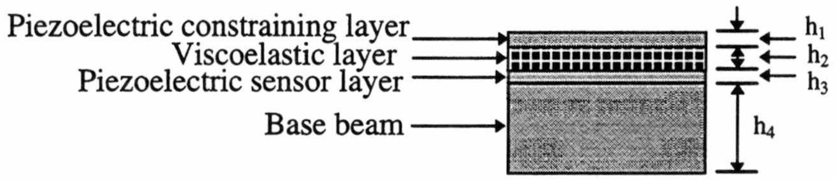

Element A: all three active treatment layers modeled

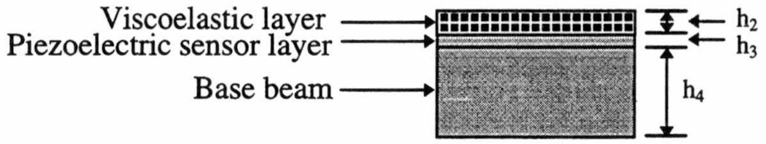

Element B: no active constraining layer

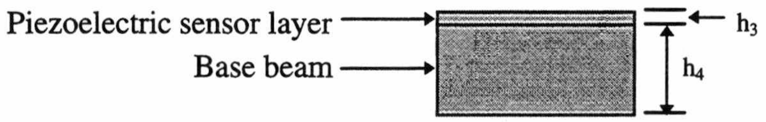

Element C: only the beam/sensor layer modeled

Figure 5.3 : Elements used to model various portions of segmented active constrained layer damping treatment

5.6 The piezoelectric control forces

The strain-voltage relations for a piezoelectric material when it acts as a sensor and an actuator are given in Appendix I.

The piezoelectric actuator strain ε_p depends on a feedback voltage V_c from the piezoelectric sensor. The control feedback voltage V_c can be manipulated using proportional and derivative control laws.

$$V_c = -K_p V_s - K_d \frac{dV_s}{dt} \tag{5.35}$$

K_p and K_d are the proportional and derivative control gains and V_s is the sensor voltage. The negative sign indicates the reverse polarity feedback to the active constraining layer.

5.7 The forcing function vector

The control forces and moments associated with each element because of the piezoelectric constraining layer can be represented by the vector given below.

$$\{F_c\} = \{F_{pj}\ 0\ 0\ M_{pj}\ F_{pk}\ 0\ 0\ M_{pk}\}^T \tag{5.36}$$

where F_{pj} and F_{pk} denote the control forces generated at nodes j and k defined as

$$F_{pj} = -F_{pk} = g(K_p + K_d p)(w'_k - w'_j) \tag{5.37}$$

where p is the d / dt operator. The constant g is defined as

$$g = -E_1 h_1 b\left(\frac{d_{31}}{h_1}\right)\left[\frac{k_{31}^2 D_d b}{g_{31} C}\right] \tag{5.38}$$

The control moments, generated at nodes j and k, M_{pj} and M_{pk}, are expressed as

$$M_{pj} = -M_{pk} = D_d F_{pj} \tag{5.39}$$

Forces F_{pj} and F_{pk} change the longitudinal displacement u_1 of the piezoelectric constraining layer. Similarly, moments M_{pj} and M_{pk} alter the angular deflection of the beam. Thus, the piezoelectric constraining layer increases the shear strain in the viscoelastic layer and it also produces a moment that tries to restore the beam to the equilibrium position. The force vector depends on a transverse displacement. Piezoelectric control force vectors (see Equations (5.37) and (5.39)) depend on the nodal displacement vector and can be represented as

$$\begin{Bmatrix} F_{pj} \\ 0 \\ 0 \\ 0 \\ F_{pk} \\ 0 \\ 0 \\ 0 \end{Bmatrix} = \begin{Bmatrix} gK_p\left(w'_k - w'_j\right) \\ 0 \\ 0 \\ 0 \\ -gK_p\left(w'_k - w'_j\right) \\ 0 \\ 0 \\ 0 \end{Bmatrix} = gK_p \begin{bmatrix} 0 & 0 & 0 & -1 & 0 & 0 & 0 & 1 \\ 0 & 0 & 0 & 0 & 0 & 0 & 0 & 0 \\ 0 & 0 & 0 & 0 & 0 & 0 & 0 & 0 \\ 0 & 0 & 0 & 0 & 0 & 0 & 0 & 0 \\ 0 & 0 & 0 & 1 & 0 & 0 & 0 & -1 \\ 0 & 0 & 0 & 0 & 0 & 0 & 0 & 0 \\ 0 & 0 & 0 & 0 & 0 & 0 & 0 & 0 \\ 0 & 0 & 0 & 0 & 0 & 0 & 0 & 0 \end{bmatrix} \begin{Bmatrix} u_{1j} \\ u_{3j} \\ w_j \\ w'_j \\ u_{1k} \\ u_{3k} \\ w_k \\ w'_k \end{Bmatrix} = \left[K_{pc}\right]\left\{\Delta_i\right\} \tag{5.40}$$

and

$$\begin{Bmatrix} 0 \\ 0 \\ 0 \\ M_{pj} \\ 0 \\ 0 \\ 0 \\ M_{pk} \end{Bmatrix} = \begin{Bmatrix} 0 \\ 0 \\ 0 \\ gK_dD_d\left(\dot{w}'_k - \dot{w}'_j\right) \\ 0 \\ 0 \\ 0 \\ -gK_dD_d\left(\dot{w}'_k - \dot{w}'_j\right) \end{Bmatrix} = gK_dD_d \begin{bmatrix} 0 & 0 & 0 & 0 & 0 & 0 & 0 & 0 \\ 0 & 0 & 0 & 0 & 0 & 0 & 0 & 0 \\ 0 & 0 & 0 & 0 & 0 & 0 & 0 & 0 \\ 0 & 0 & 0 & -1 & 0 & 0 & 0 & 1 \\ 0 & 0 & 0 & 0 & 0 & 0 & 0 & 0 \\ 0 & 0 & 0 & 0 & 0 & 0 & 0 & 0 \\ 0 & 0 & 0 & 0 & 0 & 0 & 0 & 0 \\ 0 & 0 & 0 & 1 & 0 & 0 & 0 & -1 \end{bmatrix} \begin{Bmatrix} \dot{u}_{1j} \\ \dot{u}_{3j} \\ \dot{w}_j \\ \dot{w}'_j \\ \dot{u}_{1k} \\ \dot{u}_{3k} \\ \dot{w}_k \\ \dot{w}'_k \end{Bmatrix} = \left[C_{dc}\right]\left\{\dot{\Delta}_i\right\} \tag{5.41}$$

$$\Rightarrow \{F_c\} = [K_{pc}]\{\Delta_i\} + [C_{dc}]\{\dot{\Delta}_i\} \tag{5.42}$$

Force vectors can be assembled for each element giving the following equation for each element.

$$[M_i]\{\ddot{\Delta}_i\} + [C_{dci}]\{\dot{\Delta}_i\} + ([K_i] + [K_{pc_i}])\{\Delta_i\} = \{0\} \tag{5.43}$$

The above equation can be solved after assembling all the elements taking into consideration the nodal compatibility. The method used to solve the equation is the following.

Let $\{Z_i\} = \begin{bmatrix} \Delta_i \\ \dot{\Delta}_i \end{bmatrix}$ and $[A_i] = \begin{bmatrix} 0_{8x8} & I_{8x8} \\ -[M_i]^{-1}([K_i] + [K_{pc_i}]) & [M_i]^{-1}[C_{dc_i}] \end{bmatrix}$

that reduces equation (5.43) to

$$\{\dot{Z}_i\} = [A_i]\{Z_i\} \tag{5.44}$$

Such an equation is obtained for each element. All the matrix equations are then assembled taking into consideration the nodal compatibility. The final assembled matrix equation can be solved as an Eigen Value problem. The finite element algorithm described above was coded using Matlab. Appendix VI gives the listing of the program. The program in its current version can only solve a free vibrations problem. However, it can be modified easily to give steady state solutions. The mode separation method is one possible way to obtain a steady state solution. Other time integration methods are also available to solve the steady state problem. Results obtained using the program are compared in Chapter 7 with experimental results.

CHAPTER 6

SPECIMENS TESTED

This chapter introduces the specimens tested during the course of the study. Different classes of materials were used. The characteristics and properties of the materials used are presented. The fabrication procedure is outlined and dimensions of those specimens are given.

6.1 Description of materials used

Two categories of materials were used to build tested treatments. Those were

a) piezoelectric materials, and

b) viscoelastic material.

Aluminum 6061 was used for base beams. That type of material has a modulus of elasticity of 6.91×10^{10} Pa and a density of 2800 kg/m^3.

6.1.1 Description of the piezoelectric material

Two basic types of piezoelectric material were used.

a) piezoceramic material, and

b) piezoelectric film.

a) Piezoceramic material

Piezoceramic elements used in this research were made of PZT materials and purchased from Piezo Systems Inc., Cambridge, MA. Piezoelectric and mechanical properties of those elements are listed in Table 6.1.

Table 6.1 Piezoelectric and mechanical properties of PZT piezoceramic

Composition	Lead Zirconate Titanate	
Material designation	PSI-5A-S2	
Part number	T110-A2-501	
PIEZOELECTRIC PROPERTIES		
Property name	Value	Units
Piezoelectric strain coefficient, d_{31}	171×10^{-12}	Meters/Volt
Electromechanical coupling coefficient, k_{31}	0.34	
Piezoelectric voltage coefficient, g_{31}	11.4×10^{-3}	Volt Meters/Newton
Dielectric constant, k_{3t}	1950	
MECHANICAL PROPERTIES		
Density, ρ	7750	Kg/Meter^3
Modulus of elasticity, E	6.3×10^{10}	Newtons/Meter^2

Definitions and an introduction to various piezoelectric properties mentioned in this thesis is given in Appendix VII. The material purchased was pre-poled and with nickel electrode coating on both surfaces of an element. The elements were 0.0635 meters long, 0.0381 meters wide and 2.54×10^{-4} meters thick. The designation of the high voltage face direction was done by the supplier. The high voltage faces of the elements were marked with a red strip. The material was used to generate transverse compression and tension. The response of piezoelectric elements when voltage is applied across the thickness is shown in Figure 6.1.

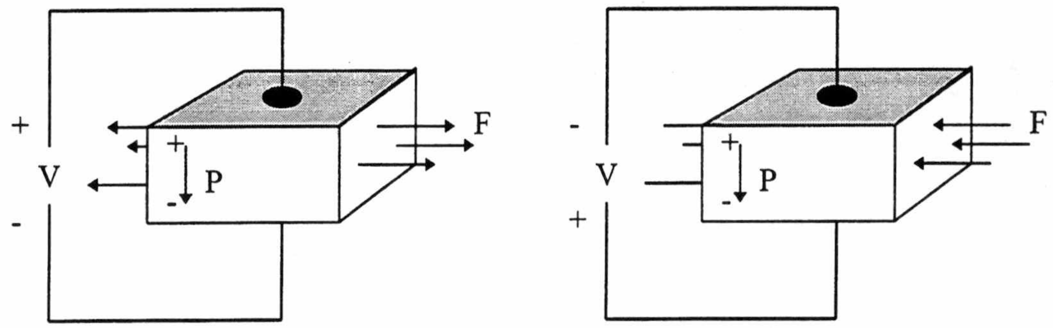

Figure 6.1 : Induced strain in piezoelectric materials

b) Piezoelectric film

Piezoelectric films used in this research were KYNAR piezofilm purchased from AMP Inc., Valley Forge, PA. Table 6.2 lists the piezoelectric and mechanical properties of the KYNAR piezoelectric film.

Table 6.2 Piezoelectric and mechanical properties of KYNAR piezofilm

Composition	Polyvinylidene fluoride (PVDF)	
Material designation	DT1-052K	
PIEZOELECTRIC PROPERTIES		
Property name	Value	Units
Piezoelectric strain coefficient, d_{31}	23×10^{-12}	Meters/Volt
Electromechanical coupling coefficient, k_{31}	0.12	
Piezoelectric voltage coefficient, g_{31}	216×10^{-3}	Volt Meters/Newton
Dielectric constant, k_{3t}	1950	
MECHANICAL PROPERTIES		
Density, ρ	1780	Kg/Meter^3
Modulus of elasticity, E	2.1×10^9	Newtons/Meter^2

As mentioned the piezoelectric films are made from Polyvinylidene fluoride (PVDF) and have the same poling characteristics as piezoceramic materials. The piezoelectric constants mentioned in Table 6.2 are defined in Appendix VII. The piezoelectric film purchased was a 0.9144 meters long, 0.3556 meters wide and 52×10^{-6}

meters thick sheet. The piezoelectric film came with a thin sputtered nickel-copper metallization on the surfaces. The poling direction and high voltage surface was marked by the supplier.

6.1.2 Description of the viscoelastic material

The viscoelastic material used was DYAD 606 from SOUNDCOAT, Deer Park, NY. Material properties for the same are listed in Table 6.3.

Table 6.3 DYAD 606 properties

Material designation	DYAD 606	
Property name	Value	Units
Density, ρ	1104	Kg/Meter^3
Poison's ratio, ν	0.5	

The complex shear modulus for the material is expressed as (Douglas and Yang 1978) :

$$G = 142000e^{0.494\ln\left(\frac{\omega}{2\pi}\right)}(1+1.46i)N/m^2 \tag{6.1}$$

The material was purchased as 20 mils and 50 mils thick sheets.

6.2 Specimens fabrication

Four different sets of specimens were fabricated. The fabrication procedure for all sets of specimens is presented below.

6.2.1 Fabrication of the first set of specimens

This set of specimens was fabricated by Thomas Christopher Widner, a graduate student at the Mechanical and Aerospace Engineering Department, at the University of Tennessee, Knoxville. A schematic diagram of a typical specimen is shown in Figure 6.2. Table 6.4 lists the geometrical characteristics of piezoelectric films and viscoelastic material used.

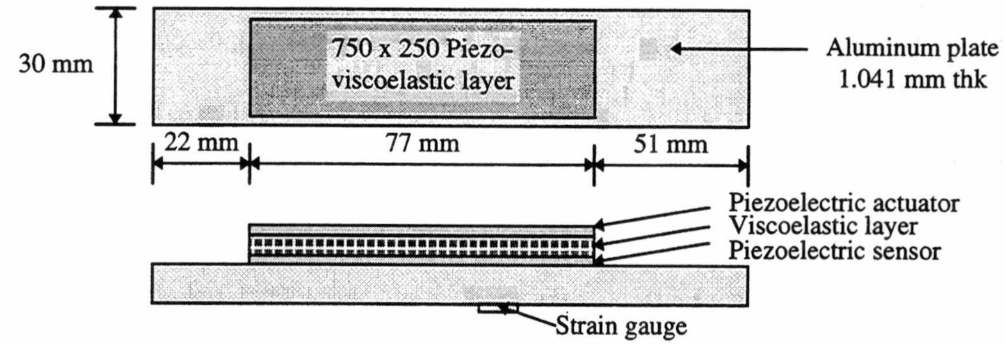

Figure 6.2 : Schamatic diagram of the PF1# (# = 1,2,3,4,5,6) specimens

Table 6.4 : Dimensions of the piezoelectric film and viscoelastic material used

Specimen name	Piezoelectric sensor thickness (m)	Viscoelastic layer thickness (m)	Piezoelectric actuator thickness (m)
PF11	28×10^{-6}	5.08×10^{-4}	28×10^{-6}
PF12	28×10^{-6}	5.08×10^{-4}	52×10^{-6}
PF13	28×10^{-6}	5.08×10^{-4}	110×10^{-6}
PF14	28×10^{-6}	12.7×10^{-4}	28×10^{-6}
PF15	28×10^{-6}	12.7×10^{-4}	52×10^{-6}
PF16	28×10^{-6}	12.7×10^{-4}	110×10^{-6}

The specimens were partially treated with an active constrained layer treatment as shown in Figure 6.2. The treatment consisted of a viscoelastic layer of DYAD 606 from SOUNDCOAT sandwiched between a segmented active constraining layer and a sensor layer, both made of DT2-052K PVDF film form AMP Inc. Component layers were bonded together using ECCOBOND 45LV epoxy resin and CATALYST 15LV epoxy resin hardener (Emersons & Cuming, Inc., Woburn, MA). Wire leads attached to actuator and sensor piezoelectric films were COPPER 1.67 x 10^{-6} meters diameter PN: TFCP-005-50 (Omega Engineering, Inc., Stamford, CT). Leads were attached to the piezoelectric films using a conductive silver paint. Strain gauges were attached at the untreated surface of the beams to measure the surface strain of the specimens. The leads were soldered to the strain gauges. Figure 6.3 shows a photograph of the specimens.

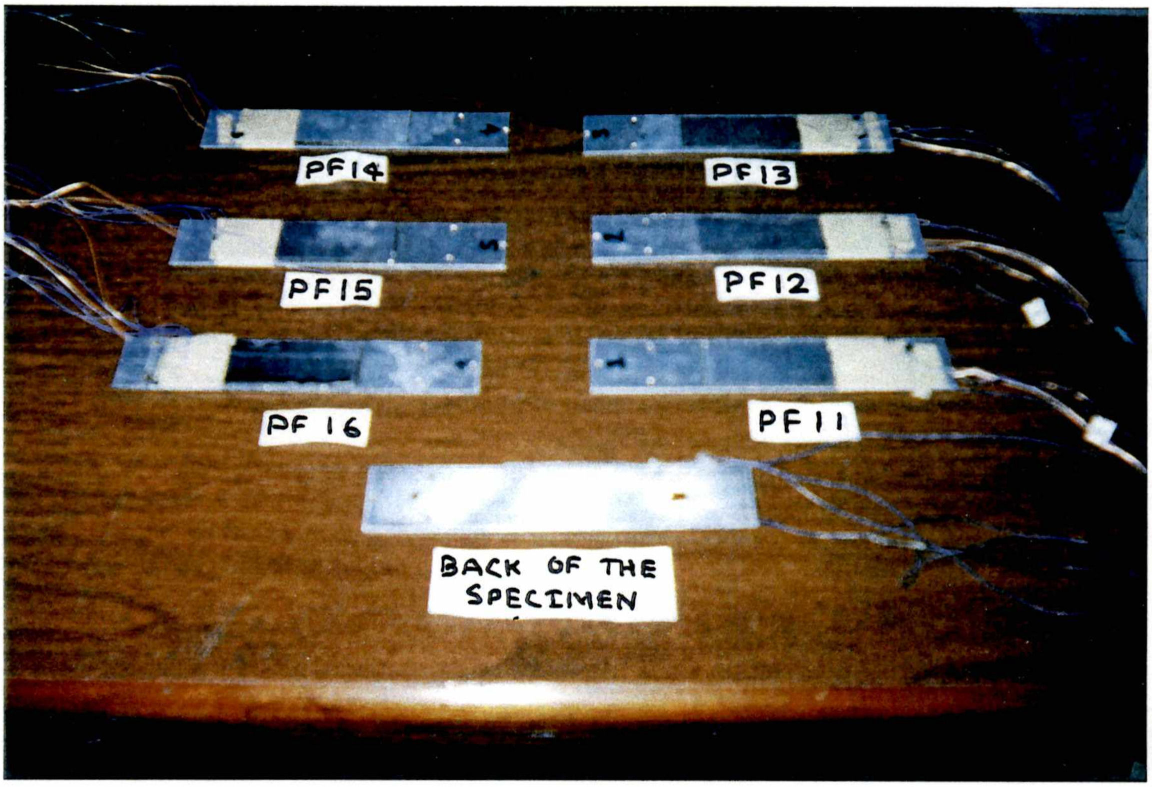

Figure 6.3 : Photograph of specimens PF1# (# = 1, 2, 3, 4, 5 and 6)

6.2.2 Fabrication of second set of specimens

This set of specimens were fabricated after the first set was tested. A schematic diagram of the specimens is shown in Figure 6.4.

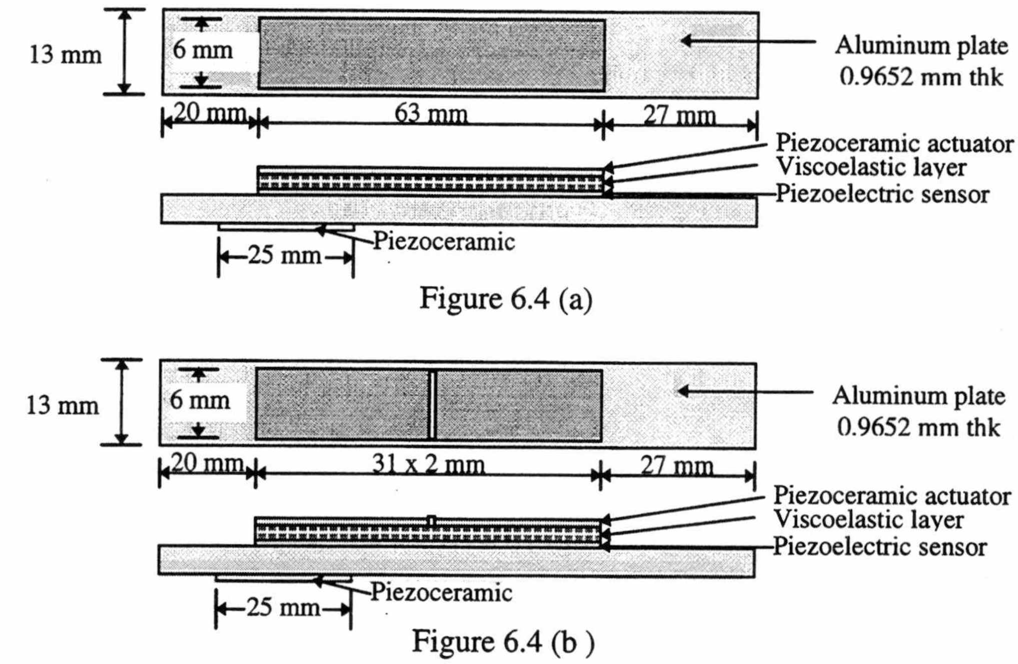

Figure 6.4 : Schematic of PZ2# specimens (a) Specimen PZ21 with unsegmented constraining layer, (b) Specimen PZ22 with constraining layer segmented

The specimens, as shown in Figure 6.4, were partially treated with an active constrained layer treatment. The treatment consisted of a viscoelastic layer of DYAD 606, 0.508 mm thick, from SOUNDCOAT sandwiched between a segmented active constraining layer made of PSI-5A-S2, 0.254 mm thick, piezoceramic material from Piezo Systems Inc. and a sensor layer made of DT2-28K PVDF film from AMP Inc. The wire leads were soldered to the piezoceramic actuator. The wire leads attached were COPPER 1.67 x 10^{-6} meters diameter PN: TFCP-005-50 (Omega Engineering, Inc., Stamford, CT). The piezoelectric film purchased had leads preattached to its surface. A piezoceramic element was attached to the untreated surface of the specimen, as seen in Figure 6.4, to actuate the beam and make it vibrate in steady state. Surfaces of all the components were cleaned using alcohol. Component layers were bonded together using ECCOBOND 45LV epoxy resin and CATALYST 15LV epoxy resin hardener from Emersons & Cuming, Inc. Resin bond was achieved by mixing 100 parts by weight of ECCOBOND 45LV with 25 parts by weight of 15LV CATALYST. After joining the component layers, the specimen was cured at room temperature for more than 24 hours.

6.2.3 Fabrication of the third and fourth set of specimens

The third and fourth set of specimens were fabricated in order to analyze the effect of active constraining layer segmentation on beams with low bending natural frequency. The schematic diagram of tested specimens is shown in Figures 6.5, 6.6 and 6.7.

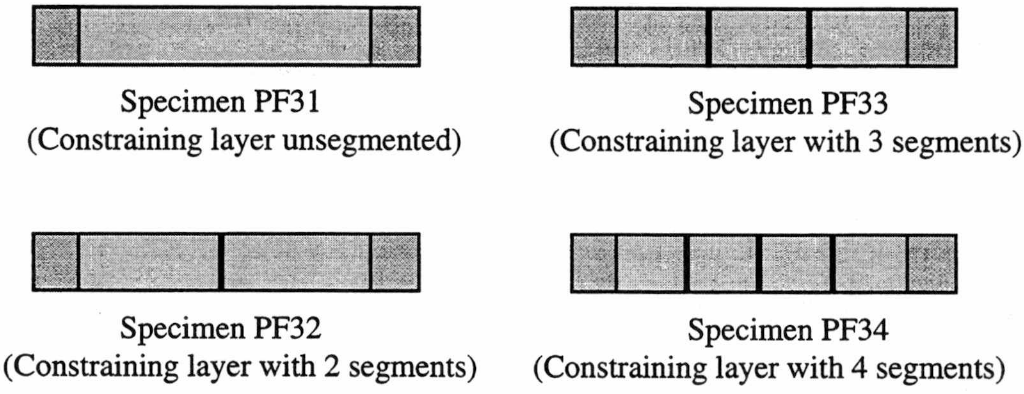

Figure 6.5 : Constraining layer segmentation for PF3# specimens (# = 1,2,3,4)
(All specimens are 25.4 mm wide)

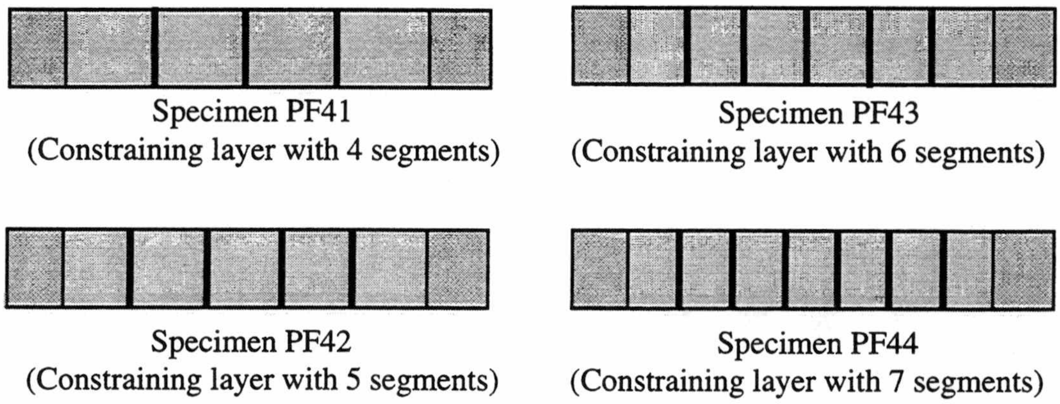

Figure 6.6 : Constraining layer segmentation for PF4# specimens (# = 1,2,3,4), (All specimens are 50.8 mm wide)

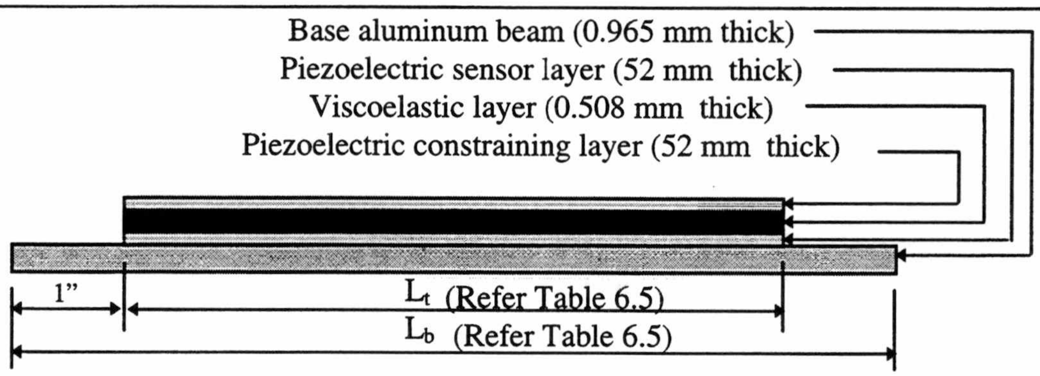

Figure 6.7 : Front view of the tested specimens (PF3# and PF4#)

Table 6.5 : Lengths L_t and L_b in Figure 6.7 for specimens PF3# and PF4#

Specimen name	L_t	L_b
PF3#	305 mm	330 mm
PF4#	565 mm	585 mm

The specimens, as shown in Figures 6.5 and 6.6, were partially treated with an active constrained layer treatment. Each specimen had different constraining layer segment lengths. The treatment consisted of a viscoelastic layer of 5.08×10^{-4} meters thick DYAD 606 from SOUNDCOAT sandwiched between a segmented active constraining layer and sensor layer made of 52 x 10^{-6} meters thick DT2-052K PVDF piezoelectric film from AMP Inc.. The piezoelectric film was cut to fit the segmentation used. The wire leads attached were COPPER 1.67 x 10^{-6} meters diameter PN: TFCP-005-50 (Omega Engineering, Inc.). The leads were attached to the piezofilm using a procedure outlined by AMP Inc. A conductive adhesive copper tape PN# 1181 (available at Wurzburg Inc., Memphis, TN) from 3M was used. The wire leads were soldered on a 25 mm long x 10 mm wide piece of the copper tape. Then the liner was removed and the tape was attached to the surface of the film with gentle pressure. The method ensured effective electrical conductivity between the wires and the piezoelectric film. The base beam was made of aluminum 9.65 x 10^{-4} meters thick. Surfaces of the aluminum beam and the viscoelastic layer were cleaned using alcohol. Component layers were bonded together using ECCOBOND 45LV epoxy resin and CATALYST 15LV epoxy resin hardener from Emersons & Cuming, Inc. Again, 100 parts by weight of ECCOBOND 45LV were mixed with 25 parts by weight of 15LV CATALYST was mixed to ensure a rigid bond. After joining the component layers, specimens were cured at room temperature for more than 24 hours. Figure 6.8 shows a photograph of the specimens.

Figure 6.8 : Photograph of specimens PF3# and PF4# (# = 1, 2, 3 and 4)

CHAPTER 7

EXPERIMENTAL INVESTIGATION

Transient and steady state vibrations of specimens described in chapter 6 were analyzed. Progress made in both fabrication technique and feedback circuit design resulted in damping treatment performance improvement. The progress will be apparent from the results presented in this chapter.

7.1 Experiments with the first set of specimens

Transient vibration analysis of the specimens was done. The experimental setup and results are outlined below.

7.1.1 Experimental setup

Figure 7.1 shows the experimental setup for testing specimens PF11, PF12, PF13, PF14, PF15 and PF16 shown in Figure 6.2. The specimens were clamped at one end as shown in Figure 7.2.

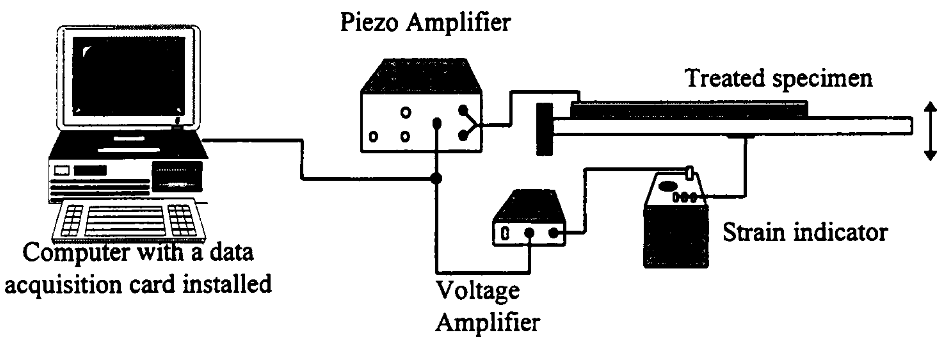

Figure 7.1 : Experimental setup for testing specimens PF1# (# = 1, 2, 3, 4, 5, 6)

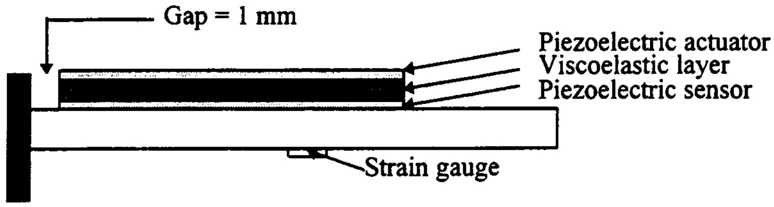

Figure 7.2 : Clamped specimen schematic

The free end was given a initial velocity with a impact. The produced strain was sensed by a strain gauge mounted on the untreated surface of the beam. A strain indicator (Automations Industries, Inc. Instruments Division, Model P-350) was connected to the strain gauge. The strain gauge indicator produced a voltage proportional to the strain. The voltage signal from the strain indicator was fed to a voltage amplifier as shown in Figure 7.1. The voltage amplifier could produce a maximum of 6 volts. The amplifier gain was constant 100 times the input. The voltage amplifier was designed and built by the department electrician Dennis Hidgon[23]. The signal from the voltage amplifier was fed to a Piezo Amplifier (Model 60.102 from Piezo Systems, Inc., Cambridge, MA). The gain in the Piezo Amplifier was 20 and it could produce ±200 volts output for a ±10 volts input maximum. The amplified signal was fed back to the piezoelectric film constraining layer. The polarity of the signal to the active constraining layer was such that it could produce a strain opposite to the strain produced on the beam surface. When the treated surface of the beam was compressed, the piezoelectric constraining layer was made to produce a extentional strain and vice versa. The amplified voltage signal from the voltage amplifier which was indicative of the strain on the surface of the specimen was fed to a data acquisition card, from Computer Boards, Inc., mounted inside a personal 486 computer.

7.1.2 Experimental results

Experiments were carried out with all six specimens. However specimen PF15 showed no improvement in the damping when the control feedback was on. A possible cause was a loose electrical connection on the active constraining layer. The silver conductive paint connection was not very reliable. A similar problem was experienced with all the specimens but could be fixed by attaching electrical tapes on the surface of the connections. The results obtained shown in Figure 7.3 for specimens PF11, PF12, PF13, PF14 and PF16.

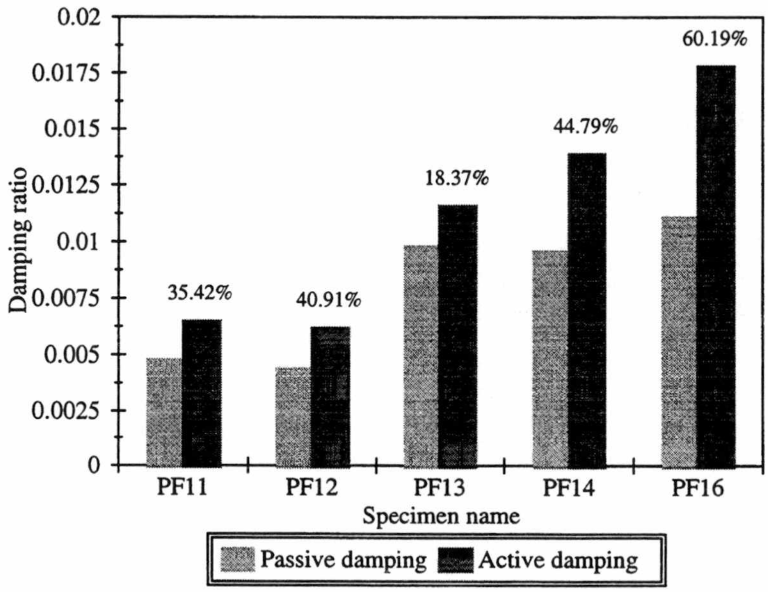

Figure 7.3 : Damping ratios for active and passive damping

Percentage improvements for the tested specimens are calculated using the equation given below.

$$\% \text{ Improvement} = \frac{\xi_{\text{passive}} - \xi_{\text{active}}}{\xi_{\text{passive}}} \bullet 100\% \qquad (7.1)$$

It can be seen from Figure 7.3 that the damping ratios for passive and active vibrations for beams with different treatment parameters were different. The active damping ratio and the passive damping ratios was the highest for specimen PF16 having a 0.11 mm thick piezoelectric film and 1.27 mm thick viscoelastic layer. Specimen PF16 also had the best percentage improvement in damping.

Another important observation was the variation of the damping ratio with the amplitude of vibration. Figure 7.4 shows the variation in the damping ratio as a function of the amplitude of vibration.

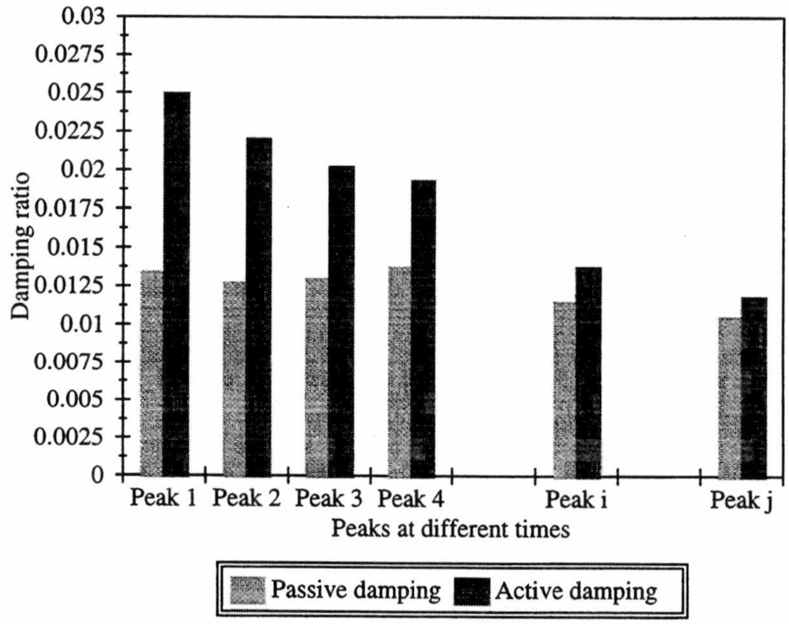

Figure 7.4 : Active vs. passive damping ratios at different amplitudes

Passive damping ratios were approximately constant for all amplitudes of vibration indicating a exponential decay. Active vibration damping ratios were higher for higher amplitudes of vibrations. This shows that the effect of the strain generated in the piezoelectric film actuator was more influensive in damping the vibrations when it had large voltage feedback. That phenomenon can be explained by a larger effect of the strain generated in the piezofilm actuator on vibrations damping for larger voltage feedback.

7.2 Experiments to examine strain producing capabilities of a piezoceramic element

Piezoceramic elements were used in the following experiments to induce steady state vibrations in a beam. These tests were preceeded with measuring the strain inducing capabalities of a piezoelectric element.

7.2.1 Experimental setup

Figure 7.5 shows the schematic of an untreated beam along with the experimental setup.

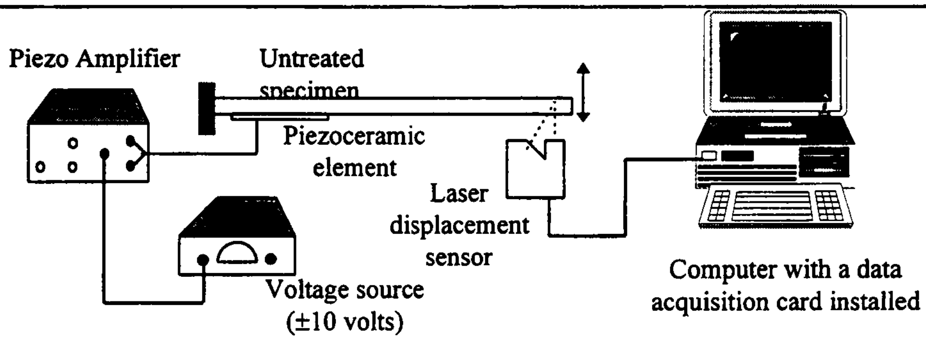

Figure 7.5 : Experimental setup for testing untreated specimens

As shown in Figure 7.5, the output from a Dual Regulated Power Supply (LAMBDA Electronic Corporation, Melville, L. I., NY, Model LPD-422A-FM) is fed to the Piezo Amplifier (Model 60.102 from Piezo Systems, Inc., Cambridge, MA) to produce the actuation voltage. The tip displacement of the beam was sensed by a laser displacement sensor (Model LM200 from Aromat Corporation, New Providence, New Jersey). The signal from the displacement sensor was fed to the data acquisition card installed in a 486 PC. The tip displacement was measured for different voltages activating the piezoceramic element. Dynamic vibrations were generated using the setup shown in Figure 7.6.

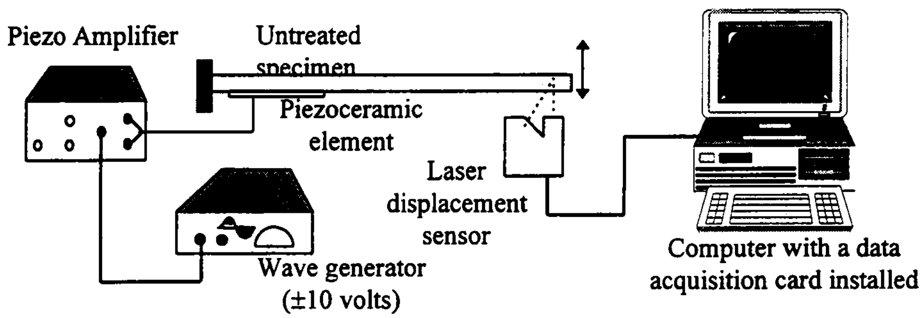

Figure 7.6 : Experimental setup for dynamic testing of the untreated specimens

A sine wave generator (Model 110 Wavetek Function Generator) output was fed to the Piezo Amplifier. The wave generator was capable of producing a ±10 volts true sine wave output. The wave generator along with the Piezo Amplifier produced a sine wave voltage supply of ±200 volts which was fed to the piezoceramic element. The piezoelement excited beam vibrations.

7.2.2 Experimental results

Figure 7.7 shows the tip displacement produced by the piezoceramic element for different activation voltages.

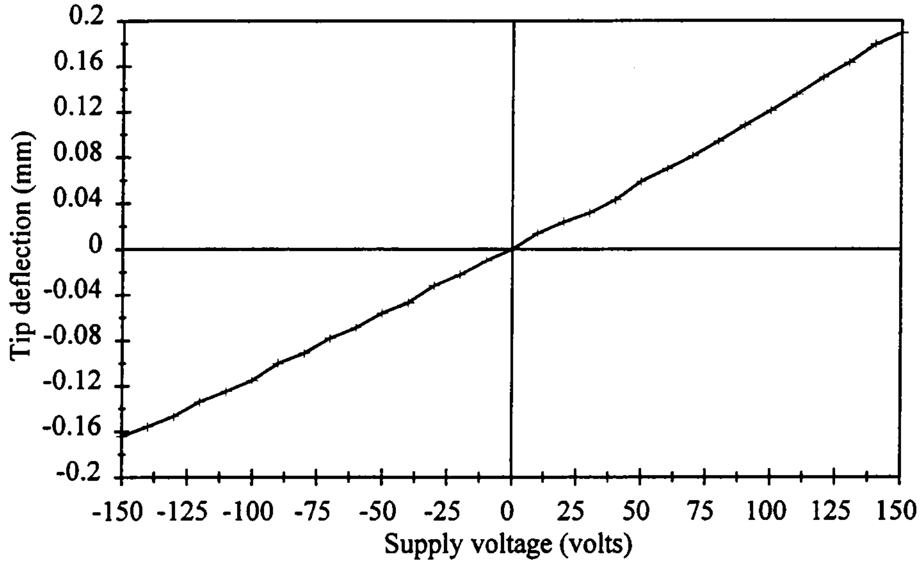

Figure 7.7 : Experimental static deflection of the untreated specimen

The response of the piezoceramic element was reasonably linear. Steady state specimen tip deflections were measured for a ±150 volt range.

Then, the piezoelectric actuator was activated with a sine wave signal with an amplitude of 120 V and a frequency of 63 Hz (first natural bending frequency of the beam). Steady state vibration amplitudes were measured.

Steady state displacements excited by a known signal made it possible to determine the magnitude of piezo induced bending moment as 2.36 N-mm.

7.3 Experiments with second set of specimens

Experiments with two specimens, PZ21 and PZ22 shown in Figure 6.4, were conducted. The main objective of these experiments was to compare the performance of active and passive damping treatments for different constraining layer segmentation.

7.3.1 Experimental setup

Figure 7.8 shows the experimental setup.

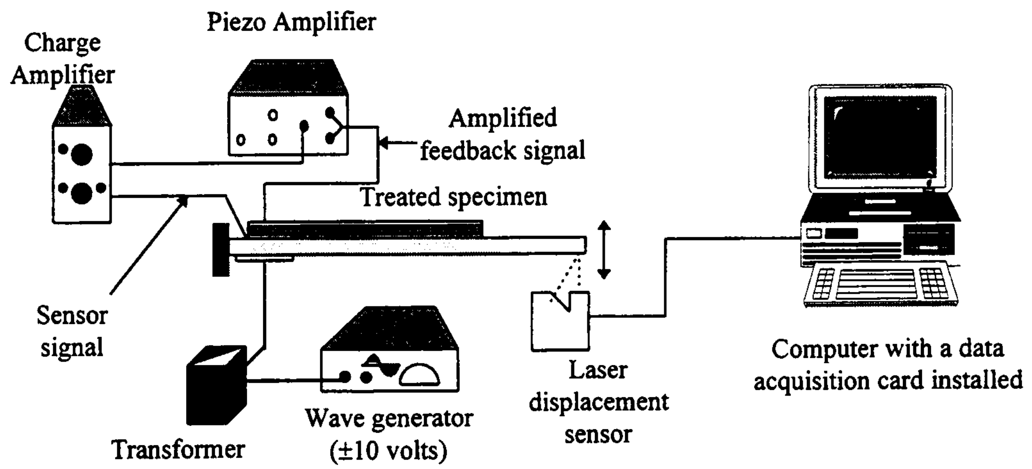

Figure 7.8 : Experimental setup for testing specimens PF21 and PF22

As seen from the figure, the sine wave generator output was fed to a transformer (capable of amplifying an AC supply of 6.3 volts by a factor of 35). The transformer, however, was used to produce a sine wave of ±100 volts at the natural frequency of the beam. The natural frequencies for the beam with different tip mass are listed in the next section. Steady state vibrations were excited by a piezoelectric actuator, as before.

The feedback active control circuit contained a Charge Amplifier (Model 503 from Kistler Instruments, Inc., Clarance, NY) which sensed the charge produced by the piezoelectric film sensor when the beam was excited. The output from the Charge Amplifier was fed to a Piezo Amplifier (Piezo Systems, Inc., Cambridge, MA) which amplified the voltage 20 times. The amplified voltage was then fed to the piezoceramic constraining layer with a reverse polarity thus closing the feedback circuit.

Tip displacements of the beam were sensed by a laser displacement sensor (Model LM200). Tip displacement data was collected by a data acquisition card as discussed in the previous section.

7.3.2 Experimental results

Specimens were tested without any end mass attached and with mass of 8.5 g. attached at the tip. The mass was used to decrease the natural frequencies of the specimens. The following arrangements were investigated.

i) Specimen PZ21 with no end mass attached (natural frequency = 73.242 Hz.)

ii) Specimen PZ21 with 8.5 g. end mass attached (natural frequency = 24.414 Hz.)

iii) Specimen PZ22 with no end mass attached (natural frequency = 68.359 Hz.)

iv) Specimen PZ22 with 8.5 g. end mass attached (natural frequency = 24.414 Hz.)

The results are presented in Figures 7.9 to 7.12.

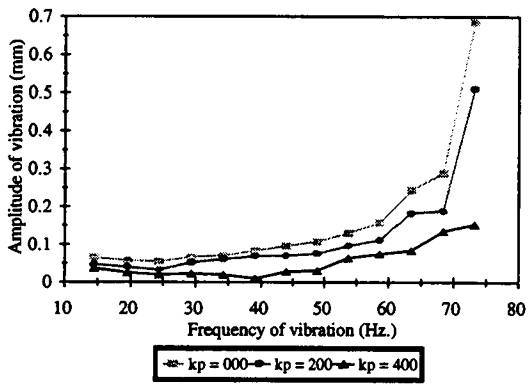

Figure 7.9 : Amplitude vs. frequency for experiments with PZ21, $f_n = 73.242$

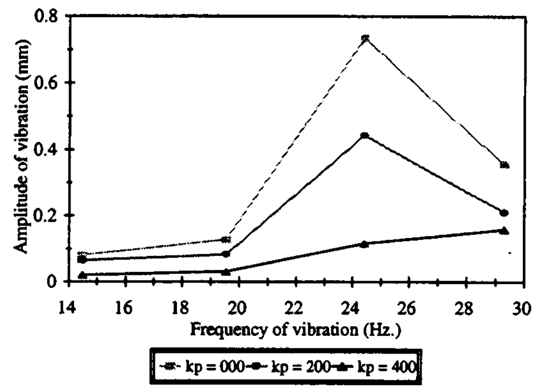

Figure 7.10 : Amplitude vs. frequency for experiments with PZ21, $f_n = 24.414$

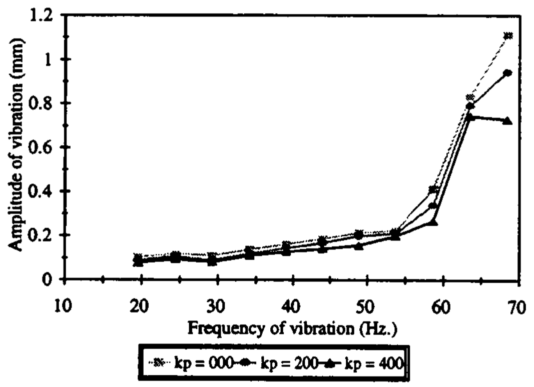

Figure 7.11 : Amplitude vs. frequency for experiments with PZ22, $f_n = 68.359$

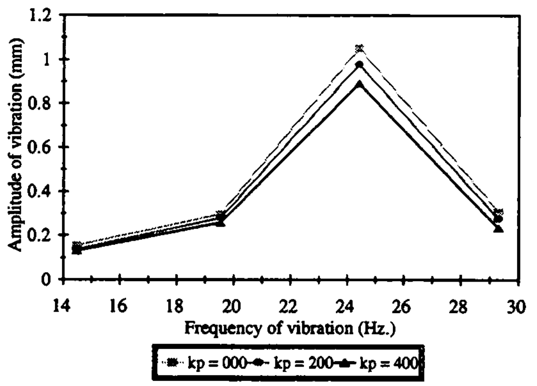

Figure 7.12 : Amplitude vs. frequency for experiments with PZ22, $f_n = 24.414$

The observations made from the results are as follows.

1) The improvement in damping was most significant when the constraining layer was continuous and when the natural frequency was low. The lowest natural frequency attained was 24.414 Hz.

2) The segmentation of the constraining layer did not improve the performance of the treatment because high frequency vibrations were analyzed and the viscoelastic layer was thick. Proper treatment parameters selection is necessary to improve the performance of the treatment.

7.4 Experiments with third and fourth set of specimens

The effect of active constraining layer segmentation on vibration damping in beams with low natural frequencies was investigated experimentally. Two types of specimens were tested as shown in Figures 6.5 and 6.6 The specimens were designated as PF3# (# = 1, 2, 3, and 4) and PF4# (# = 1, 2, 3, and 4).

7.4.1 Experimental setup

Figure 7.13 shows the experimental setup used to test the specimens.

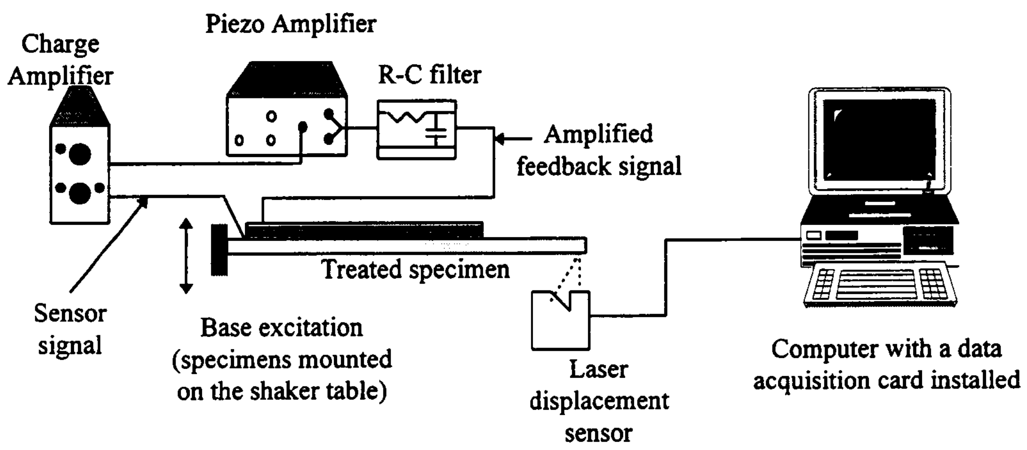

Figure 7.13 : Experimental setup for testing specimens PF3# and PF4# (# = 1, 2, 3, 4)

The only difference between the method described before and this method is that a shaker was used to excite specimens PF3# and PF4#. Thus the wave generator and the transformer shown in Figure 7.8 were not necessary. The specimen was mounted on a shaker table.

Figure 7.14 shows a schematic diagram of the shaker table.

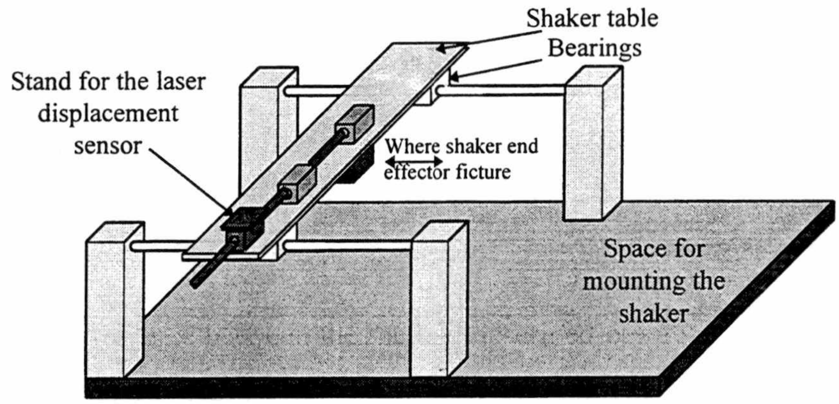

Figure 7.14 : Schematic diagram of the shaker table

The table was excited using a shaker Model VG 100-6 from Vibration Test Systems, Aurora, Ohio. The laser displacement sensor was also mounted on the table, as shown in Figure 7.14.

The sensor signal from the piezoelectric sensor layer was fed to a charge amplifier. The charge amplifier had a ±10 volts output with a variable gain. A gain of 10 was set. The output from the Charge Amplifier, as shown in Figure 7.13, was fed to the Piezo Amplifier. The gain in the Piezo Amplifier was 20. The cumulative gain of the circuit was equal to 200. A Resistance-Capacitance (R-C) filter (R= 68 kΩ, C = 1 μF) was used to filter out the noise produced by the charge amplifier and amplified in the

Piezo Amplifier. The filter was designed by Dennis Hidgon[23] to eliminate any electrical noise having frequency above 22 Hz. The noise was a problem in previous experiments and was responsible for reducing the performance of damping treatments.

The tip displacement of the beam was sensed by a laser displacement sensor as shown in Figure 7.13. The sensor signal was fed to the data acquisition card in a computer where the displacement was recorded. An oscilloscope was used to monitor the output signal from the Piezo Amplifier, i.e., the voltage supplied to the constraining layer.

For steady state analysis a shaker was used to excite the beam. Used experimental setup is shown in Figure 7.15.

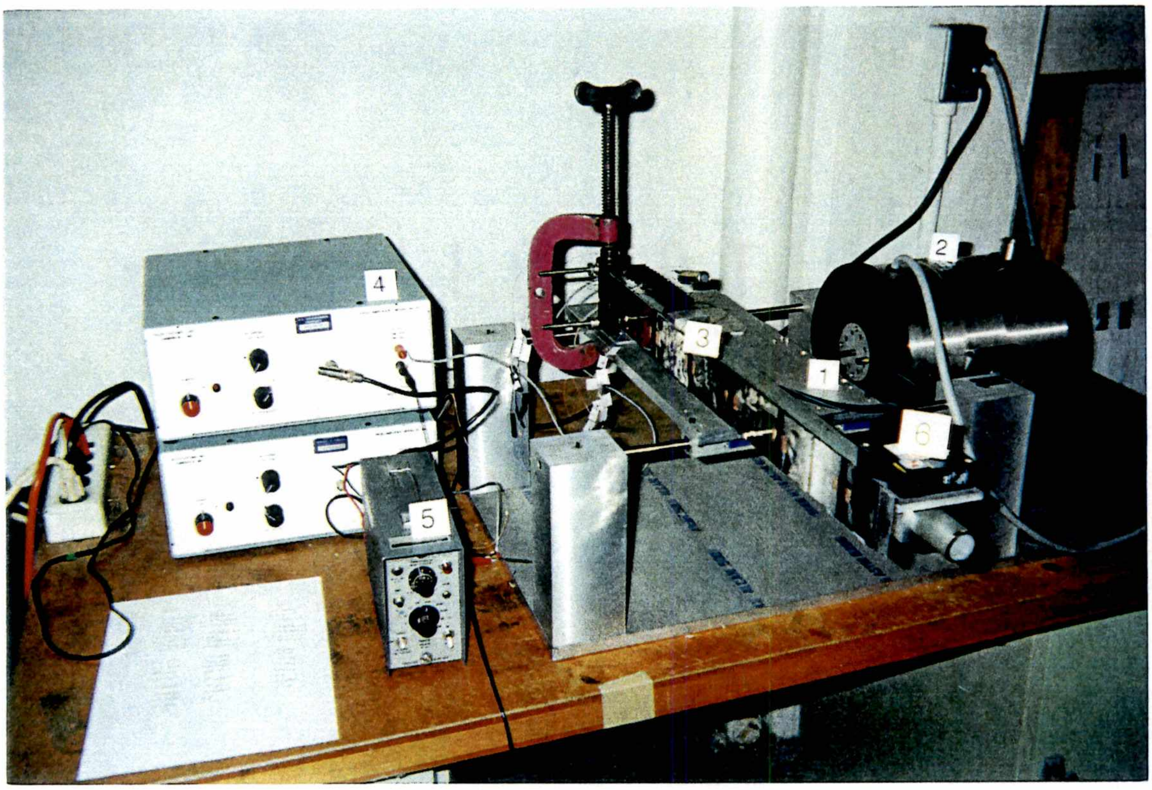

Figure 7.15 : Photograph of a typical experimental setup
1. Vibration table, 2. Shaker, 3. Specimen, 4. Piezo Amplifier,
5. Charge Amplifier, 6. Laser displacement sensor

7.4.2 Experimental procedure

Each specimen was clamped on the vibration table as shown in Figure 7.15. Free vibrations of a specimen were induced by an impact at the tip of the beam Tip displacements were sensed using the laser displacement sensor probe, fed to the A/D card and recorded on a hard disk. Sampling rate of 500 data points per second was used.

Steady state vibration tests were performed by exciting beam roots attached to the shaking table at a natural frequency of given specimen and amplitude of 0.6-0.8 mm. The tip displacement amplitude was recorded using the laser displacement sensor.

In both transient and steady state vibration cases explained above, data was collected for feedback circuits off and on. The performance of passive and active control systems was then compared.

7.4.3 Experimental results

Results obtained for transient and steady state vibrations of tested beams are outlined below. All the data associated with the graphs is given in Appendix VIII.

a) Transient vibration results

Results obtained for transient vibration damping tests for specimens PF3# are presented in Figures 7.16 and 7.17. Percentage improvements for the tested specimens are calculated using equation (7.1).

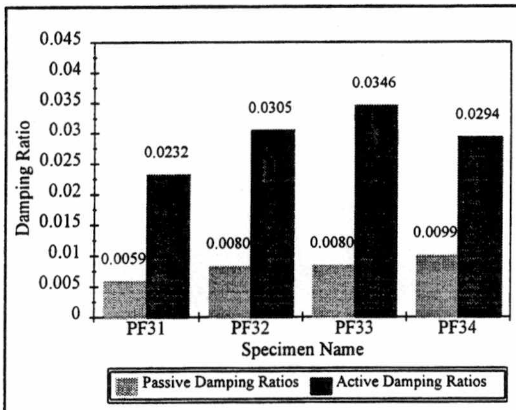

Figure 7.16 : Damping ratios for passive and active damping

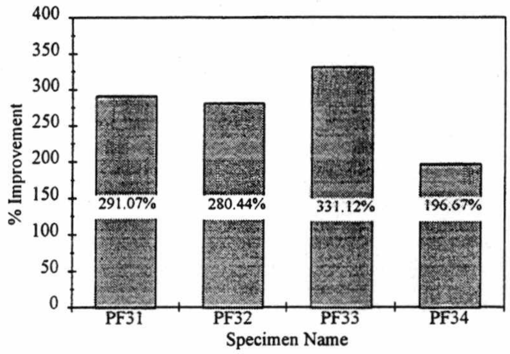

Figure 7.17 : Passive vs. active damping

The most important observations are as follows:

1) The highest damping ratio was obtained for a specimen having the constraining layer divided into three segments (PF33). We can observe that the treatment with the constraining layer divided into three segments was about 50% more effective than the treatment with no segmentation,
2) The improvement in damping ratio magnitude was most significant also for the same specimen.

Table 7.1 : Finite element analysis vs. experimental results for specimens PF3#

	Natural frequency		Damping ratio	
Specimen name	Experimental	Theoretical	Experimental	Theoretical
PF31	6.23	8.2236	0.0232	0.22144
PF32	6.73	8.1115	0.0305	0.22277
PF33	6.26	8.00393	0.0346	0.22413
PF34	6.49	7.90017	0.0294	0.22561

For the error analysis the finite element results see Appendix IX.

The transient vibration results for specimens PF4# are presented in Figures 7.18 and 7.19. Percentage improvements are again calculated using Equation (7.1).

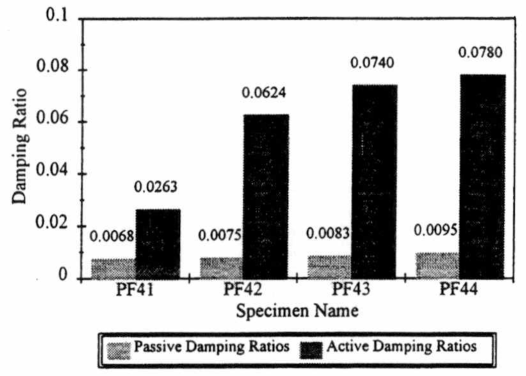

Figure 7.18 : Damping ratios for passive and active damping

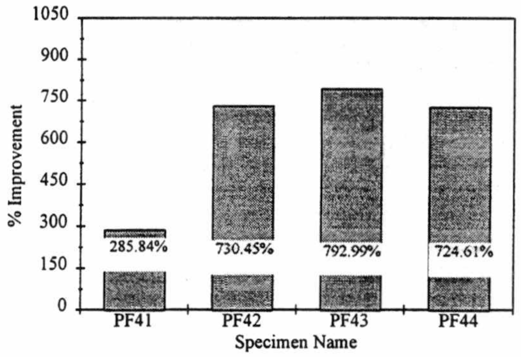

Figure 7.19 : Passive vs. active damping

This portion of the experiment has shown that:

1) The highest damping ratio was obtained for the specimen having the constraining layer divided into seven segments (PF44). We can observe that dividing the constraining layer into seven segments resulted in more than 210% improvement over the performance of the treatment with four segments,
2) The improvement in damping ratio magnitude was most significant for the specimen with six segments (PF43).

Table 7.2 : Finite element analysis vs. experimental results for specimens PF4#

	Natural frequency		Damping ratio	
Specimen name	Experimental	Theoretical	Experimental	Theoretical
PF41	2.02	2.8805	0.0263	0.28294
PF42	1.79	2.8623	0.0624	0.28573
PF43	1.91	2.8412	0.0740	0.28635
PF44	1.88	2.8222	0.0780	0.28704

For the error analysis of the finite element results see Appendix IX.

The results of transient vibrations damping tests indicate that the passive and active damping ratios vary with the change of segment length. It can be noted that the optimal segment lengths for passive and active case are not necessarily the same. For example, specimen PF43 (with the active constraining layer divided into three segments) behaves best of all specimens for active damping while specimen PF34 (with the active constraining layer divided into four segments) behaves best for passive damping.

Typical time histories of passively and actively damped transient vibrations of specimen PF44 are shown in Figures 7.20 and 7.21

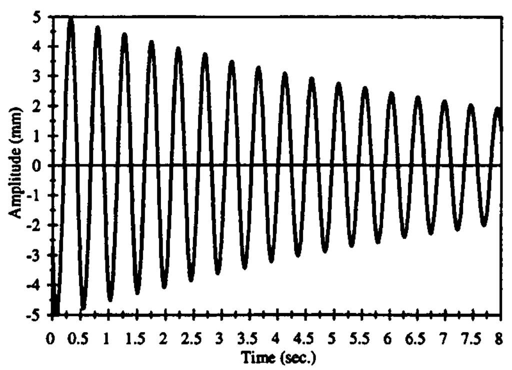

Figure 7.20 : Time history of passively damped transient vibrations

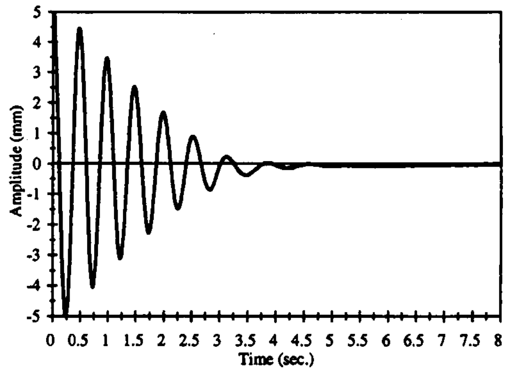

Figure 7.21 : Time history of actively damped transient vibrations

Figures 7.22 and 7.23 show improvements in a steady state vibration amplitude reduction for specimens PF3# and PF4#. Percentage improvements are calculated using the equation given below.

$$\% \quad \text{Improvement} = \frac{A_{passive} - A_{active}}{A_{active}} \bullet 100\% \tag{7.2}$$

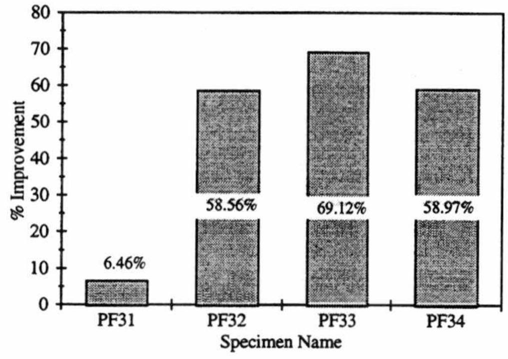

Figure 7.22 : Steady state active vs. passive damping for specimens PF3#

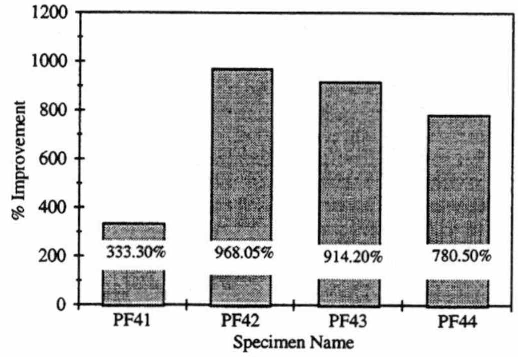

Figure 7.23 : Steady state active vs. passive damping for specimens PF4#

The most important observations are summarized below.

It is apparent that the active constraining layer segmentation improves damping in specimens with low natural frequencies (PF4#) much more than in specimens with higher natural frequencies (PF3#). This trend is compatible with observations made for segmented passive constrained layer treatments. The most significant improvement in amplitude reduction was obtained for the following specimens

1) PF33-specimen with a higher natural frequency having three active constraining layer segments.

2) PF42-specimen with a lower natural frequency having five active constraining layer segments.

Figure 7.24 shows a comparison between the experimental and the analytical results obtained for steady state vibrations of specimen PF31. The results show a fair reasonable agreement.

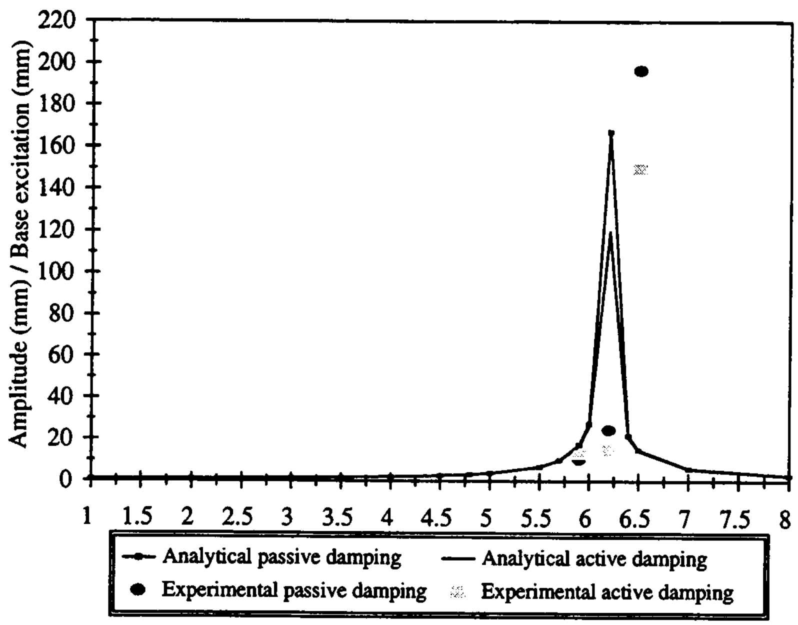

Figure 7.24 : Experimental vs. analytical results for specimen PF31

Representative steady state tip displacements of specimen PF44 for passive and active damping cases are shown in Figures 7.25 and 7.26, respectively.

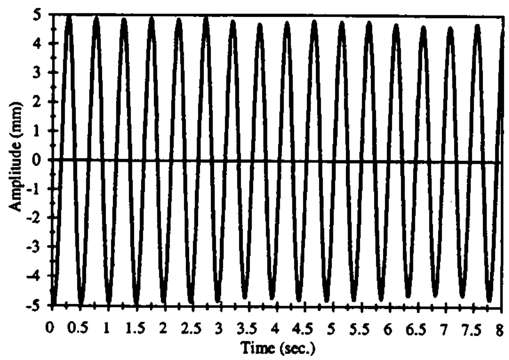

Figure 7.25 : Time history of passively damped steady state vibrations

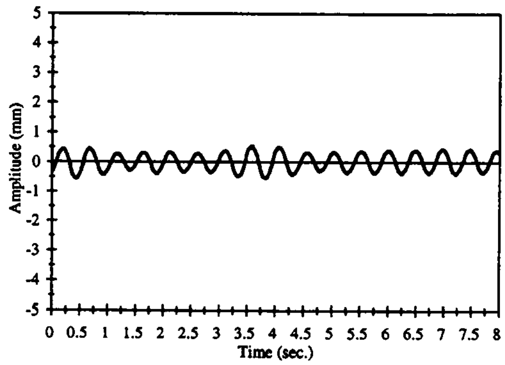

Figure 7.26 : Time history of actively damped steady state vibrations

We can note that the number of active constraining layer segments for best damping performance is different for transient vibrations damping (seven segments) than for the steady state vibration damping (five segments).

CHAPTER 8

CONCLUSIONS

The research has examined the performance of a new class of smart active damping treatment. The experimental results obtained for the novel approach used to control vibration make it a candidate for consideration in commercial application at places where vibration is a problem. Analytical evaluations show a good correspondence with experimental results. Higher proportional and derivative gains will certainly improve the performance of the damping treatments.

One of the most important issue addressed in the thesis is the effect of segmentation of the active constraining. It is evident that segmentation of the constraining layer is an effective and improves the damping in the structure without addition of extra weight. For example the damping ratio is about 0.035 for a beam with the active constraining layer partitioned into three segments as compared to 0.022 for a beam having unsegmented active constraining layer.

The numerical evaluations show a fair correspondence with the experimental results. The theory used to derive the finite element model is based on the Timoshenko beam theory and is used model thin beams. The high stiffness predicted is expected. However, it is also evident that more work in modeling of the viscoelastic layer is necessary.

The present research has placed emphasis on investigating the effect of constraining layer segmentation. The results of this project show that the segmentation of a constraining layer can improve the performance of a damping treatment by a factor of three or more.

REFERENCES

1. Mead, D. J. and Markus, S., "The Forced Vibration of a Three-Layer, Damped Sandwich Beam with Arbitrary Boundary Conditions," Journal of Sound and Vibration, 10(2), pp. 163-175, 1969.
2. Baz, A. "Active Constrained Layer Damping," Damping '93 Conference, San Francisco, CA, February 1993, pp. IBB 1-23.
3. Baz, A. and Ro, J. "Partial Treatment of Flexible Beams with Active Constrained Layer Damping," Conference of Engineering Science Society, ASME-AMD- Vol. 167, Charlottesville, VA, pp. 61-80, June 1993.
4. Plunkett, R. and Lee, C. T., "Length Optimization for Constrained Viscoelastic Layer Damping," The Journal of the Acoustical Society of America, Vol. 48, No. 1 (Part 2), pp. 150-161, 1970.
5. Parfitt, G. G. and Lambeth, D., "The Damping of Structural Vibrations," A. R. C. C. P. No. 569, 1960.
6. Parfitt, G. G., "The Effect of Cuts in Damping Tapes," Fourth International Congress on Acoustics, Copenhagen, P21, 1962.
7. Lifshitz, J. M. and Leibowitz, M., "Optimal Sandwich Beam Design for Maximum Viscoelastic Damping," Int. J. Solids Structures, Vol. 23, No. 7, pp. 1027-1034, 1987.
8. Mantena, P. R., Gibson, Ronald F. and Hwang, Shwilong J., "Optimal Constrained Viscoelastic Tape Lengths for Maximizing Damping in Laminated Composites," AIAA Journal Vol. 29, No. 10, pp.1678-1685, 1990.
9. Crawley, Edward F., "Intelligent Structures for Aerospace: A Technology Overview and Assessment," AIAA Journal, Vol. 32, No. 8, pp. 1689-1699, 1994.

10. Ashley, Stevens, "Smart skis and other adaptive structures," Mechanical Engineering, Vol. 117 No. 11, pp. 76-81, 1995.

11. Trompette, P., Boillot, D. and Ravanel, M. A., "The Effect of Boundary Conditions on the Vibration of a Viscoelastically Damped Cantilever Beams," Journal of Sound and Vibration 60(3), 345-350, 1978.

12. Baz, A. and Ro, J., "Finite Element Modeling and Performance of Active Constrained Layer Damping," Ninth VPI & SU Conference on Dynamics & Control of Large Structures, Blacksburg, VA, pp. 345-358, May 1993.

13. Johnson Conor D. and Kienholz David A., "Finite Element Prediction of Damping in Structures with Constrained Viscoelastic Layers," AIAA Journal, Vol. 20, No. 9, pp. 1284-1290, 1981.

14. Douglas, B. E., "The Transverse Vibratory Response of Partially Constrained Elastic-Viscoelastic-Elastic Beams," PhD. Dissertation, University of Maryland, 1977.

15. Kerwin, Edward M. Jr., "Damping of Flexural Waves by a Constrained Viscoelastic Layer," The Journal of the Acoustical Society of America, Vol. 31, No. 7, pp. 952-962, 1959.

16. Ungar, Eric E. and Kerwin, Edward M. Jr., "Loss factors of Viscoelastic Systems in Terms of Energy Concepts," The Journal of the Acoustical Society of America, Vol. 34, No. 7, pp. 954-957, 1962.

17. Asnani, N. T. and Nakara, B. C., "Vibration Damping Characteristics of Multilayered Beams with Constrained Viscoelastic Layers," Journal of Engineering for Industry, pp. 895-901, August 1976.

18. DiTaranto, R. A., "Theory of Vibratory Bending for Elastic and Viscoelastic Layered Finite-Length Beams," Journal of Applied Mechanics, pp. 881-886, December 1965.

19. Nasif, A. D., Jones, D. I. G. and Henderson, J. P., Vibration Damping, A Wiley-Interscience Publication, John Wiley & Sons, ©1985.

20. Petyt, Maurice, Introduction to Finite Element Vibration Analysis, Cambridge University Press, Cambridge, ©1990.

21. Meirovitch, Leonard, Analytical Methods In Vibrations, Macmillan Publishing Co., Inc., New York, ©1967.

22. Kawiecki, Grzegorz, Assistant Professor, Department of Mechanical and Aerospace Engineering, University of Tennessee, Knoxville, TN., Personal Communication.

23. Higdon, Dennis, Electronics Specialist, Department of Mechanical and Aerospace Engineering, University of Tennessee, Knoxville, TN., Personal Communication.

24. Smith, Winthrop P., "Validation of Torsional-Bending Piezoelectric Actuator Concept," Master's Thesis, The University of Tennessee, Knoxville, 1993.

25. Chinyi Hu, "Torisonal Control of Thin-Walled Structures by Piezoelectric Actuators," Master's Thesis, The University of Tennessee, Knoxville, 1994.

26. Mead D. J., "Criteria for Comparing the Effectiveness of Damping Treatments," Noise Control, pp. 27-38, May/June 1961.

27. Liu, M. and Gorman, D. G., "Improved Method for Evaluating Damping Ratios of a Vibrating System," AIAA Journal, Vol. 31, No. 7, pp. 1357-1362, 1993.

28. Zeinetdinova, R. Z., Naumkina, N. I. and Tartakovskii, B. D., "Effectiveness of a Vibration-Absorbing Coating with a Cut Constraining Layer," Sov. Phys. Acoust. 24(4), pp. 347-348, 1978.

29. Park, C and Chopra, I., "Modeling Piezoceramic Actuation of Beams in Torsion," AIAA Journal, AIAA-94-1781-CP.

30. Bathe, Klaus-Jürgen, Finite Element Procedures, Prentice Hall, Englewood Cliffs, New Jersey, ©1996.

APPENDICES

APPENDIX I

PIEZOELECTRIC STRAINS

The piezoelectric actuator :

Strain is induced in the piezoelectric actuator when subjected to a voltage applied across the thickness. For a typical piezoelectric actuator the strain induced is given as follows (Baz and Ro[3]).

$$\varepsilon_p = \left(\frac{d_{31}}{h_1}\right)V_c$$

where V_c is the voltage across the constraining piezoelectric actuator layer.

The piezoelectric sensor :

The piezoelectric sensor layer is bonded to the beam surface. Therefore, the strain induced in the sensor layer is proportional to the curvature of the beam (Baz and Ro[3]).

$$\varepsilon_s = D_d \frac{\partial^2 w_2}{\partial x^2}$$

The sensor voltage is obtained by integration of the induced strain over the length of the sensor layer (Baz and Ro[3]).

$$V_s = -\left[\frac{k_{31}^2 D_d b}{g_{31} C}\right] \int_{L_1}^{L_2} \frac{\partial^2 w_2}{\partial x^2} dx$$

The capacitance of the sensor C is given by (Baz and Ro[3])

$$C = 8.854\left(10^{-12}\right)\frac{Ak_{3t}}{h_3}$$

APPENDIX II

MATHEMATICA PROGRAM TO SOLVE THE ANALYTICAL EQUATION OF MOTION

```
Off[General::spell1,General::spell]
Clear["Global`*"];
timall = TimeUsed[];
```

■ Geometric definition and Material Properties

Numerical P number value

```
pPi = N[Pi];
```

Thickness of the piezoactuator

```
hL1 = 0.000052;
```

Thickness of the viscoelastic core

```
hL2 = 0.000508;
```

Thickness of the piezosensor

```
hL3 = 0.000052;
```

Thickness of the beam

```
hL4 = 0.0009652;
```

Length of the beam

```
lL  = 0.3327;
```

Distance from the beam tip to the tip end of the piezoactuator

```
lL1 = 0.0254;
```

Distance from the beam tip to the base end of the piezoactuator

```
lL2 = 0.3302;
```

Width of the beam

```
b   = 0.0254;
```

Width of the piezoactuator

```
bp    = 0.0254;
```

Density of the piezoactuator

```
roL1 = 1800.0;
```

Density of the viscoelastic material

```
roL2 = 1104.0;
```

Density of the piezosensor

```
roL3 = 1800.0;
```

Density of the beam

```
roL4 = 2776.156867;
```

Elasticity modulus of the piezoactuator

```
eEL1 = 2.25 10^9;
```

```
eEL3 = 2.25 10^9;
```

Elasticity modulus of the beam

```
eEL4 = 6.32661 10^10;
```

Second area moment of inertia of the piezoactuator layer

```
iIL1 = N[1.0/12.0 bp hL1^3];
```

Second area moment of inertia of the viscoelastic layer

```
iIL2 = N[1.0/12.0 b hL2^3];
```

Second area moment of inertia of the piezosensor layer

```
iIL3 = N[1.0/12.0 b hL3^3];
```

Second area moment of inertia of the beam

```
iIL4 = N[1.0/12.0 b hL4^3];
```

Beam - piezoactuator- piezosensor rigidity per unit width

```
dDLt = (eEL1 iIL1 + eEL3 iIL3 + eEL4 iIL4)/b;
```

■ External force

Excitation frequency [Hz]

```
f = 6.2;
ome = 2 pPi f;
```

Base excitation displacement [mm]

```
w = 0.1;
```

■ Piezo-Electric constraining layer

Piezoelectric strain constant

```
dL31 = 23 10^(-12);
```

Electromechanical coupling factor

```
kL31 = 0.12;
```

Piezoelectric voltage constant of the piezosensor

```
gL31 = 216*10^(-3);
```

Dielectric constant

```
kL3t = 1950.0;
```

Sensor area

```
aALp = b (lL2-lL1);
```

Capacitance of the sensor

```
c = 8.854 10^(-12) aALp kL3t/hL3;
```

Control gain (Kp = 0 for passive damping)

```
kKLp = 0200.0;
```

■ Visco-elastic layer

Complex shear modulus of the viscoelastic core (Baz93a/51/14)

```
gG = Simplify[142000.0  Exp[0.494 Log[ome/(2.0 pPi)]]
              (1.0+1.46I)];
```

■ Intermediate Variables

```
g = gG/hL2 ((eEL1 hL1 + eEL3 hL3 + eEL4 hL4)/
           (eEL1 hL1  (eEL3 hL3 + eEL4 hL4)));
```

Distance between the neutral axis of the beam-sensor layer and the interface between the beam-sensor layer and the viscoelastic layer

```
dD = (eEL3 hL3^2 + 2.0 eEL4 hL3 hL4 + eEL4 hL4^2)/
     (2.0 (eEL3 hL3 +  eEL4 hL4));
```

Distance between the neutral axis of the beam-sensor layer and the neutral axis of the piezoelectric layer (Baz93a/2/8)

```
d  = hL2 + hL1/2.0 + dD;
```

Distance between neutral axis of entire sandwiched beam and the interface between the sensor and the viscoelastic layer

```
dDLd = dD;
```

Auxiliary constant (Baz93a/12/9)

```
yY = d^2/dDLt (eEL1 hL1  (eEL3 hL3 + eEL4 hL4))/
              (eEL1 hL1 + eEL3 hL3 + eEL4 hL4);
```

Auxiliary constant (Baz93b/25/70)

```
k = Sqrt[roL4 ome^2/eEL4];
```

Mass per unit length of the beam

```
mL4   = roL4 hL4 b;
```

Flexural rigidity of the beam

```
dDL4 = eEL4 iIL4/b;
```

Mass per unit surface area of the sandwiched part of the beam

```
m=(roL1 hL1 b/bp + roL2 hL2 + roL3 hL3 + roL4 hL4);
```

■ Governing Equations

Auxiliary constants necessary to compute Eqs. 1/66 Baz93b

```
eWL1=DSolve[eEL4 iIL4 wWL1''''[x] - mL4 ome^2 wWL1[x]==
     0.0, wWL1, x, DSolveConstants->aA]

                                        2        3        4
{{wWL1 -> Function[x, 0. + 0. x + 0. x  + 0. x  + 0. x  +

       aA[1]        5.41179 x             aA[3] Cos[5.41179 x]
      ------------ + E           aA[4] + ------------------------ -
       5.41179 x                                       -19
      E                                     2.02224 10    x
                                           E

      aA[2] Sin[5.41179 x]
      ----------------------]}}
                   -19
        2.02224 10    x
       E

eWL2=DSolve[wWL2''''''[x] - g (1+yY) wWL2''''[x] -
     m ome^2/dDLt wWL2''[x] + m g ome^2/dDLt wWL2[x]==
     0, wWL2, x, DSolveConstants->bB]

                            (-91.6144 - 48.2941 I) x
{{wWL2 -> Function[x, E                                bB[1] +

       (-5.71557 - 0.000101163 I) x
      E                                  bB[2] +
```

```
  (-0.000100471 - 5.71571 I) x
E                               bB[3] +

  (0.000100471 + 5.71571 I) x
E                              bB[4] +

  (5.71557 + 0.000101163 I) x
E                              bB[5] +

  (91.6144 + 48.2941 I) x
E                         bB[6]]}}
```

```
eWL3=DSolve[eEL4 iIL4 wWL3''''[x] - mL4 ome^2 wWL3[x]==
      0.0, wWL3, x, DSolveConstants->cC]
```

```
                                                 2        3        4
{{wWL3 -> Function[x, 0. + 0. x + 0. x  + 0. x  + 0. x  +

     cC[1]          5.41179 x           cC[3] Cos[5.41179 x]
   ----------- + E           cC[4] + ---------------------- -
    5.41179 x                                     -19
   E                                   2.02224 10     x
                                      E

   cC[2] Sin[5.41179 x]
   --------------------]}}
                 -19
     2.02224 10     x
    E
```

■ Induced Strain

Output voltage from the sensor layer

```
vVLs = -(kL31^2 dDLd b/(gL31 c)) Integrate[(wWL2''[x]/.eWL2),
        {x,lL1,lL2}];
```

Actuator voltage (Baz93b/41/72)

```
vVLa = -kKLp vVLs;
```

Free strain (Baz93b/37/71)

```
epsLp = dL31 / hL1 vVLa;
```

■ Boundary and Compatibility Conditions

```
eqL1  = wWL1'''[0]/.eWL1;
eqL2  = wWL1''[0]/.eWL1;
eqL3  = wWL3[lL] - w/.eWL3;
eqL4  = wWL3'[lL]/.eWL3;
eqL5  = (wWL1[lL1]/.eWL1) - (wWL2[lL1]/.eWL2);
eqL6  = (wWL1'[lL1]/.eWL1) - (wWL2'[lL1]/.eWL2);
eqL7  = (wWL1''[lL1]/.eWL1) - (wWL2''[lL1]/.eWL2);
eqL8  = (wWL1'''[lL1]/.eWL1) - (wWL2'''[lL1]/.eWL2);
eqL9  = (wWL3[lL2]/.eWL3) - (wWL2[lL2]/.eWL2);
eqL10 = (wWL3'[lL2]/.eWL3) - (wWL2'[lL2]/.eWL2);
eqL11 = (wWL3''[lL2]/.eWL3) - (wWL2''[lL2]/.eWL2);
eqL12 = (wWL3'''[lL2]/.eWL3) - (wWL2'''[lL2]/.eWL2);
```

```
eqL13 =  ((1.0/k) Cot[k lL1] (1.0/g (wWL2''''[lL1]/.eWL2) -
          yY (wWL2''[lL1]/.eWL2) -
          m ome^2/(dDLt g) (wWL2[lL1]/.eWL2) -
          yY/d epsLp) + 1.0/g^2 (wWL2'''''[lL1]/.eWL2) -
          yY/g (wWL2'''[lL1]/.eWL2) -
         (yY + m ome^2/(dDLt g)) (wWL2'[lL1]/.eWL2) -
          yY/d x epsLp)/.x->lL1;

eqL14 =  ((1.0/k) Tan[k (lL2 - lL)]
         (1.0/g (wWL2''''[lL2]/.eWL2) -
          yY (wWL2''[lL2]/.eWL2) -
          m ome^2/(dDLt g) (wWL2[lL2]/.eWL2) - yY/d epsLp)-
         (1.0/g^2 (wWL2'''''[lL2]/.eWL2) -
          yY/g (wWL2'''[lL2]/.eWL2) -
         (yY + m ome^2/(dDLt g)) (wWL2'[lL2]/.eWL2) -
          yY/d x epsLp ))/.x->lL2;
```

■ Solution

```
 sol=Solve[{eqL1==0, eqL2==0, eqL3==0, eqL4==0,eqL5==0,
            eqL6==0, eqL7==0, eqL8==0, eqL9==0,eqL10==0,
            eqL11==0,eqL12==0,eqL13==0,eqL14==0},
           {aA[1], aA[2], aA[3], aA[4],
            bB[1], bB[2], bB[3], bB[4], bB[5], bB[6],
            cC[1], cC[2], cC[3], cC[4]}];

actvol    = Abs[vVLa/.sol]//N;

pasvol    = Abs[vVLs/.sol]//N;

result    = wWL1[0.0]/.eWL1/.sol;

amplit    = Abs[result]

{{12.0003}}
```

APPENDIX III

PROGRAM TO GET SHEAR IN THE VISCOELASTIC LAYER

```
Off[General::spell1,General::spell];
Clear["Global`*"];
timall = TimeUsed[];
```

■ Geometric definition and Material Properties

Numerical P number value

```
pPi = N[Pi];
```

Thickness of the piezoactuator

```
hL1 = 0.000052;
```

Thickness of the viscoelastic core

```
hL2 = 0.000508;
```

Thickness of the piezosensor

```
hL3 = 0.000052;
```

Thickness of the beam

```
hL4 = 0.000965;
```

Length of the beam

```
lL  = 0.3327;
```

Distance from the beam tip to the tip end of the piezoactuator

```
lL1 = 0.0254;
```

Distance from the beam tip to the base end of the piezoactuator

```
lL2 = 0.3302;
```

Width of the beam

```
b   = 0.0254;
```

Density of the piezoactuator

```
roL1 = 1800.0;
```

Density of the viscoelastic material

```
roL2 = 1104.0;
```

Density of the piezosensor

```
roL3 = 1800.0;
```

Density of the beam

```
roL4 = 2800.0;
```

Elasticity modulus of the piezoactuator

```
eEL1 = 2.25 10^9;
```

Elasticity modulus of the piezosensor

```
eEL3 = 2.25 10^9;
```

Elasticity modulus of the beam

```
eEL4 = 6.911 10^10;
```

■ External force

Forcing frequency [Hz]

```
f = 16;
ome = 2 pPi f;
```

External force amplitude [N]

```
pPL0 = 5.0;
```

■ Visco-elastic layer

Complex shear modulus of the viscoelastic core (Baz93a/51/14)

```
gG = Simplify[142000.0  Exp[0.494 Log[ome/(2.0 pPi)]]
            (1.0+1.46I)];
gG1 = Im[gG];
gG2 = Re[gG];
```

Subroutine to extract data from the program to a ASCII text file

```
writeMatrixToSpreadSheet[filename_String,data_List]:=
        Block[{
                file = OpenWrite[filename]
                },
                Scan[
                        (
                        WriteString[file,First[#]];
                        Scan[
                                WriteString[file,"\t",#]&,
                                Rest[#]
                        ];
                        WriteString[file,"\n"]
                        )&,
                        data
                ];
                Close[file]
                ]
```

■ Intermediate Variables

System Characteristic Constant

```
bB0 = Abs[(hL1 hL2 eEL1/gG)^0.5];
```

Segment Length

```
l1 = 0.05;
```

Shear Strain

```
gGma = (2 eps0 bB0 Sinh[x/bB0]/Cosh[l1/(2 bB0)])/hL2;
```

Shear strain energy

```
shr = pPi gG1 gGma^2 hL2/eps0^2;
```

Strain energy distribution plot

```
Plot[shr,{x,-0.025,0.025},PloStyle ->{Thickness[0.01]},
        GridLines->Automatic,
        Frame->True,Axes -> None];
```

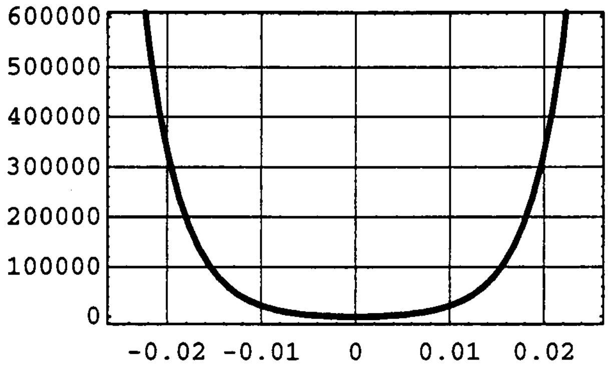


```
dDw =  2 Integrate[pPi gG1 gGma^2 hL2,{x,0,11/2}]/eps0^2
```

```
9184.44
```

Energy Lost

```
dDw =  2 Integrate[pPi gG1 gGma^2 hL2,{x,0,11/2}];
```

System Energy

```
w =  eps0^2 eEL1 hL1 11/2;
```

```
y[x]=(2 pPL0 /(eEL4 b hL4^3)) (x^3 - 3 lL x^2);
y1 = D[y[x],x];
iI = Integrate[y1^2,{x,lL-lL2,lL-lL1}];
iI1 = Integrate[y1^2,{x,0,lL}];
```

■ Loss Coefficient

```
ow = l1/bB0;
```

```
n = dDw/w;
```

■ Overall Loss Factor

```
nL = (3 n eEL1 hL1/(2 pPi eEL4 hL4)) iI/iI1;
```

APPENDIX IV

FINITE ELEMENT INTEGRATIONS

```
Off[General::spell1,General::spell]
Clear["Global`*"];
```

■ Finite element formulation

The following module defines the functions which are used in the calculation of the mass and stiffness matrix.
The following nomenclature is used.
nNj[z,i] = The shape functions for element i and layer j
tnj[z,i] = Transpose of the shape functions for element i and layer j.
' indicates the derivative of the function

```
l[i_]:=lL1;
cC[i_]:=1/4 List[c1,c2,c3,c4,c5,c6,c7,c8];
f1[z_]:= List[z,1,0,0,0,0,0,0];
f2[z_]:= List[0,0,z,1,0,0,0,0];
f3[z_]:= List[0,0,0,0,z^3,z^2,z,1];
f4[z_]:= List[0,0,0,0,3 z^2,2 z,1,0];
nN1[{z_,i_}]:=f1[z].cC[i];
tn1[{z_,i_}]:=Partition[nN1[{z,i}],1];
nN2[{z_,i_}]:=f2[z].cC[i];
tn2[{z_,i_}]:=Partition[nN2[{z,i}],1];
nN3[{z_,i_}]:=f3[z].cC[i];
tn3[{z_,i_}]:=Partition[nN3[{z,i}],1];
nN4[{z_,i_}]:=f4[z].cC[i];
n1'[{z_,i_}]:=D[nN1[{z,i}],z];
tn1'[{z_,i_}]:=Partition[n1'[{z,i}],1];
n2'[{z_,i_}]:=D[nN2[{z,i}],z];
tn2'[{z_,i_}]:=Partition[n2'[{z,i}],1];
n3'[{z_,i_}]:=D[nN3[{z,i}],z];
tn3'[{z_,i_}]:=Partition[n3'[{z,i}],1];
n3''[{z_,i_}]:=D[n3'[{z,i}],z];
tn3''[{z_,i_}]:=Partition[n3''[{z,i}],1];
nN5[{z_,i_}]:=1/2 (n1'[{z,i}]/(l[i]/2) + n2'[{z,i}]/(l[i]/2) +
                  (h1-h3-h4) n3''[{z,i}]/((l[i]/2)^2));
tn5[{z_,i_}]:=Partition[nN5[{z,i}],1];
nN6[{z_,i_}]:=(1/h2) (n1'[{z,i}]/(l[i]/2) - n2'[{z,i}]/(l[i]/2) +
                  ((h1+h3+h4)/2) n3''[{z,i}]/((l[i]/2)^2));
tn6[{z_,i_}]:=Partition[nN6[{z,i}],1];
nN7[{z_,i_}]:=(nN1[{z,i}] - nN2[{z,i}] + d n3'[{z,i}]/(l[i]/2));
tn7[{z_,i_}]:=Partition[nN7[{z,i}],1];
nN8[{z_,i_}]:=(nN1[{z,i}] + nN2[{z,i}] +
                  (h1-h3-h4) n3'[{z,i}]/(l[i]/2))/2;
tn8[{z_,i_}]:=Partition[nN8[{z,i}],1];
```

The following module calculates the cC[i] matrix for each element (Inverse of the coefficient coupling matrix).

```
c1=List[-2,0,0,0,2,0,0,0];
c2=List[2,0,0,0,2,0,0,0];
c3=List[0,-2,0,0,0,2,0,0];
c4=List[0,2,0,0,0,2,0,0];
c5=List[0,0,1,l[i]/2,0,0,-1,l[i]/2];
c6=List[0,0,0,-l[i]/2,0,0,0,l[i]/2];
c7=List[0,0,-3,-l[i]/2,0,0,3,-l[i]/2];
c8=List[0,0,2,l[i]/2,0,0,2,-l[i]/2];
cC[i]=1/4 List[c1,c2,c3,c4,c5,c6,c7,c8];
```

The following module calculates the mass and stiffness multiplier matrices for each element.
Multiplier matrices indicate the terms in the integral of the various stiffness and mass matrices
ki = the stiffness multiplier matrices
mi = the mass multiplier matrices

```
k1=Integrate[(tn1'[{z,i}].{n1'[{z,i}]}),{z,-1,1}]
```

$$\left\{\left\{\frac{1}{2}, 0, 0, 0, -\left(\frac{1}{2}\right), 0, 0, 0\right\}, \{0, 0, 0, 0, 0, 0, 0, 0\}, \{0, 0, 0, 0, 0, 0, 0, 0\}, \{0, 0, 0, 0, 0, 0, 0, 0\}, \left\{-\left(\frac{1}{2}\right), 0, 0, 0, \frac{1}{2}, 0, 0, 0\right\}, \{0, 0, 0, 0, 0, 0, 0, 0\}, \{0, 0, 0, 0, 0, 0, 0, 0\}, \{0, 0, 0, 0, 0, 0, 0, 0\}\right\}$$

```
k2=Integrate[(tn3''[{z,i}].{n3''[{z,i}]}),{z,-1,1}]
```

$$\left\{\{0, 0, 0, 0, 0, 0, 0, 0\}, \{0, 0, 0, 0, 0, 0, 0, 0\}, \left\{0, 0, \frac{3}{2}, \frac{3\,lL1}{4}, 0, 0, -\left(\frac{3}{2}\right), \frac{3\,lL1}{4}\right\}, \left\{0, 0, \frac{3\,lL1}{4}, \frac{lL1^2}{2}, 0, 0, \frac{-3\,lL1}{4}, \frac{lL1^2}{4}\right\}, \{0, 0, 0, 0, 0, 0, 0, 0\}, \{0, 0, 0, 0, 0, 0, 0, 0\}, \left\{0, 0, -\left(\frac{3}{2}\right), \frac{-3\,lL1}{4}, 0, 0, \frac{3}{2}, \frac{-3\,lL1}{4}\right\}, \left\{0, 0, \frac{3\,lL1}{4}, \frac{lL1^2}{4}, 0, 0, \frac{-3\,lL1}{4}, \frac{lL1^2}{2}\right\}\right\}$$

```
k3=Integrate[(tn5[{z,i}].{nN5[{z,i}]}),{z,-1,1}]
```

$$\left\{\left\{\frac{1}{2\,lL1^2}, \frac{1}{2\,lL1^2}, 0, \frac{h1 - h3 - h4}{2\,lL1^2}, \frac{-1}{2\,lL1^2}, \frac{-1}{2\,lL1^2}, 0, \frac{-h1 + h3 + h4}{2\,lL1^2}\right\},\right.$$

$$\left\{\frac{1}{2\,lL1^2}, \frac{1}{2\,lL1^2}, 0, \frac{h1 - h3 - h4}{2\,lL1^2}, \frac{-1}{2\,lL1^2}, \frac{-1}{2\,lL1^2}, 0, \frac{-h1 + h3 + h4}{2\,lL1^2}\right\},$$

$$\left\{0, 0, \frac{6\,(-h1 + h3 + h4)^2}{lL1^4}, \frac{3\,(-h1 + h3 + h4)^2}{lL1^3}, 0, 0, \frac{-6\,(-h1 + h3 + h4)^2}{lL1^4}, \frac{3\,(-h1 + h3 + h4)^2}{lL1^3}\right\},$$

$$\left\{\frac{h1 - h3 - h4}{2\,lL1^2}, \frac{h1 - h3 - h4}{2\,lL1^2}, \frac{3\,(-h1 + h3 + h4)^2}{lL1^3}, \frac{2\,(-h1 + h3 + h4)^2}{lL1^2}, \frac{-h1 + h3 + h4}{2\,lL1^2}, \frac{-h1 + h3 + h4}{2\,lL1^2}, \frac{-3\,(-h1 + h3 + h4)^2}{lL1^3}, \frac{(-h1 + h3 + h4)^2}{lL1^2}\right\},$$

$$\left\{\frac{-1}{2\,lL1^2}, \frac{-1}{2\,lL1^2}, 0, \frac{-h1 + h3 + h4}{2\,lL1^2}, \frac{1}{2\,lL1^2}, \frac{1}{2\,lL1^2}, 0, \frac{h1 - h3 - h4}{2\,lL1^2}\right\},$$

$$\left\{\frac{-1}{2\,lL1^2}, \frac{-1}{2\,lL1^2}, 0, \frac{-h1 + h3 + h4}{2\,lL1^2}, \frac{1}{2\,lL1^2}, \frac{1}{2\,lL1^2}, 0, \frac{h1 - h3 - h4}{2\,lL1^2}\right\},$$

$$\left\{0, 0, \frac{-6\,(-h1 + h3 + h4)^2}{lL1^4}, \frac{-3\,(-h1 + h3 + h4)^2}{lL1^3}, 0, 0, \frac{6\,(-h1 + h3 + h4)^2}{lL1^4}, \frac{-3\,(-h1 + h3 + h4)^2}{lL1^3}\right\},$$

$$\left.\left\{\frac{-h1 + h3 + h4}{2\,lL1^2}, \frac{-h1 + h3 + h4}{2\,lL1^2}, \frac{3\,(-h1 + h3 + h4)^2}{lL1^3}, \frac{(-h1 + h3 + h4)^2}{lL1^2}, \frac{h1 - h3 - h4}{2\,lL1^2}, \frac{h1 - h3 - h4}{2\,lL1^2}, \frac{-3\,(-h1 + h3 + h4)^2}{lL1^3}, \frac{2\,(-h1 + h3 + h4)^2}{lL1^2}\right\}\right\}$$

```
k4=Integrate[(tn6[{z,i}].{nN6[{z,i}]}),{z,-1,1}]
```

$$\left\{\left\{\frac{2}{h2^2\,lL1^2}, \frac{-2}{h2^2\,lL1^2}, 0, \frac{h1+h3+h4}{h2^2\,lL1^2}, \frac{-2}{h2^2\,lL1^2}, \frac{2}{h2^2\,lL1^2}, 0, -\left(\frac{h1+h3+h4}{h2^2\,lL1^2}\right)\right\},\right.$$

$$\left\{\frac{-2}{h2^2\,lL1^2}, \frac{2}{h2^2\,lL1^2}, 0, -\left(\frac{h1+h3+h4}{h2^2\,lL1^2}\right), \frac{2}{h2^2\,lL1^2}, \frac{-2}{h2^2\,lL1^2}, 0, \frac{h1+h3+h4}{h2^2\,lL1^2}\right\},$$

$$\left\{0, 0, \frac{6\,(h1+h3+h4)^2}{h2^2\,lL1^4}, \frac{3\,(h1+h3+h4)^2}{h2^2\,lL1^3}, 0, 0, \frac{-6\,(h1+h3+h4)^2}{h2^2\,lL1^4}, \frac{3\,(h1+h3+h4)^2}{h2^2\,lL1^3}\right\},$$

$$\left\{\frac{h1+h3+h4}{h2^2\,lL1^2}, -\left(\frac{h1+h3+h4}{h2^2\,lL1^2}\right), \frac{3\,(h1+h3+h4)^2}{h2^2\,lL1^3}, \frac{2\,(h1+h3+h4)^2}{h2^2\,lL1^2}, -\left(\frac{h1+h3+h4}{h2^2\,lL1^2}\right),\right.$$

$$\left.\frac{h1+h3+h4}{h2^2\,lL1^2}, \frac{-3\,(h1+h3+h4)^2}{h2^2\,lL1^3}, \frac{(h1+h3+h4)^2}{h2^2\,lL1^2}\right\},$$

$$\left\{\frac{-2}{h2^2\,lL1^2}, \frac{2}{h2^2\,lL1^2}, 0, -\left(\frac{h1+h3+h4}{h2^2\,lL1^2}\right), \frac{2}{h2^2\,lL1^2}, \frac{-2}{h2^2\,lL1^2}, 0, \frac{h1+h3+h4}{h2^2\,lL1^2}\right\},$$

$$\left\{\frac{2}{h2^2\,lL1^2}, \frac{-2}{h2^2\,lL1^2}, 0, \frac{h1+h3+h4}{h2^2\,lL1^2}, \frac{-2}{h2^2\,lL1^2}, \frac{2}{h2^2\,lL1^2}, 0, -\left(\frac{h1+h3+h4}{h2^2\,lL1^2}\right)\right\},$$

$$\left\{0, 0, \frac{-6\,(h1+h3+h4)^2}{h2^2\,lL1^4}, \frac{-3\,(h1+h3+h4)^2}{h2^2\,lL1^3}, 0, 0, \frac{6\,(h1+h3+h4)^2}{h2^2\,lL1^4}, \frac{-3\,(h1+h3+h4)^2}{h2^2\,lL1^3}\right\},$$

$$\left\{-\left(\frac{h1+h3+h4}{h2^2\,lL1^2}\right), \frac{h1+h3+h4}{h2^2\,lL1^2}, \frac{3\,(h1+h3+h4)^2}{h2^2\,lL1^3}, \frac{(h1+h3+h4)^2}{h2^2\,lL1^2}, \frac{h1+h3+h4}{h2^2\,lL1^2}, -\left(\frac{h1+h3+h4}{h2^2\,lL1^2}\right),\right.$$

$$\left.\left.\frac{-3\,(h1+h3+h4)^2}{h2^2\,lL1^3}, \frac{2\,(h1+h3+h4)^2}{h2^2\,lL1^2}\right\}\right\}$$

```
k5=Integrate[(tn7[{z,i}].{nN7[{z,i}]}),{z,-1,1}]
```

$$\left\{\left\{\frac{2}{3}, -\left(\frac{2}{3}\right), -\left(\frac{d}{lL1}\right), \frac{d}{6}, \frac{1}{3}, -\left(\frac{1}{3}\right), \frac{d}{lL1}, \frac{-d}{6}\right\}, \left\{-\left(\frac{2}{3}\right), \frac{2}{3}, \frac{d}{lL1}, \frac{-d}{6}, -\left(\frac{1}{3}\right), \frac{1}{3}, -\left(\frac{d}{lL1}\right), \frac{d}{6}\right\},\right.$$

$$\left\{-\left(\frac{d}{lL1}\right), \frac{d}{lL1}, \frac{12\,d^2}{5\,lL1^2}, \frac{d^2}{5\,lL1}, -\left(\frac{d}{lL1}\right), \frac{d}{lL1}, \frac{-12\,d^2}{5\,lL1^2}, \frac{d^2}{5\,lL1}\right\}, \left\{\frac{d}{6}, \frac{-d}{6}, \frac{d^2}{5\,lL1}, \frac{4\,d^2}{15}, \frac{-d}{6}, \frac{d}{6}, \frac{-d^2}{5\,lL1}, \frac{-d^2}{15}\right\},$$

$$\left\{\frac{1}{3}, -\left(\frac{1}{3}\right), -\left(\frac{d}{lL1}\right), \frac{-d}{6}, \frac{2}{3}, -\left(\frac{2}{3}\right), \frac{d}{lL1}, \frac{d}{6}\right\}, \left\{-\left(\frac{1}{3}\right), \frac{1}{3}, \frac{d}{lL1}, \frac{d}{6}, -\left(\frac{2}{3}\right), \frac{2}{3}, -\left(\frac{d}{lL1}\right), \frac{-d}{6}\right\},$$

$$\left.\left\{\frac{d}{lL1}, -\left(\frac{d}{lL1}\right), \frac{-12\,d^2}{5\,lL1^2}, \frac{-d^2}{5\,lL1}, \frac{d}{lL1}, -\left(\frac{d}{lL1}\right), \frac{12\,d^2}{5\,lL1^2}, \frac{-d^2}{5\,lL1}\right\}, \left\{\frac{-d}{6}, \frac{d}{6}, \frac{d^2}{5\,lL1}, \frac{-d^2}{15}, \frac{d}{6}, \frac{-d}{6}, \frac{-d^2}{5\,lL1}, \frac{4\,d^2}{15}\right\}\right\}$$

```
k6=Integrate[(tn2'[{z,i}].{n2'[{z,i}]}),{z,-1,1}]
```

$$\left\{\{0, 0, 0, 0, 0, 0, 0, 0\}, \left\{0, \frac{1}{2}, 0, 0, 0, -\left(\frac{1}{2}\right), 0, 0\right\}, \{0, 0, 0, 0, 0, 0, 0, 0\},\right.$$

$$\{0, 0, 0, 0, 0, 0, 0, 0\}, \{0, 0, 0, 0, 0, 0, 0, 0\}, \left\{0, -\left(\frac{1}{2}\right), 0, 0, 0, \frac{1}{2}, 0, 0\right\},$$

$$\left.\{0, 0, 0, 0, 0, 0, 0, 0\}, \{0, 0, 0, 0, 0, 0, 0, 0\}\right\}$$

k7=Integrate[(tn3''[{z,i}].{n3''[{z,i}]}),{z,-1,1}]

$$\{\{0, 0, 0, 0, 0, 0, 0, 0\}, \{0, 0, 0, 0, 0, 0, 0, 0\}, \{0, 0, \frac{3}{2}, \frac{3\ lL1}{4}, 0, 0, -(\frac{3}{2}), \frac{3\ lL1}{4}\},$$

$$\{0, 0, \frac{3\ lL1}{4}, \frac{lL1^{2}}{2}, 0, 0, \frac{-3\ lL1}{4}, \frac{lL1^{2}}{4}\}, \{0, 0, 0, 0, 0, 0, 0, 0\}, \{0, 0, 0, 0, 0, 0, 0, 0\},$$

$$\{0, 0, -(\frac{3}{2}), \frac{-3\ lL1}{4}, 0, 0, \frac{3}{2}, \frac{-3\ lL1}{4}\}, \{0, 0, \frac{3\ lL1}{4}, \frac{lL1^{2}}{4}, 0, 0, \frac{-3\ lL1}{4}, \frac{lL1^{2}}{2}\}\}$$

m1=Integrate[(tn3[{z,i}].{nN3[{z,i}]} +
tn1[{z,i}].{nN1[{z,i}]}),{z,-1,1}]

$$\{\{\frac{2}{3}, 0, 0, 0, \frac{1}{3}, 0, 0, 0\}, \{0, 0, 0, 0, 0, 0, 0, 0\}, \{0, 0, \frac{26}{35}, \frac{11\ lL1}{105}, 0, 0, \frac{9}{35}, \frac{-13\ lL1}{210}\},$$

$$\{0, 0, \frac{11\ lL1}{105}, \frac{2\ lL1^{2}}{105}, 0, 0, \frac{13\ lL1}{210}, \frac{-lL1^{2}}{70}\}, \{\frac{1}{3}, 0, 0, 0, \frac{2}{3}, 0, 0, 0\}, \{0, 0, 0, 0, 0, 0, 0, 0\},$$

$$\{0, 0, \frac{9}{35}, \frac{13\ lL1}{210}, 0, 0, \frac{26}{35}, \frac{-11\ lL1}{105}\}, \{0, 0, \frac{-13\ lL1}{210}, \frac{-lL1^{2}}{70}, 0, 0, \frac{-11\ lL1}{105}, \frac{2\ lL1^{2}}{105}\}\}$$

```
a=(tn3[{z,i}].{nN3[{z,i}]} +
              tn8[{z,i}].{nN8[{z,i}]});
m2=Integrate[a,{z,-1,1}];
Simplify[m2]
```

$$\{\{\frac{1}{6}, \frac{1}{6}, \frac{-h1 + h3 + h4}{4\ lL1}, \frac{h1 - h3 - h4}{24}, \frac{1}{12}, \frac{1}{12}, \frac{h1 - h3 - h4}{4\ lL1}, \frac{-h1 + h3 + h4}{24}\},$$

$$\{\frac{1}{6}, \frac{1}{6}, \frac{-h1 + h3 + h4}{4\ lL1}, \frac{h1 - h3 - h4}{24}, \frac{1}{12}, \frac{1}{12}, \frac{h1 - h3 - h4}{4\ lL1}, \frac{-h1 + h3 + h4}{24}\},$$

$$\{\frac{-h1 + h3 + h4}{4\ lL1}, \frac{-h1 + h3 + h4}{4\ lL1}, \frac{21\ h1^2 - 42\ h1\ h3 + 21\ h3^2 - 42\ h1\ h4 + 42\ h3\ h4 + 21\ h4^2 + 26\ lL1^2}{35\ lL1^2},$$

$$\frac{21\ h1^2 - 42\ h1\ h3 + 21\ h3^2 - 42\ h1\ h4 + 42\ h3\ h4 + 21\ h4^2 + 44\ lL1^2}{420\ lL1}, \frac{-h1 + h3 + h4}{4\ lL1}, \frac{-h1 + h3 + h4}{4\ lL1},$$

$$\frac{3\ (-7\ h1^2 + 14\ h1\ h3 - 7\ h3^2 + 14\ h1\ h4 - 14\ h3\ h4 - 7\ h4^2 + 3\ lL1^2)}{35\ lL1^2},$$

$$\frac{21\ h1^2 - 42\ h1\ h3 + 21\ h3^2 - 42\ h1\ h4 + 42\ h3\ h4 + 21\ h4^2 - 26\ lL1^2}{420\ lL1}\},$$

$$\{\frac{h1 - h3 - h4}{24}, \frac{h1 - h3 - h4}{24}, \frac{21\ h1^2 - 42\ h1\ h3 + 21\ h3^2 - 42\ h1\ h4 + 42\ h3\ h4 + 21\ h4^2 + 44\ lL1^2}{420\ lL1},$$

$$\frac{7\ h1^2 - 14\ h1\ h3 + 7\ h3^2 - 14\ h1\ h4 + 14\ h3\ h4 + 7\ h4^2 + 2\ lL1^2}{105}, \frac{-h1 + h3 + h4}{24}, \frac{-h1 + h3 + h4}{24},$$

$$\frac{-21\ h1^2 + 42\ h1\ h3 - 21\ h3^2 + 42\ h1\ h4 - 42\ h3\ h4 - 21\ h4^2 + 26\ lL1^2}{420\ lL1},$$

$$\frac{-7\ h1^2 + 14\ h1\ h3 - 7\ h3^2 + 14\ h1\ h4 - 14\ h3\ h4 - 7\ h4^2 - 6\ lL1^2}{420}\},$$

$$\{\frac{1}{12}, \frac{1}{12}, \frac{-h1 + h3 + h4}{4\ lL1}, \frac{-h1 + h3 + h4}{24}, \frac{1}{6}, \frac{1}{6}, \frac{h1 - h3 - h4}{4\ lL1}, \frac{h1 - h3 - h4}{24}\},$$

$$\{\frac{1}{12}, \frac{1}{12}, \frac{-h1 + h3 + h4}{4\ lL1}, \frac{-h1 + h3 + h4}{24}, \frac{1}{6}, \frac{1}{6}, \frac{h1 - h3 - h4}{4\ lL1}, \frac{h1 - h3 - h4}{24}\},$$

$$\{\frac{h1 - h3 - h4}{4\ lL1}, \frac{h1 - h3 - h4}{4\ lL1}, \frac{3\ (-7\ h1^2 + 14\ h1\ h3 - 7\ h3^2 + 14\ h1\ h4 - 14\ h3\ h4 - 7\ h4^2 + 3\ lL1^2)}{35\ lL1^2},$$

$$\frac{-21\ h1^2 + 42\ h1\ h3 - 21\ h3^2 + 42\ h1\ h4 - 42\ h3\ h4 - 21\ h4^2 + 26\ lL1^2}{420\ lL1}, \frac{h1 - h3 - h4}{4\ lL1}, \frac{h1 - h3 - h4}{4\ lL1},$$

$$\frac{21\ h1^2 - 42\ h1\ h3 + 21\ h3^2 - 42\ h1\ h4 + 42\ h3\ h4 + 21\ h4^2 + 26\ lL1^2}{35\ lL1^2},$$

$$\frac{-21\ h1^2 + 42\ h1\ h3 - 21\ h3^2 + 42\ h1\ h4 - 42\ h3\ h4 - 21\ h4^2 - 44\ lL1^2}{420\ lL1}\},$$

$$\{\frac{-h1 + h3 + h4}{24}, \frac{-h1 + h3 + h4}{24}, \frac{21\ h1^2 - 42\ h1\ h3 + 21\ h3^2 - 42\ h1\ h4 + 42\ h3\ h4 + 21\ h4^2 - 26\ lL1^2}{420\ lL1},$$

$$\frac{-7\ h1^2 + 14\ h1\ h3 - 7\ h3^2 + 14\ h1\ h4 - 14\ h3\ h4 - 7\ h4^2 - 6\ lL1^2}{420}, \frac{h1 - h3 - h4}{24}, \frac{h1 - h3 - h4}{24},$$

$$\frac{-21\ h1^2 + 42\ h1\ h3 - 21\ h3^2 + 42\ h1\ h4 - 42\ h3\ h4 - 21\ h4^2 - 44\ lL1^2}{420\ lL1},$$

$$\frac{7\,h1^{2} - 14\,h1\,h3 + 7\,h3^{2} - 14\,h1\,h4 + 14\,h3\,h4 + 7\,h4^{2} + 2\,lL1^{2}}{105}\}\}$$

```
m3=Integrate[(tn3[{z,i}].{nN3[{z,i}]} +
              tn2[{z,i}].{nN2[{z,i}]}),{z,-1,1}]
```

$$\{\{0,\ 0,\ 0,\ 0,\ 0,\ 0,\ 0,\ 0\},\ \{0,\ \frac{2}{3},\ 0,\ 0,\ 0,\ \frac{1}{3},\ 0,\ 0\},\ \{0,\ 0,\ \frac{26}{35},\ \frac{11\ lL1}{105},\ 0,\ 0,\ \frac{9}{35},\ \frac{-13\ lL1}{210}\},$$

$$\{0,\ 0,\ \frac{11\ lL1}{105},\ \frac{2\ lL1^{2}}{105},\ 0,\ 0,\ \frac{13\ lL1}{210},\ \frac{-lL1^{2}}{70}\},\ \{0,\ 0,\ 0,\ 0,\ 0,\ 0,\ 0,\ 0\},\ \{0,\ \frac{1}{3},\ 0,\ 0,\ 0,\ \frac{2}{3},\ 0,\ 0\},$$

$$\{0,\ 0,\ \frac{9}{35},\ \frac{13\ lL1}{210},\ 0,\ 0,\ \frac{26}{35},\ \frac{-11\ lL1}{105}\},\ \{0,\ 0,\ \frac{-13\ lL1}{210},\ \frac{-lL1^{2}}{70},\ 0,\ 0,\ \frac{-11\ lL1}{105},\ \frac{2\ lL1^{2}}{105}\}\}$$

APPENDIX V

ENERGIES ASSOCIATED WITH THE VISCOELASTIC LAYER

A] Strain energy in the viscoelastic layer

a) Energy due to extension of the viscoelastic layer

$$U_3 = \frac{1}{2}\int EA\left(\frac{\partial \bar{u}_2}{\partial x}\right)\left(\frac{\partial u_2}{\partial x}\right)dx$$

Now $u_2 = \frac{1}{2}\left[(u_1 + u_3) + (h_1 - h_3 - h_4)\frac{\partial w}{\partial x}\right]$

$$\therefore \frac{\partial u_2}{\partial x} = \frac{1}{2}\left[\left(\frac{\partial u_1}{\partial x} + \frac{\partial u_3}{\partial x}\right) + (h_1 - h_3 - h_4)\frac{\partial^2 w}{\partial x^2}\right]$$

$$\frac{\partial u_1}{\partial x} = \frac{[N'_1(\xi)]}{(L_i/2)}\{\Delta_i\},\quad \frac{\partial u_3}{\partial x} = \frac{[N'_{21}(\xi)]}{(L_i/2)}\{\Delta_i\}$$

and $\frac{\partial^2 w}{\partial x^2} = \frac{[N''_3(\xi)]}{(L_i/2)^2}\{\Delta_i\}$

$$\therefore \frac{\partial u_2}{\partial x} = \underbrace{\frac{1}{2}\left[\left(\frac{[N'_1(\xi)]}{(L_i/2)} + \frac{[N'_2(\xi)]}{(L_i/2)}\right) + (h_1 - h_3 - h_4)\frac{[N''_3(\xi)]}{(L_i/2)^2}\right]}_{[N_5(\xi)]}\{\Delta_i\}$$

which gives $U_3 = \frac{1}{2}EA\{\Delta_i\}^T\int_{-1}^{1}[N_5(\xi)]^T[N_5(\xi)](L_i/2)d\xi\{\Delta_i\}$

b) Strain energy due to bending strain in the viscoelastic layer

$$U_4 = \frac{1}{2}\int EI\left(\frac{\partial^2 \overline{w}}{\partial x^2}\right)\left(\frac{\partial^2 w}{\partial x^2}\right)dx$$

Now $$\frac{\partial w}{\partial x} = \frac{1}{h_2}\left[(u_1 - u_3) + \left(\frac{h_1 + h_3 + h_4}{2}\right)\frac{\partial w}{\partial x}\right]$$

$$\frac{\partial^2 w}{\partial x^2} = \frac{1}{h_2}\left[\left(\frac{\partial u_1}{\partial x} - \frac{\partial u_3}{\partial x}\right) + \left(\frac{h_1 + h_3 + h_4}{2}\right)\frac{\partial^2 w}{\partial x^2}\right]$$

$$\therefore \frac{\partial^2 w}{\partial x^2} = \underbrace{\frac{1}{h_2}\left[\left(\frac{[N'_1(\xi)]}{(L_i/2)} - \frac{[N'_2(\xi)]}{(L_i/2)}\right) + \left(\frac{h_1 + h_3 + h_4}{2}\right)\frac{[N''_3(\xi)]}{(L_i/2)^2}\right]}_{[N_6(\xi)]}\{\Delta_i\}$$

which gives $$U_4 = \frac{1}{2}EI\{\Delta_i\}^T \int_{-1}^{1} [N_6(\xi)]^T [N_6(\xi)](L_i/2)d\xi\{\Delta_i\}$$

c) Strain energy due to shear in the viscoelastic layer

$$U_5 = \frac{1}{2}\int GA(\overline{\gamma})(\gamma)dx$$

Now $$\gamma = \frac{d}{h_2}\left(\frac{\partial w}{\partial x}\right) + \frac{(u_1 - u_3)}{h_2}$$

$$\therefore \gamma = \underbrace{\frac{1}{h_2}\left[([N_1(\xi)] - [N_2(\xi)]) + d\frac{[N'_3(\xi)]}{(L_i/2)}\right]}_{[N_7(\xi)]}\{\Delta_i\}$$

which gives $$U_5 = \frac{1}{2}GA\{\Delta_i\}^T \int_{-1}^{1} [N_7(\xi)]^T [N_7(\xi)](L_i/2)d\xi\{\Delta_i\}$$

B] Kinetic energy in the viscoelastic layer

$$T_2 = \frac{1}{2}\rho A \int \left(\dot{\overline{w}}\dot{w} + \dot{\overline{u}}\dot{u} \right) dx$$

$$u_2 = \frac{1}{2}\left[(u_1 + u_3) + (h_1 - h_3 - h_4)\frac{\partial w}{\partial x} \right]$$

$$\therefore \dot{u}_2 = \underbrace{\frac{1}{2}\left[\left([N_1(\xi)] + [N_2(\xi)] \right) + (h_1 - h_3 - h_4)\frac{[N'_3(\xi)]}{(L_i/2)} \right]}_{[N_8(\xi)]} \{\dot{\Delta}_i\}$$

$$T_2 = \frac{1}{2}\rho A \{\dot{\Delta}_i\}^T \int_{-1}^{1} \left([N_3(\xi)]^T [N_3(\xi)] + [N_8(\xi)]^T [N_8(\xi)] \right) (L_i/2) d\xi \{\dot{\Delta}_i\}$$

APPENDIX VI

FINITE ELEMENT PROGRAM LISTING

```
%%%%%%%%%%%%%%%%PROGRAM BAZFEM.M FILE-MAIN PROGRAM%%%%%%%%%%%%%%%%%%%%%%%%
%%%%%%%%%%%%%%%%%%%%%%%%%%%%%%%%%%%%%%%%%%%%%%%%%%%%%%%%%%%%%%%%%%%%%%%%%
%       THE PROGRAM FOR THE FINITE ELEMENT FORMULATION FOR PREDICTING     %
%       THE PERFORMANCE OF ACTIVE CONSTRAINED LAYER DAMPING TREATMENT     %
%       APPLIED TO SLENDER BEAMS TO IMPROVE DAMPING CHARACTERISTICS       %
%       OF THE BEAM.                                                      %
%%%%%%%%%%%%%%%%%%%%%%%%%%%%%%%%%%%%%%%%%%%%%%%%%%%%%%%%%%%%%%%%%%%%%%%%%
%
%
% INPUT THE NUMBER OF ELEMENTS OF SECTION 1, UNTREATED PORTION OF THE
% BEAM TOWARDS THE FIXED END.
%
fprintf('Input the number of elements of untreated portion of')
fprintf('beam towards the fixed end desired')
X = input('X =');
%
%
% INPUT THE NUMBER OF SEGMENTS OF ACTIVE LAYER OF THE TREATED PORTION
% OF THE BEAM.
%
fprintf('Input the number of segments of active layer of the treatment')
N = input('N =');
GAP = 0.00254;          %Gap between the active layer segments(m)
%
%
% INPUT THE NUMBER OF ELEMENTS OF TREATED PORTION OF THE
% BEAM AT THE CENTER.
%
fprintf('Input the number of elements of treated portion of each')
fprintf('segment of the active layer of beam desired')
Y = input('Y =');
%
% INTERMEDIATE PARAMETER
RATIO = Y/N;
%
% INPUT THE NUMBER OF ELEMENTS OF SECTION 3, UNTREATED PORTION OF THE
% BEAM TOWARDS THE FREE END.
%
fprintf('Input the number of elements of untreated portion of')
fprintf('beam towards the free end desired')
Z = input('Z =');
%
%%%%%%%%%%%%%%%%%%%%%%%%%%%%%%%%%%%%%%%%%%%%%%%%%%%%%%%%%%%%%%%%%%%%%
%       DEFINITION OF MATERIAL GEOMETRIC PARAMETERS AND PROPERTIES    %
%%%%%%%%%%%%%%%%%%%%%%%%%%%%%%%%%%%%%%%%%%%%%%%%%%%%%%%%%%%%%%%%%%%%%
HPAL1 = 0.000052;          %Thickness of the Piezoactuator(m)
HVEL2 = 0.000508;          %Thickness of the Viscoelastic Layer(m)
HPSL3 = 0.000052;          %Thickness of the Piezosensor(m)
HBML4 = 0.000965;          %Thickness of the Beam(m)
%

LFDU1 = 0.002540;          %Length of the untreated beam at fixed end(m)
LMDTX = 0.304800;          %Length of the treated portion of the beam(m)
LFEUN = 0.025400;          %Length of the untreated beam at free end(m)
%
BSAND = 0.025400;          %Width of the treated beam(m)
%
```

```
APAL1 = HPAL1*BSAND;        %Cross-Sectional Area of the Piezoactuator(MPa)
AVEL2 = HVEL2*BSAND;        %Cross-Sectional Area of the Viscoelastic Layer(MPa)
APSL3 = HPSL3*BSAND;        %Cross-Sectional Area of the Piezosensor(MPa)
ABML4 = HBML4*BSAND;        %Cross-Sectional Area of the Beam(MPa)
%
APSLS = LMDTX*BSAND;        %Surface Area of the Beam(MPa)
%
ROPA1 = 1800.00;            %Density of the Piezoactuator(kg/m^3)
ROVE2 = 1104.00;            %Density of the Viscoelastic Layer(kg/m^3)
ROPS3 = 1800.00;            %Density of the Piezosensor(kg/m^3)
ROBM4 = 2800.00;            %Density of the Beam(kg/m^3)
%
%%%%%%%%%%%%%%%%%%%%%%%%%%%%%%%%%%%%%%%%%%%%%%%%%%%%%%%%%%%%%%%%%%%%%%%%%
% Complex Shear Modulus of the Viscoelastic Core (Baz93)
OMNAF = 2*pi*6.5534;
GVESH = 142000.00*exp(0.494*log(OMNAF/(2*pi)))*(1.00+1.46*i);

EPAL1 = 2.25e9;             %Elastic Modulus of the Piezoactuator(MPa)
EVEL2 = 3*GVESH;            %Elastic Modulus of the Viscoelastic Layer(MPa)
EPSL3 = 2.25e9;             %Elastic Modulus of the Piezosensor(MPa)
EBML4 = 6.911e10;           %Elastic Modulus of the Beam(MPa)
%
%Second area Moment of Inertia of the Piezoactuator Layer(m^4)
IPAL1 = BSAND*HPAL1^3/12;
%Second area Moment of Inertia of the Viscoelastic Layer(m^4)
IVEL2 = BSAND*HVEL2^3/12;
%Second area Moment of Inertia of the Piezosensor Layer(m^4)
IPSL3 = BSAND*HPSL3^3/12;
%Second area Moment of Inertia of the Beam(m^4)
IBML4 = BSAND*HBML4^3/12;
%%%%%%%%%%%%%%%%%%%%%%%%%%%%%%%%%%%%%%%%%%%%%%%%%%%%%%%%%%%%%%%%%%%%%%%%%
% Distance between neutral axis of the beam sensor layer and the
% interface between the beam beam-sensor layer and the Viscoelastic
% Layer
%
DBMSI = (EPSL3*HPSL3^2 + 2*EBML4*HPSL3*HBML4 + EBML4*HBML4^2)/...
              (2*(EPSL3*HPSL3 + EBML4*HBML4));
%%%%%%%%%%%%%%%%%%%%%%%%%%%%%%%%%%%%%%%%%%%%%%%%%%%%%%%%%%%%%%%%%%%%%%%%%
% Distance between neutral axis of sandwiched beam and the interface
% between the Sensor and the Viscoelastic Layer
DNASI = HVEL2 + HPAL1/2 + DBMSI;
%%%%%%%%%%%%%%%%%%%%%%%%%%%%%%%%%%%%%%%%%%%%%%%%%%%%%%%%%%%%%%%%%%%%%%%%%
%                    PIEZO-CONTROL FORCES AND MOMENTS                   %
%%%%%%%%%%%%%%%%%%%%%%%%%%%%%%%%%%%%%%%%%%%%%%%%%%%%%%%%%%%%%%%%%%%%%%%%%
%
PIZD31 = 18.6*10^(-11);     %Piezoelectric strain constant
PIZK31 = 0.34;              %Electromechanical coupling factor
PIZG31 = 11.6*10^(-3);      %Piezoelectric voltage constant of sensor
PIZK3T = 1950.0;            %Dielectric constant
%
%%%%%%%%%%%%%%%%%%%%%%%%%%%%%%%%%%%%%%%%%%%%%%%%%%%%%%%%%%%%%%%%%%%%%%%%%
%Capacitance of the sensor
PIZCAP = 8.854*10^(-12)*APSLS*PIZK3T/HPSL3;
%%%%%%%%%%%%%%%%%%%%%%%%%%%%%%%%%%%%%%%%%%%%%%%%%%%%%%%%%%%%%%%%%%%%%%%%%
% Proportional and derivative gains for the control loop
CONKP = 0000.0;
CONKD = 0000.0;
%%%%%%%%%%%%%%%%%%%%%%%%%%%%%%%%%%%%%%%%%%%%%%%%%%%%%%%%%%%%%%%%%%%%%%%%%
% Force and Moment calculation (intermediate constant)
CFMGC = -EPAL1*(BSAND^2)*(PIZK31^2)*DNASI*PIZD31/(PIZG31*PIZCAP);
```

```
%%%%%%%%%%%%%%%%%%%%%%%%%%%%%%%%%%%%%%%%%%%%%%%%%%%%%%%%%%%%%%%%%%%%%%%%
%
% SUBROUTINE PROGRAM CALL FOR GETTING THE MASTER MATRIX FOR A UNTREATED
% BEAM WITH LENGTH "LEN"(LENGTH OF ONE ELEMENT OF SEGMENT 1 OF THE BEAM)
LEN = LFDU1/X;
[MEQU1,KEQU1] = km_mat1(LEN,ABML4,ROBM4,IBML4,EBML4,HPAL1,...
                        HVEL2,HPSL3,HBML4,DNASI,CFMGC);
%
%%%%%%%%%%%%%%%%%%%%%%%%%%%%%%%%%%%%%%%%%%%%%%%%%%%%%%%%%%%%%%%%%%%%%%%%
% SUBROUTINE PROGRAM CALL FOR GETTING THE MASTER MATRIX FOR A TREATED
% BEAM WITH LENGTH "LEN"(LENGTH OF ONE ELEMENT OF SEGMENT 2 SANDWICHED
% PORTION OF THE BEAM)
%
LEN = (LMDTX-((N-1)*GAP))/Y;
[MEQU2,CEQU2,KEQU2] = km_mat2(LEN,...
             APAL1,AVEL2,APSL3,ABML4,ROPA1,ROVE2,ROPS3,ROBM4,...
             IPAL1,IVEL2,IPSL3,IBML4,EPAL1,EVEL2,EPSL3,EBML4,...
             HPAL1,HVEL2,HPSL3,HBML4,DNASI,GVESH,CFMGC,CONKP,CONKD);
%
%%%%%%%%%%%%%%%%%%%%%%%%%%%%%%%%%%%%%%%%%%%%%%%%%%%%%%%%%%%%%%%%%%%%%%%%
% SUBROUTINE PROGRAM CALL FOR GETTING THE MASTER MATRIX FOR A TREATED
% BEAM(WITH PIEZO-SENSOR LAYER AND VISCOELASTIC LAYER) WITH LENGTH "LEN"
% (LENGTH OF ONE GAP ELEMENT OF THE BEAM)
%
LEN = GAP;
[MEQUP,KEQUP] = km_mat3(LEN,...
                AVEL2,APSL3,ABML4,ROVE2,ROPS3,ROBM4,...
                IVEL2,IPSL3,IBML4,EVEL2,EPSL3,EBML4,...
                HPAL1,HVEL2,HPSL3,HBML4,DNASI,GVESH,CFMGC);
%
%%%%%%%%%%%%%%%%%%%%%%%%%%%%%%%%%%%%%%%%%%%%%%%%%%%%%%%%%%%%%%%%%%%%%%%%
% SUBROUTINE PROGRAM CALL FOR GETTING THE MASTER MATRIX FOR A UNTREATED
% BEAM WITH LENGTH "LEN"(LENGTH OF ONE ELEMENT OF SEGMENT 3 OF THE BEAM)
%
LEN = LFEUN/Z;
[MEQU3,KEQU3] = km_mat1(LEN,ABML4,ROBM4,IBML4,EBML4,HPAL1,...
                        HVEL2,HPSL3,HBML4,DNASI,CFMGC);
%%%%%%%%%%%%%%%%%%%%%%%%%%%%%%%%%%%%%%%%%%%%%%%%%%%%%%%%%%%%%%%%%%%%%%%%

%%%%%%%%%%%%%%%%%%%%%%%%%%%%%%%%%%%%%%%%%%%%%%%%%%%%%%%%%%%%%%%%%%%%%%%%
% MASS AND STIFFNESS EQUIVALENT MATRICES FOR THE UNTREATED PORTIONS OF
% THE BEAM REDUCED BY ELEMINATING THE ZERO ROWS AND COLUMNS PRESENT DUE
% TO THE ABSENCE OF THE CONSTRAINING LAYER
% "*EQU**R" = MATRIX WITH 1ST AND 5TH ROW AND COLUMN ELIMINATED
% "*EQU**P" = MATRIX WITH 1ST OR 5TH ROW AND COLUMN ELIMINATED
%
MEQU1R = [MEQU1(2:4,2:4),MEQU1(2:4,6:8);MEQU1(6:8,2:4),MEQU1(6:8,6:8)];
MEQU1P = [MEQU1(2:8,2:8)];
MEQU3R = [MEQU3(2:4,2:4),MEQU3(2:4,6:8);MEQU3(6:8,2:4),MEQU3(6:8,6:8)];
MEQU3P = [MEQU3(1:4,1:4),MEQU3(1:4,6:8);MEQU3(6:8,1:4),MEQU3(6:8,6:8)];
KEQU1R = [KEQU1(2:4,2:4),KEQU1(2:4,6:8);KEQU1(6:8,2:4),KEQU1(6:8,6:8)];
KEQU1P = [KEQU1(2:8,2:8)];
KEQU3R = [KEQU3(2:4,2:4),KEQU3(2:4,6:8);KEQU3(6:8,2:4),KEQU3(6:8,6:8)];
KEQU3P = [KEQU3(1:4,1:4),KEQU3(1:4,6:8);KEQU3(6:8,1:4),KEQU3(6:8,6:8)];
%%%%%%%%%%%%%%%%%%%%%%%%%%%%%%%%%%%%%%%%%%%%%%%%%%%%%%%%%%%%%%%%%%%%%%%%
%
% Maximum Matrix size after Assembly
%
M = 3*(X + Z) + 4*(Y + (N-1)) + 4;
IDEN = eye(M);
```

```
%
% GLOBAL EQUIVALENT MATRICES BEFORE ASSEMBLY FOR ALL THREE SEGMENTS
% K=STIFNESS MATRIX, M=MASS MATRIX, C=DAMPING MATRIX
GKEQU1 = zeros(M);
GMEQU1 = zeros(M);
GKEQU2 = zeros(M);
GCEQU2 = zeros(M);
GMEQU2 = zeros(M);
GKEQU3 = zeros(M);
GMEQU3 = zeros(M);
%
%%%%%%%%%%%%%%%%%%%%%%%%%%%%%%%%%%%%%%%%%%%%%%%%%%%%%%%%%%%%%%%%%%%%%%%
% ASSEMBLY PROCESS FOR THE UNTREATED PORTION OF THE BEAM (SEGMENT 1)
%
for I = 1:X
if X-I > 0
A = IDEN((3*I-2):(3*I+3),1:M);
GKEQU1 = A'*KEQU1R*A + GKEQU1;
GMEQU1 = A'*MEQU1R*A + GMEQU1;
else
A = IDEN((3*I-2):(3*I+4),1:M);
GKEQU1 = A'*KEQU1P*A + GKEQU1;
GMEQU1 = A'*MEQU1P*A + GMEQU1;
end
end
%%%%%%%%%%%%%%%%%%%%%%%%%%%%%%%%%%%%%%%%%%%%%%%%%%%%%%%%%%%%%%%%%%%%%%%

%%%%%%%%%%%%%%%%%%%%%%%%%%%%%%%%%%%%%%%%%%%%%%%%%%%%%%%%%%%%%%%%%%%%%%%
% ASSEMBLY PROCESS FOR THE TREATED PORTION OF THE BEAM (SEGMENT 2)
%
COUNT = 1;
for I = (X+1):(X+Y+N-1)
if I-X == (RATIO+1)*COUNT
COUNT = COUNT + 1;
A = IDEN((4*I-X-3):(4*I-X+4),1:M);
GKEQU2 = A'*KEQUP*A + GKEQU2;
GMEQU2 = A'*MEQUP*A + GMEQU2;
else
A = IDEN((4*I-X-3):(4*I-X+4),1:M);
GKEQU2 = A'*KEQU2*A + GKEQU2;
GCEQU2 = A'*CEQU2*A + GCEQU2;
GMEQU2 = A'*MEQU2*A + GMEQU2;
end
end
%%%%%%%%%%%%%%%%%%%%%%%%%%%%%%%%%%%%%%%%%%%%%%%%%%%%%%%%%%%%%%%%%%%%%%%
%%%%%%%%%%%%%%%%%%%%%%%%%%%%%%%%%%%%%%%%%%%%%%%%%%%%%%%%%%%%%%%%%%%%%%%
% ASSEMBLY PROCESS FOR THE UNTREATED PORTION OF THE BEAM (SEGMENT 3)
%
I = (X+Y+N);
A = IDEN((4*I-X-3):(4*I-X+3),1:M);
GKEQU3 = A'*KEQU3P*A + GKEQU3;
GMEQU3 = A'*MEQU3P*A + GMEQU3;
%
%%%%%%%%%%%%%%%%%%%%%%%%%%%%%%%%%%%%%%%%%%%%%%%%%%%%%%%%%%%%%%%%%%%%%%%
%
% ASSEMBLY OF THE STIFFNESS, DAMPING AND MASS MATRICES FOR THE ENTIRE
% BEAM (SEGMENT 1 + SEGMENT 2 + SEGMENT 3)
%
GKEQU = GKEQU1(5:M,5:M) + GKEQU2(5:M,5:M) + GKEQU3(5:M,5:M);
GCEQU = GCEQU2(5:M,5:M);
GMEQU = GMEQU1(5:M,5:M) + GMEQU2(5:M,5:M) + GMEQU3(5:M,5:M);
```

```
%%%%%%%%%%%%%%%%%%%%%%%%%%%%%%%%%%%%%%%%%%%%%%%%%%%%%%%%%%%%%%%%%%%%%%%%%%%
%
% EIGEN-VALUE AND NATURAL FREQUENCIES CALCULATION
% d = VECTOR OF THE NATURAL FREQUENCIES OF THE BEAM
%
IGMEQU = inv(GMEQU);
EIGMAT = (IGMEQU*GKEQU);
[Q,D] = eig(EIGMAT);
d=(D^0.5)/(2*pi);
NATURAL FREQUENCY IN Hz.
f=diag(d)
%%%%%%%%%%%%%%%%%%%%%%%%%%%%%%%%%%%%%%%%%%%%%%%%%%%%%%%%%%%%%%%%%%%%%%%%%%%
```

```
%%%%%%%%%%%%%%%%%%%SUBROUTINE PROGRAM KM_MAT1.M-FUNCTION FILE%%%%%%%%%%%%%%%%
%%%%%%%%%%%%%%%%%%%%%%%%%%%%%%%%%%%%%%%%%%%%%%%%%%%%%%%%%%%%%%%%%%%%%%%%%%%%%
%       ELEMENT MASS AND STIFFNESS MATRICES FOR UNTREATED BEAM             %
%%%%%%%%%%%%%%%%%%%%%%%%%%%%%%%%%%%%%%%%%%%%%%%%%%%%%%%%%%%%%%%%%%%%%%%%%%%%%
%
%
function [MEQU1,KEQU1] = km_mat1(LEN,ABML4,ROBM4,IBML4,EBML4,HPAL1,...
                                HVEL2,HPSL3,HBML4,DNASI,CFMGC);
%
%%%%%%%%%%%%%%%%%%%%%%%%%%%%%%%%%%%%%%%%%%%%%%%%%%%%%%%%%%%%%%%%%%%%%%%%%%%%%
% FUNCTION CALL TO GET MASTER MATRIX LIBRARY
%
[EXTNUL1,BENDUL1,EXTNUL2,BENDUL2,SHEARUL2,EXTNUL34,...
                BENDUL34,KESEG1,KESEG2,KESEG3,CONTFRC] = basisfn(LEN,...
                HPAL1,HVEL2,HPSL3,HBML4,DNASI,CFMGC);
%
%%%%%%%%%%%%%%%%%%%%%%%%%%%%%%%%%%%%%%%%%%%%%%%%%%%%%%%%%%%%%%%%%%%%%%%%%%%%%
% STIFNESS AND MASS MATRICES DEFINED
%
KEBML4 = 2*EBML4*ABML4*EXTNUL34/LEN;
KBBML4 = 8*EBML4*IBML4*BENDUL34/(LEN^3);
MBML4 = ROBM4*ABML4*KESEG3*LEN/2;
%
%%%%%%%%%%%%%%%%%%%%%%%%%%%%%%%%%%%%%%%%%%%%%%%%%%%%%%%%%%%%%%%%%%%%%%%%%%%%%
% EQUAVIVALENT STIFFNESS AND MASS MATRICES FOR SEGMENT 1 OR SEGMENT 3
%
KEQU1 = KEBML4 + KBBML4;
MEQU1 = MBML4;
%%%%%%%%%%%%%%%%%%%%%%%%%%%%%%%%%%%%%%%%%%%%%%%%%%%%%%%%%%%%%%%%%%%%%%%%%%%%%
```

```
%%%%%%%%%%%%%%SUBROUTINE PROGRAM KM_MAT2.M-FUNCTION FILE%%%%%%%%%%%%%%%%%%%%%
%%%%%%%%%%%%%%%%%%%%%%%%%%%%%%%%%%%%%%%%%%%%%%%%%%%%%%%%%%%%%%%%%%%%%%%%%%%%%
%       ELEMENT MASS AND STIFFNESS MATRICES FOR TREATED BEAM               %
%%%%%%%%%%%%%%%%%%%%%%%%%%%%%%%%%%%%%%%%%%%%%%%%%%%%%%%%%%%%%%%%%%%%%%%%%%%%%
%
%
function [MEQU2,CEQU2,KEQU2] = km_mat2(LEN,...
                APAL1,AVEL2,APSL3,ABML4,ROPA1,ROVE2,ROPS3,ROBM4,...
                IPAL1,IVEL2,IPSL3,IBML4,EPAL1,EVEL2,EPSL3,EBML4,...
                HPAL1,HVEL2,HPSL3,HBML4,DNASI,GVESH,CFMGC,CONKP,CONKD);

%
%%%%%%%%%%%%%%%%%%%%%%%%%%%%%%%%%%%%%%%%%%%%%%%%%%%%%%%%%%%%%%%%%%%%%%%%%%%%%
% FUNCTION CALL FOR MASTER MATRIX LIBRARY
%
[EXTNUL1,BENDUL1,EXTNUL2,BENDUL2,SHEARUL2,EXTNUL34,BENDUL34,...
                KESEG1,KESEG2,KESEG3,CONTFRC] = basisfn(LEN,HPAL1,...
                HVEL2,HPSL3,HBML4,DNASI,CFMGC);
%
%%%%%%%%%%%%%%%%%%%%%%%%%%%%%%%%%%%%%%%%%%%%%%%%%%%%%%%%%%%%%%%%%%%%%%%%%%%%%
% STIFFNESS AND MASS MATRICES DEFINED FOR CONSTRAINING LAYER
%
KEPAL1 = 2*EPAL1*APAL1*EXTNUL1/LEN;
KBPAL1 = 8*EPAL1*IPAL1*BENDUL1/(LEN^3);
MPAL1 = ROPA1*APAL1*KESEG1*LEN/2;
%
%%%%%%%%%%%%%%%%%%%%%%%%%%%%%%%%%%%%%%%%%%%%%%%%%%%%%%%%%%%%%%%%%%%%%%%%%%%%%
% STIFFNESS AND MASS MATRICES DEFINED FOR THE VISCOELASTIC LAYER
%
KEVEL2 = EVEL2*AVEL2*EXTNUL2*LEN/2;
KBVEL2 = EVEL2*IVEL2*BENDUL2*LEN/2;
KSVEL2 = (5/6)*GVESH*AVEL2*SHEARUL2*LEN/(2*HVEL2^2);
MVEL2 = ROVE2*AVEL2*KESEG2*LEN/2;
%
%%%%%%%%%%%%%%%%%%%%%%%%%%%%%%%%%%%%%%%%%%%%%%%%%%%%%%%%%%%%%%%%%%%%%%%%%%%%%
% STIFFNESS AND MASS MATRICES DEFINED FOR THE SENSOR-BEAM LAYER
%
EABML34 = EPSL3*APSL3 + EBML4*ABML4;
EIBML34 = EPSL3*IPSL3 + EBML4*IBML4;
ROABM34 = (ROPS3*APSL3*HPSL3 + ROBM4*ABML4*HBML4)/(HPSL3 + HBML4);
KEBML34 = 2*EABML34*EXTNUL34/LEN;
KBBML34 = 8*EIBML34*BENDUL34/(LEN^3);
MBML34 = ROABM34*KESEG3*LEN/2;
%
%%%%%%%%%%%%%%%%%%%%%%%%%%%%%%%%%%%%%%%%%%%%%%%%%%%%%%%%%%%%%%%%%%%%%%%%%%%%%
% STIFFNESS AND DAMPING MATRIX WHEN THE CONSTRAINING LAYER IS ACTIVE
%
KCONT1 = -CONKP*CONTFRC;
CCONT1 = CONKD*CONTFRC;
%
%%%%%%%%%%%%%%%%%%%%%%%%%%%%%%%%%%%%%%%%%%%%%%%%%%%%%%%%%%%%%%%%%%%%%%%%%%%%%
% STIFFNESS, DAMPING AND MASS MATIRCES ASSEMBLED FOR THE SANDWICHED
% PORTION OF ONE EMEMENT OF THE BEAM
%
KEQU2 = KEPAL1+KBPAL1+KEVEL2+KBVEL2+KSVEL2+KEBML34+KBBML34+KCONT1;
CEQU2 = CCONT1;
MEQU2 = MPAL1+MVEL2+MBML34;
%%%%%%%%%%%%%%%%%%%%%%%%%%%%%%%%%%%%%%%%%%%%%%%%%%%%%%%%%%%%%%%%%%%%%%%%%%%%%
```

```
%%%%%%%%%%%%%%%%%%SUBROUTINE PROGRAM KM_MAT3.M-FUNCTION FILE%%%%%%%%%%%%%%%%%
%%%%%%%%%%%%%%%%%%%%%%%%%%%%%%%%%%%%%%%%%%%%%%%%%%%%%%%%%%%%%%%%%%%%%%%%%%%%%%
%       ELEMENT MASS AND STIFFNESS MATIRCES FOR THE BEAM TREATED WITH       %
%                    SENSOR AND VISCOELASTIC LAYERS                           %
%%%%%%%%%%%%%%%%%%%%%%%%%%%%%%%%%%%%%%%%%%%%%%%%%%%%%%%%%%%%%%%%%%%%%%%%%%%%%%
%
%
function [MEQUP,KEQUP] = km_mat3(LEN,...
                AVEL2,APSL3,ABML4,ROVE2,ROPS3,ROBM4,...
                IVEL2,IPSL3,IBML4,EVEL2,EPSL3,EBML4,...
                HPAL1,HVEL2,HPSL3,HBML4,DNASI,GVESH,CFMGC);

%
%%%%%%%%%%%%%%%%%%%%%%%%%%%%%%%%%%%%%%%%%%%%%%%%%%%%%%%%%%%%%%%%%%%%%%%%%%%%%%
% FUNCTION CALL TO GET THE MASTER MATRIX LIBRARY
%
[EXTNUL1,BENDUL1,EXTNUL2,BENDUL2,SHEARUL2,EXTNUL34,...
                BENDUL34,KESEG1,KESEG2,KESEG3,CONTFRC] = basisfn(LEN,...
                HPAL1,HVEL2,HPSL3,HBML4,DNASI,CFMGC);
%
%%%%%%%%%%%%%%%%%%%%%%%%%%%%%%%%%%%%%%%%%%%%%%%%%%%%%%%%%%%%%%%%%%%%%%%%%%%%%%
% STIFFNESS AND MASS MATRICES DEFINED FOR THE VISCOELASTIC LAYER
%
KEVEL2 = EVEL2*AVEL2*EXTNUL2*LEN/2;
KBVEL2 = EVEL2*IVEL2*BENDUL2*LEN/2;
KSVEL2 = GVESH*AVEL2*SHEARUL2*LEN/2;
MVEL2 = ROVE2*AVEL2*KESEG2*LEN/2;
%
%%%%%%%%%%%%%%%%%%%%%%%%%%%%%%%%%%%%%%%%%%%%%%%%%%%%%%%%%%%%%%%%%%%%%%%%%%%%%%
% STIFFNESS AND MASS MATRICES DEFINED FOR THE BEAM-SENSOR LAYER
%
EABML34 = EPSL3*APSL3 + EBML4*ABML4;
EIBML34 = EPSL3*IPSL3 + EBML4*IBML4;
ROABM34 = (ROPS3*APSL3*HPSL3 + ROBM4*ABML4*HBML4)/(HPSL3 + HBML4);
KEBML34 = 2*EABML34*EXTNUL34/LEN;
KBBML34 = 8*EIBML34*BENDUL34/(LEN^3);
MBML34 = ROABM34*KESEG3*LEN/2;
%
%%%%%%%%%%%%%%%%%%%%%%%%%%%%%%%%%%%%%%%%%%%%%%%%%%%%%%%%%%%%%%%%%%%%%%%%%%%%%%
% EQUIVALENT STIFFNESS AND MASS MATRICES ASSEMBLED FOR THE GAP ELEMENT
%
KEQUP = KEVEL2 + KBVEL2 + KSVEL2 + KEBML34 + KBBML34;
MEQUP = MVEL2 + MBML34;
%%%%%%%%%%%%%%%%%%%%%%%%%%%%%%%%%%%%%%%%%%%%%%%%%%%%%%%%%%%%%%%%%%%%%%%%%%%%%%
```

```
%%%%%%%%%%%%%%%%%%%SUBROUTINE PROGRAM BASISFN.M-FUNCTION FILE%%%%%%%%%%%%%%%%
%%%%%%%%%%%%%%%%%%%%%%%%%%%%%%%%%%%%%%%%%%%%%%%%%%%%%%%%%%%%%%%%%%%%%%%%%%%%%%%%
%       BASIS FUNCTIONS INTEGRATED OVER THE LENGTH OF THE ELEMENT            %
%%%%%%%%%%%%%%%%%%%%%%%%%%%%%%%%%%%%%%%%%%%%%%%%%%%%%%%%%%%%%%%%%%%%%%%%%%%%%%%%
function [EXTNUL1,BENDUL1,EXTNUL2,BENDUL2,SHEARUL2,EXTNUL34,...
              BENDUL34,KESEG1,KESEG2,KESEG3,CONTFRC] = basisfn(LEN,...
              HPAL1,HVEL2,HPSL3,HBML4,DNASI,CFMGC)
% ALL VARIABLES DEFINED IN PROGRAM FILE BAZFEM.M
%%%%%%%%%%%%%%%%%%%%%%%%%%%%%%%%%%%%%%%%%%%%%%%%%%%%%%%%%%%%%%%%%%%%%%%%%%%%%%%%
% Matrix multiplier for the Extentional Internal Energy of the
% Constraining layer
%
EXTNUL1 = [0.5,  0.0,  0.0,  0.0,  -0.5,  0.0,  0.0,  0.0
       0.0,  0.0,  0.0,  0.0,  0.0,  0.0,  0.0,  0.0
       0.0,  0.0,  0.0,  0.0,  0.0,  0.0,  0.0,  0.0
       0.0,  0.0,  0.0,  0.0,  0.0,  0.0,  0.0,  0.0
       -0.5,  0.0,  0.0,  0.0,  0.5,  0.0,  0.0,  0.0
       0.0,  0.0,  0.0,  0.0,  0.0,  0.0,  0.0,  0.0
       0.0,  0.0,  0.0,  0.0,  0.0,  0.0,  0.0,  0.0
       0.0,  0.0,  0.0,  0.0,  0.0,  0.0,  0.0,  0.0];
%%%%%%%%%%%%%%%%%%%%%%%%%%%%%%%%%%%%%%%%%%%%%%%%%%%%%%%%%%%%%%%%%%%%%%%%%%%%%%%%
% Matrix multiplier for the Bending Internal Energy of the
% Constraining layer
%
BENDUL1 = [0.0,  0.0,  0.0,  0.0,  0.0,  0.0,  0.0,  0.0
        0.0,  0.0,  0.0,  0.0,  0.0,  0.0,  0.0,  0.0
        0.0,  0.0,  1.5,  0.75*LEN,  0.0,  0.0,  -1.5,  0.75*LEN
        0.0,  0.0,  0.75*LEN, 0.5*LEN^2, 0.0, 0.0, -0.75*LEN, 0.25*LEN^2
        0.0,  0.0,  0.0,  0.0,  0.0,  0.0,  0.0,  0.0
        0.0,  0.0,  0.0,  0.0,  0.0,  0.0,  0.0,  0.0
        0.0,  0.0,  -1.5,  -0.75*LEN,  0.0,  0.0,  1.5,  -0.75*LEN
        0.0,  0.0,  0.75*LEN, 0.25*LEN^2, 0.0, 0.0, -0.75*LEN, 0.5*LEN^2];
%%%%%%%%%%%%%%%%%%%%%%%%%%%%%%%%%%%%%%%%%%%%%%%%%%%%%%%%%%%%%%%%%%%%%%%%%%%%%%%%
% Matrix multiplier for the Extentional Internal Energy of the
% Viscoelastic layer
%
THK = (-HPAL1 + HPSL3 + HBML4);
EXTNUL2 = [0.5/(LEN^2), 0.5/(LEN^2) , 0.0, -THK/(2*LEN^2),...
             -0.5/(LEN^2), -0.5/(LEN^2) , 0.0, THK/(2*LEN^2)
       0.5/(LEN^2), 0.5/(LEN^2) , 0.0, -THK/(2*LEN^2),...
             -0.5/(LEN^2), -0.5/(LEN^2) , 0.0, THK/(2*LEN^2)
       0.0, 0.0, (6*THK^2)/(LEN^4), (3*THK^2)/(LEN^3), 0.0, 0.0,...
             -(6*THK^2)/(LEN^4), (3*THK^2)/(LEN^3)
       -THK/(2*LEN^2), -THK/(2*LEN^2), (3*THK^2)/(LEN^3),...
             2*(THK^2)/(LEN^2),THK/(2*LEN^2), THK/(2*LEN^2),...
             -(3*THK^2)/(LEN^3), (THK^2)/(LEN^2)
       -0.5/(LEN^2), -0.5/(LEN^2) , 0.0, THK/(2*LEN^2),...
             0.5/(LEN^2), 0.5/(LEN^2) , 0.0, -THK/(2*LEN^2)
       -0.5/(LEN^2), -0.5/(LEN^2) , 0.0, THK/(2*LEN^2),...
             0.5/(LEN^2), 0.5/(LEN^2) , 0.0, -THK/(2*LEN^2)
       0.0, 0.0, -(6*THK^2)/(LEN^4), -(3*THK^2)/(LEN^3), 0.0, 0.0,...
             (6*THK^2)/(LEN^4), -(3*THK^2)/(LEN^3)
       THK/(2*LEN^2), THK/(2*LEN^2), (3*THK^2)/(LEN^3), (THK^2)/(LEN^2),...
             -THK/(2*LEN^2), -THK/(2*LEN^2), -(3*THK^2)/(LEN^3),...
             2*(THK^2)/(LEN^2)];
```

```
%%%%%%%%%%%%%%%%%%%%%%%%%%%%%%%%%%%%%%%%%%%%%%%%%%%%%%%%%%%%%%%%%%%%%%%%%%%%
% Matrix multiplier for the Bending Internal Energy of the
% Viscoelastic layer
%
HEI = (HPAL1 + HPSL3 + HBML4);
BENDUL2 = [2/(HVEL2^2*LEN^2), -2/(HVEL2^2*LEN^2), 0.0,...
              HEI/(8*HVEL2^2*LEN^2),-2/(HVEL2^2*LEN^2),...
              2/(HVEL2^2*LEN^2),0.0, -HEI/(HVEL2^2*LEN^2)
        -2/(HVEL2^2*LEN^2), 2/(HVEL2^2*LEN^2), 0.0, -HEI/(8*HVEL2^2*LEN^2),...
              2/(HVEL2^2*LEN^2), -2/(HVEL2^2*LEN^2),0.0,...
              HEI/(HVEL2^2*LEN^2)
        0.0,0.0,6*(HEI^2)/(HVEL2^2*LEN^4),3*(HEI^2)/(HVEL2^2*LEN^3),...
              0.0, 0.0,-6*(HEI^2)/(HVEL2^2*LEN^4),...
              3*(HEI^2)/(HVEL2^2*LEN^3)
        HEI/(HVEL2^2*LEN^2),-HEI/(HVEL2^2*LEN^2),3*(HEI^2)/(HVEL2^2*LEN^3),...
        2*(HEI^2)/(HVEL2^2*LEN^2),-HEI/(HVEL2^2*LEN^2),HEI/(HVEL2^2*LEN^2),...
              -3*(HEI^2)/(HVEL2^2*LEN^3),(HEI^2)/(HVEL2^2*LEN^2)
        -2/(HVEL2^2*LEN^2), 2/(HVEL2^2*LEN^2), 0.0, -HEI/(8*HVEL2^2*LEN^2),...
              2/(HVEL2^2*LEN^2), -2/(HVEL2^2*LEN^2),0.0, HEI/(HVEL2^2*LEN^2)
        2/(HVEL2^2*LEN^2), -2/(HVEL2^2*LEN^2), 0.0, HEI/(8*HVEL2^2*LEN^2),...
              -2/(HVEL2^2*LEN^2), 2/(HVEL2^2*LEN^2),0.0, -HEI/(HVEL2^2*LEN^2)
        0.0,0.0,-6*(HEI^2)/(HVEL2^2*LEN^4),-3*(HEI^2)/(HVEL2^2*LEN^3),...
              0.0, 0.0,6*(HEI^2)/(HVEL2^2*LEN^4),...
              -3*(HEI^2)/(HVEL2^2*LEN^3)
        -HEI/(HVEL2^2*LEN^2),HEI/(HVEL2^2*LEN^2),3*(HEI^2)/(HVEL2^2*LEN^3),...
              (HEI^2)/(HVEL2^2*LEN^2),HEI/(HVEL2^2*LEN^2),...
              -HEI/(HVEL2^2*LEN^2),-3*(HEI^2)/(HVEL2^2*LEN^3),...
              2*(HEI^2)/(HVEL2^2*LEN^2)];
%%%%%%%%%%%%%%%%%%%%%%%%%%%%%%%%%%%%%%%%%%%%%%%%%%%%%%%%%%%%%%%%%%%%%%%%%%%%
% Matrix multiplier for the Shear Internal Energy of the
% Viscoelastic layer
%
SHEARUL2 = [2/3, -2/3, -DNASI/LEN, DNASI/6,1/3, -1/3,...
              DNASI/LEN, -DNASI/6
        -2/3, 2/3, DNASI/LEN, -DNASI/6,-1/3, 1/3,...
              -DNASI/LEN, DNASI/6
        -DNASI/LEN,DNASI/LEN,(12*DNASI^2)/(5*LEN^2),(DNASI^2)/(5*LEN),...
              -DNASI/LEN,DNASI/LEN,-(12*DNASI^2)/(5*LEN^2),...
              (DNASI^2)/(5*LEN)
        DNASI/6, -DNASI/6, (DNASI^2)/5*LEN,4*(DNASI^2)/15, -DNASI/6,...
              DNASI/6,-(DNASI^2)/5*LEN,-(DNASI^2)/15
        1/3, -1/3, -DNASI/LEN, -DNASI/6,2/3, -2/3,...
              DNASI/LEN, DNASI/6
        -1/3, 1/3, DNASI/LEN, DNASI/6,-2/3, 2/3,...
              -DNASI/LEN, -DNASI/6
      DNASI/LEN,-DNASI/LEN,-(12*DNASI^2)/(5*LEN^2),-(DNASI^2)/(5*LEN),...
              DNASI/LEN,-DNASI/LEN,...
              (12*DNASI^2)/(5*LEN^2),-(DNASI^2)/(5*LEN)
        -DNASI/6, DNASI/6, (DNASI^2)/(5*LEN),-(DNASI^2)/15, DNASI/6,...
              -DNASI/6,-(DNASI^2)/(5*LEN),(4*DNASI^2)/(15)];

%%%%%%%%%%%%%%%%%%%%%%%%%%%%%%%%%%%%%%%%%%%%%%%%%%%%%%%%%%%%%%%%%%%%%%%%%%%%
% Matrix multiplier for the Extentional Internal Energy of the
% Beam and Sensor layer considered as one.
%
EXTNUL34 = [0.0, 0.0, 0.0, 0.0, 0.0, 0.0, 0.0, 0.0
         0.0, 0.5, 0.0, 0.0, 0.0, -0.5, 0.0, 0.0
         0.0, 0.0, 0.0, 0.0, 0.0, 0.0, 0.0, 0.0
         0.0, 0.0, 0.0, 0.0, 0.0, 0.0, 0.0, 0.0
         0.0, 0.0, 0.0, 0.0, 0.0, 0.0, 0.0, 0.0
         0.0, -0.5, 0.0, 0.0, 0.0, 0.5, 0.0, 0.0
         0.0, 0.0, 0.0, 0.0, 0.0, 0.0, 0.0, 0.0
         0.0, 0.0, 0.0, 0.0, 0.0, 0.0, 0.0, 0.0];
```

```
%%%%%%%%%%%%%%%%%%%%%%%%%%%%%%%%%%%%%%%%%%%%%%%%%%%%%%%%%%%%%%%%%%%%%%%%%%%%%%%%%%%%
% Matrix multiplier for the Bending Internal Energy of the
% Beam and Sensor layer considered as one.
%
BENDUL34 = [0.0,  0.0,  0.0,  0.0,  0.0,  0.0,  0.0,  0.0
        0.0,  0.0,  0.0,  0.0,  0.0,  0.0,  0.0,  0.0
        0.0,  0.0,  1.5,  0.75*LEN,  0.0,  0.0,  -1.5,  0.75*LEN
        0.0,  0.0, 0.75*LEN, (LEN^2)/2, 0.0, 0.0, -0.75*LEN, (LEN^2)/4
        0.0,  0.0,  0.0,  0.0,  0.0,  0.0,  0.0,  0.0
        0.0,  0.0,  0.0,  0.0,  0.0,  0.0,  0.0,  0.0
        0.0,  0.0,  -1.5,  -0.75*LEN,  0.0,  0.0,  1.5,  -0.75*LEN
        0.0,  0.0, 0.75*LEN, (LEN^2)/4, 0.0, 0.0, -0.75*LEN, (LEN^2)/2];
%%%%%%%%%%%%%%%%%%%%%%%%%%%%%%%%%%%%%%%%%%%%%%%%%%%%%%%%%%%%%%%%%%%%%%%%%%%%%%%%%%%%
% Matrix multiplier for the Kinetic Energy of the Constraining Layer
%
KESEG1 = [2/3,  0.0,  0.0,   0.0,   1/3,  0.0,  0.0,   0.0
       0.0,  0.0,  0.0,  0.0,  0.0,  0.0,  0.0,  0.0
       0.0,0.0,26/35,11*LEN/105,0.0,0.0,9/35,-13*LEN/210
       0.0, 0.0, 11*LEN/105, 2*(LEN^2)/105, 0.0, 0.0, 13*LEN/210,...
                                                      -(LEN^2)/70
       1/3,  0.0,  0.0,   0.0,   2/3,  0.0,  0.0,   0.0
       0.0,  0.0,  0.0,  0.0,  0.0,  0.0,  0.0,  0.0
       0.0,0.0,9/35,13*LEN/210,0.0,0.0,26/35,-11*LEN/105
       0.0, 0.0, -13*LEN/210, -(LEN^2)/70, 0.0, 0.0, -11*LEN/105,...
                                                    2*(LEN^2)/105];
%%%%%%%%%%%%%%%%%%%%%%%%%%%%%%%%%%%%%%%%%%%%%%%%%%%%%%%%%%%%%%%%%%%%%%%%%%%%%%%%%%%%
% Matrix multiplier for the Kinetic Energy of the Viscoelastic Layer
%
K11 = 1/6;
K12 = 1/6;
K13 = THK/(4*LEN);
K14 = -THK/24;
K15 = 1/12;
K16 = 1/12;
K17 = -THK/(4*LEN);
K18 = THK/24;
K31 = THK/(4*LEN);
K32 = THK/(4*LEN);
K33 = 26/35 + 3*(THK^2)/(5*LEN^2);
K34 = 11*LEN/105 + (THK^2)/(20*LEN);
K35 = THK/(4*LEN);
K36 = THK/(4*LEN);
K37 = 9/35 - 3*(THK^2)/(5*LEN^2);
K38 = -13*LEN/210 + (THK^2)/(20*LEN);
K41 = -THK/24;
K42 = -THK/24;
K43 = 11*LEN/105 + (THK^2)/(20*LEN);
K44 = 2*(LEN^2)/105 + (THK^2)/15;
K45 = THK/24;
K46 = THK/24;
K47 = 13*LEN/210 - (THK^2)/(20*LEN);
K48 = -(LEN^2)/70 - (THK^2)/60;
KESEG2 = [K11, K12, K13, K14, K15, K16, K17, K18
       K11, K12, K13, K14, K15, K16, K17, K18
       K31, K32, K33, K34, K35, K36, K37, K38
       K41, K42, K43, K44, K45, K46, K47, K48
       K15, K16, K13,-K14, K11, K12, K17,-K18
       K15, K16, K13,-K14, K11, K12, K17,-K18
       -K35,-K36, K37,-K38,-K31,-K32, K33,-K34
       K45, K46,-K47, K48, K41, K42,-K43, K44];
```

```
%%%%%%%%%%%%%%%%%%%%%%%%%%%%%%%%%%%%%%%%%%%%%%%%%%%%%%%%%%%%%%%%%%%%%%%%%%%
% Matrix multiplier for the Kinetic Energy of the Beam and Sensor
% layer considered as one.
%
KESEG3 = [0.0,  0.0,  0.0,  0.0,  0.0,  0.0,  0.0,  0.0
       0.0,   2/3,   0.0,   0.0,   0.0,  1/3,  0.0,   0.0
       0.0,0.0, 26/35,11*LEN/105,0.0,0.0,9/35,-13*LEN/210
       0.0,  0.0,  11*LEN/105,  2*(LEN^2)/105,  0.0,  0.0,...
                                        13*LEN/210,  -(LEN^2)/70
       0.0,  0.0,  0.0,  0.0,  0.0,  0.0,  0.0,  0.0
       0.0,  1/3,  0.0,  0.0,   0.0,   2/3,  0.0,  0.0
       0.0,0.0, 9/35,13*LEN/210,0.0,0.0,26/35,-11*LEN/105
       0.0,  0.0,  -13*LEN/210,  -(LEN^2)/70,  0.0,  0.0,...
                                  -11*LEN/105,  2*(LEN^2)/105];
%%%%%%%%%%%%%%%%%%%%%%%%%%%%%%%%%%%%%%%%%%%%%%%%%%%%%%%%%%%%%%%%%%%%%%%%%%%
% Matrix multiplier for the Control Forces due to the active layer
%
CONTFRC = [0.0,  0.0,  0.0, (-CFMGC),  0.0,  0.0,  0.0, (CFMGC)
         0.0,  0.0,  0.0,  0.0,  0.0,  0.0,  0.0,  0.0
         0.0,  0.0,  0.0,  0.0,  0.0,  0.0,  0.0,  0.0
         0.0, 0.0, 0.0, (-CFMGC*DNASI), 0.0, 0.0, 0.0,(CFMGC*DNASI)
         0.0,  0.0,  0.0,  (CFMGC),  0.0,  0.0,  0.0, (-CFMGC)
         0.0,  0.0,  0.0,  0.0,  0.0,  0.0,  0.0,  0.0
         0.0,  0.0,  0.0,  0.0,  0.0,  0.0,  0.0,  0.0
         0.0, 0.0, 0.0, (CFMGC*DNASI), 0.0, 0.0, 0.0,(-CFMGC*DNASI)];
%%%%%%%%%%%%%%%%%%%%%%%%%%%%%%%%%%%%%%%%%%%%%%%%%%%%%%%%%%%%%%%%%%%%%%%%%%%
```

APPENDIX VII

PIEZOELECTRIC MATERIALS

When a piezoelectric material is subjected to an electric voltage across the thickness, it produces a compressive strain or a tensile strain depending upon the applied voltage. Also, when it is strained mechanically, it can produce positive or negative charge depending on the kind of the applied stress~~, charge induced may be positive or negative~~. Thus, piezoelectric material can act as a sensor and as an actuator. Some terms associated with the piezoelectric effect are explained below.

Poling axes

Relationships between applied forces and the resultant responses depend upon the piezoelectric properties of the material, the size and shape of the piece and the direction of the electrical and mechanical excitation. In order to identify the directions in a piezoelectric element, three axes are used. These axes are termed as 1, 2 and 3 and are analogous to X, Y and Z axes of the classical three dimensional orthogonal set. Figure A7.1 shows the location of the three axes with respect to the poling direction. The polarization vector "P" is represented by an arrow pointing from the positive to the negative poling electrode.

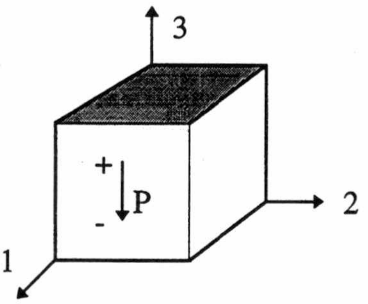

Figure A7.1 : Poling direction and the 1, 2 and 3 axes

Piezoelectric coefficients with double subscripts link electrical and mechanical quantities. The first subscript gives the direction of the electrical field associated with the voltage applied, or the charge induced. The second subscript gives the direction of the mechanical stress or strain. Also, frequently the constants have a second subscript, a character, not a number, which indicate the associated electrical or mechanical boundary conditions. For example t as the second subscript in k_{3t} expresses the relative dielectric constant measured in the polar direction 3 with no mechanical clamping applied.

"d" constant

The piezoelectric constants relating the mechanical strain produced by an applied electric field are termed as ~~the~~ strain constants, or ~~the~~ "d" coefficients. The ir units may ~~then~~ be expressed as meters per volt.

$$d = \frac{\text{strain developed}}{\text{applied electical field}} \quad \text{m/V}$$

Thus, d_{31} applies to a situation when the charge is produced across the planes perpendicular to the 3 axis, while the strain is produced between the planes perpendicular the 1 axis.

"g" constant

The piezoelectic constants relating the electrical field produced by the mechanical stress are termed the voltage constants, or the "g" coefficients. The units then may be expressed as volts/meter per newton/square meter.

$$g = \frac{\text{open circuit electric field}}{\text{applied mechanical stress}}$$

Coupling coefficient

Electromechanical coupling k_{31} describe the conversion of energy by the element from electrical to mechanical form or vice versa.

$$k = \sqrt{\frac{\text{mechanical energy stored}}{\text{electrical energy applied}}}$$

or

$$k = \sqrt{\frac{\text{electrical energy stored}}{\text{mechanical energy applied}}}$$

Dielectric constants

The relative dielectric constant is the ratio of the permittivity of the material, ε, to the permittivity of free space, ε_0, in the unconstrained condition.

$$k_{3t} = \frac{\text{permittivity of material}}{\text{permittivity of free space}} = \frac{\varepsilon}{\varepsilon_0}$$

APPENDIX VIII

EXPERIMENTAL DATA

Experimental results for active vs. passive damping for specimen PF31

Data for high amplitude of passively damped vibration

Amplitude (10^{-2} mm)	Time (sec.)	p(j)~p(j+1)	p(j)~p(j+2)	p(j)~p(j+3)	p(j)~p(j+4)	p(j)~p(j+5)	p(j)~p(j+6)
448.2	0.194	0.006083	0.006089	0.005735	0.005824	0.005892	0.005742
431.4	0.344	0.006095	0.005560	0.005737	0.005844	0.005674	0.005602
415.2	0.496	0.005026	0.005559	0.005760	0.005568	0.005504	0.005475
402.3	0.646	0.006092	0.006127	0.005749	0.005624	0.005565	0.005516
387.2	0.796	0.006163	0.005578	0.005468	0.005433	0.005401	
372.5	0.946	0.004993	0.005120	0.005190	0.005210		
361.0	1.098	0.005246	0.005288	0.005283			
349.3	1.248	0.005331	0.005301				
337.8	1.398	0.005272					
326.8	1.550						

Average Damping Ratio = 0.005583 **Average natural frequency = 6.637427**

Data for intermediate amplitude of passively damped vibration

Amplitude (10^{-2} mm)	Time (sec.)	p(j)~p(j+1)	p(j)~p(j+2)	p(j)~p(j+3)	p(j)~p(j+4)	p(j)~p(j+5)	p(j)~p(j+6)
370.1	0.136	0.005917	0.006240	0.005975	0.006165	0.006182	0.005992
356.6	0.296	0.006563	0.006003	0.006248	0.006248	0.006007	0.006079
342.2	0.454	0.005443	0.006090	0.006143	0.005868	0.005982	0.005937
330.7	0.614	0.006737	0.006493	0.006009	0.006116	0.006036	0.006049
317.0	0.774	0.006249	0.005646	0.005910	0.005861	0.005911	
304.8	0.932	0.005042	0.005740	0.005732	0.005826		
295.3	1.090	0.006437	0.006077	0.006088			
283.6	1.250	0.005716	0.005913				
273.6	1.408	0.006110					
263.3	1.568						

Average Damping Ratio = 0.006020 **Average natural frequency = 6.285162**

Data for low amplitude of passively damped vibration

Amplitude (10^{-2} mm)	Time (sec.)	p(j)~p(j+1)	p(j)~p(j+2)	p(j)~p(j+3)	p(j)~p(j+4)	p(j)~p(j+5)	p(j)~p(j+6)
213.2	1.216	0.005162	0.004296	0.004627	0.004628	0.004570	0.004700
206.4	1.364	0.003431	0.004360	0.004450	0.004422	0.004607	0.004777
202.0	1.516	0.005290	0.004960	0.004752	0.004901	0.005046	0.005161
195.4	1.664	0.004630	0.004484	0.004772	0.004985	0.005135	0.005156
189.8	1.814	0.004337	0.004842	0.005104	0.005262	0.005261	
184.7	1.964	0.005348	0.005487	0.005570	0.005492		
178.6	2.112	0.005626	0.005681	0.005539			
172.4	2.264	0.005736	0.005496				
166.3	2.410	0.005256					
160.9	2.526						

Average Damping Ratio = 0.004957 **Average natural frequency = 6.914611**

Data for high amplitude of actively damped vibration

Amplitude (10^{-2} mm)	Time (sec.)	p(j)~p(j+1)	p(j)~p(j+2)	p(j)~p(j+3)	p(j)~p(j+4)	p(j)~p(j+5)	p(j)~p(j+6)
471.7	0.610	0.013153	0.012908	0.013263	0.013491	0.013625	0.013964
434.3	0.770	0.012662	0.013318	0.013604	0.013743	0.014126	0.014328
401.1	0.930	0.013973	0.014075	0.014103	0.014492	0.014662	0.015083
367.4	1.090	0.014177	0.014169	0.014665	0.014834	0.015305	0.015612
336.1	1.248	0.014160	0.014909	0.015053	0.015586	0.015899	
307.5	1.408	0.015657	0.015499	0.016062	0.016334		
278.7	1.568	0.015341	0.016264	0.016559			
253.1	1.728	0.017188	0.017168				
227.2	1.886	0.017149					
204.0	2.048						

Average Damping Ratio = 0.014773 **Average natural frequency = 6.259007**

Data for intermediate amplitude of actively damped vibration

Amplitude (10^{-2} mm)	Time (sec.)	p(j)~p(j+1)	p(j)~p(j+2)	p(j)~p(j+3)	p(j)~p(j+4)	p(j)~p(j+5)	p(j)~p(j+6)
343.4	0.296	0.013694	0.014477	0.014786	0.015098	0.015690	0.016043
315.1	0.454	0.015261	0.015332	0.015566	0.016190	0.016513	0.017231
286.3	0.614	0.015403	0.015719	0.016499	0.016826	0.017625	0.017906
259.9	0.772	0.016035	0.017047	0.017300	0.018181	0.018406	0.019043
235.0	0.934	0.018059	0.017933	0.018896	0.018999	0.019645	
209.8	1.094	0.017807	0.019315	0.019313	0.020042		
187.6	1.254	0.020823	0.020066	0.020786			
164.6	1.414	0.019309	0.020768				
145.8	1.578	0.022228					
126.8	1.738						

Average Damping Ratio = 0.017586 **Average natural frequency = 6.242070**

Data for low amplitude of actively damped vibration

Amplitude (10^{-2} mm)	Time (sec.)	p(j)~p(j+1)	p(j)~p(j+2)	p(j)~p(j+3)	p(j)~p(j+4)	p(j)~p(j+5)	p(j)~p(j+6)
256.2	0.956	0.016279	0.017014	0.017251	0.018072	0.018323	0.018979
231.3	1.114	0.017749	0.017738	0.018670	0.018835	0.019519	0.020282
206.9	1.276	0.017726	0.019131	0.019196	0.019961	0.020788	0.021188
185.1	1.436	0.020535	0.019931	0.020706	0.021553	0.021881	0.022625
162.7	1.598	0.019328	0.020791	0.021893	0.022217	0.023043	
144.1	1.756	0.022255	0.023175	0.023180	0.023971		
125.3	1.916	0.024095	0.023643	0.024543			
107.7	2.080	0.023190	0.024767				
93.1	2.242	0.026343					
78.9	2.408						

Average Damping Ratio = 0.020779 **Average natural frequency = 6.199823**

Experimental results for active vs. passive damping for specimen PF32

Data for high amplitude of passively damped vibration

Amplitude (10^{-2} mm)	Time (sec.)	p(j)~p(j+1)	p(j)~p(j+2)	p(j)~p(j+3)	p(j)~p(j+4)	p(j)~p(j+5)	p(j)~p(j+6)
454.8	0.208	0.008522	0.009351	0.008418	0.008344	0.008451	0.008392
431.1	0.356	0.010180	0.008366	0.008285	0.008433	0.008366	0.008260
404.4	0.504	0.006551	0.007337	0.007850	0.007913	0.007875	0.007925
388.1	0.65	0.008122	0.008500	0.008367	0.008206	0.008200	0.008213
368.8	0.798	0.008878	0.008489	0.008235	0.008219	0.008231	
348.8	0.946	0.008100	0.007913	0.008000	0.008069		
331.5	1.094	0.007726	0.007949	0.008059			
315.8	1.24	0.008173	0.008226				
300	1.388	0.008279					
284.8	1.536						

Average Damping Ratio = 0.008230 **Average natural frequency = 6.777325**

Data for intermediate amplitude of passively damped vibration

Amplitude (10^{-2} mm)	Time (sec.)	p(j)~p(j+1)	p(j)~p(j+2)	p(j)~p(j+3)	p(j)~p(j+4)	p(j)~p(j+5)	p(j)~p(j+6)
388.1	0.65	0.008122	0.008500	0.008367	0.008206	0.008200	0.008213
368.8	0.798	0.008878	0.008489	0.008235	0.008219	0.008231	0.008050
348.8	0.946	0.008100	0.007913	0.008000	0.008069	0.007885	0.007859
331.5	1.094	0.007726	0.007949	0.008059	0.007831	0.007810	0.007970
315.8	1.24	0.008173	0.008226	0.007866	0.007832	0.008019	
300	1.388	0.008279	0.007713	0.007718	0.007981		
284.8	1.536	0.007147	0.007437	0.007881			
272.3	1.684	0.007728	0.008249				
259.4	1.83	0.008769					
245.5	1.978						

Average Damping Ratio = **0.008049** **Average natural frequency = 6.777325**

Data for low amplitude of passively damped vibration

Amplitude (10^{-2} mm)	Time (sec.)	p(j)~p(j+1)	p(j)~p(j+2)	p(j)~p(j+3)	p(j)~p(j+4)	p(j)~p(j+5)	p(j)~p(j+6)
292.6	1.012	0.008036	0.008249	0.007865	0.007872	0.007958	0.007884
278.2	1.158	0.008463	0.007780	0.007817	0.007939	0.007853	0.007705
263.8	1.304	0.007097	0.007495	0.007764	0.007701	0.007553	0.007601
252.3	1.454	0.007892	0.008098	0.007902	0.007667	0.007702	0.007765
240.1	1.602	0.008304	0.007907	0.007592	0.007654	0.007739	
227.9	1.748	0.007511	0.007236	0.007438	0.007598		
217.4	1.894	0.006962	0.007402	0.007627			
208.1	2.042	0.007842	0.007960				
198.1	2.19	0.008079					
188.3	2.338						

Average Damping Ratio = 0.007757 **Average natural frequency = 6.787884**

Date for high amplitude of actively damped vibration

Amplitude (10^{-2} mm)	Time (sec.)	p(j)~p(j+1)	p(j)~p(j+2)	p(j)~p(j+3)	p(j)~p(j+4)	p(j)~p(j+5)	p(j)~p(j+6)
454.8	0.35	0.015042	0.014809	0.014989	0.015579	0.015870	0.015996
413.8	0.5	0.014576	0.014962	0.015757	0.016077	0.016187	0.016752
377.6	0.646	0.015348	0.016348	0.016577	0.016589	0.017187	0.017685
342.9	0.794	0.017348	0.017191	0.017003	0.017647	0.018153	0.018462
307.5	0.942	0.017034	0.016831	0.017746	0.018354	0.018685	
276.3	1.09	0.016628	0.018103	0.018794	0.019098		
248.9	1.24	0.019577	0.019877	0.019921			
220.1	1.388	0.020177	0.020093				
193.9	1.536	0.020009					
171	1.68						

Average Damping Ratio = 0.017258 **Average natural frequency = 6.767875**

Data for intermediate amplitude of actively damped vibration

Amplitude (10^{-2} mm)	Time (sec.)	p(j)~p(j+1)	p(j)~p(j+2)	p(j)~p(j+3)	p(j)~p(j+4)	p(j)~p(j+5)	p(j)~p(j+6)
374.7	0.456	0.015005	0.015476	0.016091	0.016604	0.016869	0.017413
341	0.606	0.015947	0.016634	0.017137	0.017335	0.017894	0.018315
308.5	0.752	0.017320	0.017731	0.017798	0.018381	0.018788	0.019311
276.7	0.902	0.018142	0.018037	0.018734	0.019155	0.019709	0.020559
246.9	1.05	0.017932	0.019030	0.019493	0.020101	0.021042	
220.6	1.198	0.020129	0.020274	0.020824	0.021819		
194.4	1.346	0.020418	0.021171	0.022383			
171	1.496	0.021924	0.023365				
149	1.646	0.024806					
127.5	1.796						

Average Damping Ratio = 0.018951 **Average natural frequency = 6.716991**

Data for low amplitude of actively damped vibration

Amplitude (10^{-2} mm)	Time (sec.)	p(j)~p(j+1)	p(j)~p(j+2)	p(j)~p(j+3)	p(j)~p(j+4)	p(j)~p(j+5)	p(j)~p(j+6)
271.1	0.17	0.017226	0.018493	0.019004	0.019451	0.020233	0.020948
243.3	0.316	0.019761	0.019893	0.020192	0.020985	0.021692	0.022296
214.9	0.466	0.020025	0.020408	0.021393	0.022175	0.022803	0.024083
189.5	0.612	0.020791	0.022077	0.022892	0.023498	0.024895	0.025637
166.3	0.762	0.023363	0.023942	0.024400	0.025920	0.026606	
143.6	0.912	0.024520	0.024918	0.026773	0.027417		
123.1	1.06	0.025316	0.027899	0.028383			
105	1.212	0.030480	0.029915				
86.7	1.362	0.029350					
72.1	1.514						

Average Damping Ratio = 0.023335 **Average natural frequency = 6.697772**

Experimental Results for Active Vs. Passive Damping for Specimen PF33

Data for high amplitude of passively damped vibration

Amplitude (10^{-2} mm)	Time (sec.)	p(j)~p(j+1)	p(j)~p(j+2)	p(j)~p(j+3)	p(j)~p(j+4)	p(j)~p(j+5)	p(j)~p(j+6)
475.8	0.690	0.008559	0.008671	0.008617	0.008533	0.008512	0.008485
450.9	0.850	0.008784	0.008646	0.008524	0.008501	0.008470	0.008559
426.7	1.008	0.008508	0.008395	0.008406	0.008391	0.008514	0.008292
404.5	1.166	0.008281	0.008355	0.008353	0.008515	0.008248	0.008243
384.0	1.324	0.008430	0.008388	0.008593	0.008240	0.008235	
364.2	1.482	0.008347	0.008675	0.008177	0.008187		
345.6	1.640	0.009004	0.008092	0.008133			
326.6	1.798	0.007180	0.007698				
312.2	1.958	0.008216					
296.5	2.116						

Average Damping Ratio = 0.008384 **Average natural frequency = 6.311533**

Data for intermediate amplitude of passively damped vibration

Amplitude (10^{-2} mm)	Time (sec.)	p(j)~p(j+1)	p(j)~p(j+2)	p(j)~p(j+3)	p(j)~p(j+4)	p(j)~p(j+5)	p(j)~p(j+6)
387.4	0.300	0.008570	0.008402	0.008431	0.008349	0.008377	0.008343
367.1	0.458	0.008234	0.008362	0.008276	0.008328	0.008297	0.008133
348.6	0.620	0.008490	0.008297	0.008360	0.008313	0.008113	0.008266
330.5	0.776	0.008104	0.008295	0.008254	0.008019	0.008222	0.008162
314.1	0.934	0.008485	0.008329	0.007991	0.008251	0.008173	
297.8	1.092	0.008173	0.007743	0.008173	0.008095		
282.9	1.252	0.007314	0.008173	0.008069			
270.2	1.408	0.009032	0.008447				
255.3	1.568	0.007862					
243.0	1.724						

Average Damping Ratio = 0.008239 **Average natural frequency = 6.321217**

Data for low amplitude of passively damped vibration

Amplitude (10^{-2} mm)	Time (sec.)	p(j)~p(j+1)	p(j)~p(j+2)	p(j)~p(j+3)	p(j)~p(j+4)	p(j)~p(j+5)	p(j)~p(j+6)
203.0	0.084	0.007057	0.007220	0.007245	0.007344	0.007580	0.007470
194.2	0.242	0.007384	0.007338	0.007440	0.007711	0.007552	0.007462
185.4	0.402	0.007293	0.007468	0.007820	0.007594	0.007478	0.007644
177.1	0.560	0.007643	0.008084	0.007695	0.007524	0.007714	0.007421
168.8	0.716	0.008525	0.007720	0.007484	0.007732	0.007376	
160.0	0.876	0.006915	0.006964	0.007468	0.007089		
153.2	1.034	0.007012	0.007744	0.007147			
146.6	1.192	0.008476	0.007214				
139.0	1.350	0.005952					
133.9	1.508						

Average Damping Ratio = 0.007462 **Average natural frequency = 6.320549**

Data for high amplitude of actively damped vibration

Amplitude (10^{-2} mm)	Time (sec.)	p(j)~p(j+1)	p(j)~p(j+2)	p(j)~p(j+3)	p(j)~p(j+4)	p(j)~p(j+5)	p(j)~p(j+6)
480.0	0.536	0.014579	0.014634	0.014974	0.015205	0.015599	0.016056
438.0	0.696	0.014689	0.015171	0.015414	0.015854	0.016351	0.016522
399.4	0.856	0.015654	0.015776	0.016242	0.016767	0.016889	0.017427
362.0	1.014	0.015898	0.016536	0.017138	0.017197	0.017782	0.018613
327.6	1.174	0.017175	0.017757	0.017630	0.018253	0.019156	
294.1	1.332	0.018340	0.017858	0.018612	0.019652		
262.1	1.492	0.017376	0.018749	0.020089			
235.0	1.650	0.020121	0.021445				
207.1	1.810	0.022769					
179.5	1.972						

Average Damping Ratio = 0.017229 **Average natural frequency = 6.267798**

Data for intermediate amplitude of actively damped vibration

Amplitude (10^{-2} mm)	Time (sec.)	p(j)~p(j+1)	p(j)~p(j+2)	p(j)~p(j+3)	p(j)~p(j+4)	p(j)~p(j+5)	p(j)~p(j+6)
382.8	0.826	0.015817	0.016229	0.016653	0.017166	0.017449	0.018076
346.6	0.986	0.016642	0.017072	0.017615	0.017858	0.018527	0.019169
312.2	1.144	0.017502	0.018102	0.018263	0.018999	0.019674	0.020459
279.7	1.302	0.018702	0.018643	0.019498	0.020218	0.021050	0.022254
248.7	1.462	0.018584	0.019895	0.020723	0.021637	0.022965	
221.3	1.622	0.021207	0.021792	0.022655	0.024060		
193.7	1.780	0.022377	0.023379	0.025011			
168.3	1.940	0.024381	0.026327				
144.4	2.100	0.028273					
120.9	2.258						

Average Damping Ratio = 0.020126 **Average natural frequency = 6.285162**

Data for low amplitude of actively damped vibration

Amplitude (10^{-2} mm)	Time (sec.)	p(j)~p(j+1)	p(j)~p(j+2)	p(j)~p(j+3)	p(j)~p(j+4)	p(j)~p(j+5)	p(j)~p(j+6)
307.0	0.464	0.017236	0.017247	0.018388	0.018826	0.019693	0.020570
275.5	0.626	0.017257	0.018964	0.019356	0.020307	0.021237	0.022073
247.2	0.784	0.020671	0.020406	0.021324	0.022232	0.023037	0.024765
217.1	0.942	0.020142	0.021650	0.022752	0.023628	0.025584	0.027089
191.3	1.102	0.023159	0.024058	0.024790	0.026944	0.028478	
165.4	1.260	0.024956	0.025605	0.028205	0.029807		
141.4	1.422	0.026254	0.029829	0.031424			
119.9	1.582	0.033403	0.034008				
97.2	1.742	0.034613					
78.2	1.902						

Average Damping Ratio = 0.023845 **Average natural frequency = 6.259225**

Experimental Results for Active Vs. Passive Damping for Specimen PF34

Data for high amplitude of passively damped vibration

Amplitude (10^{-2} mm)	Time (sec.)	p(j)~p(j+1)	p(j)~p(j+2)	p(j)~p(j+3)	p(j)~p(j+4)	p(j)~p(j+5)	p(j)~p(j+6)
457.0	0.702	0.010365	0.010288	0.010228	0.010234	0.010205	0.010095
428.2	0.854	0.010212	0.010160	0.010190	0.010165	0.010041	0.009970
401.6	1.006	0.010107	0.010179	0.010149	0.009998	0.009921	0.010021
376.9	1.160	0.010251	0.010171	0.009962	0.009875	0.010003	0.009894
353.4	1.312	0.010090	0.009818	0.009749	0.009941	0.009823	
331.7	1.464	0.009545	0.009578	0.009892	0.009756		
312.4	1.618	0.009612	0.010065	0.009827			
294.1	1.770	0.010518	0.009934				
275.3	1.922	0.009350					
259.6	2.076						

Average Damping Ratio = 0.010005 **Average natural frequency = 6.550467**

Data for intermediate amplitude of passively damped vibration

Amplitude (10^{-2} mm)	Time (sec.)	p(j)~p(j+1)	p(j)~p(j+2)	p(j)~p(j+3)	p(j)~p(j+4)	p(j)~p(j+5)	p(j)~p(j+6)
385.9	0.868	0.010841	0.010598	0.010222	0.010196	0.010136	0.009944
360.5	1.020	0.010356	0.009912	0.009981	0.009960	0.009765	0.009905
337.8	1.172	0.009468	0.009794	0.009828	0.009617	0.009815	0.009857
318.3	1.326	0.010120	0.010008	0.009667	0.009902	0.009934	0.009790
298.7	1.476	0.009897	0.009441	0.009830	0.009888	0.009724	
280.7	1.630	0.008985	0.009797	0.009885	0.009681		
265.3	1.782	0.010609	0.010336	0.009913			
248.2	1.936	0.010063	0.009566				
233.0	2.086	0.009069					
220.1	2.240						

Average Damping Ratio = 0.009905 **Average natural frequency = 6.560467**

Data for low amplitude of passively damped vibration

Amplitude (10^{-2} mm)	Time (sec.)	p(j)~p(j+1)	p(j)~p(j+2)	p(j)~p(j+3)	p(j)~p(j+4)	p(j)~p(j+5)	p(j)~p(j+6)
314.9	1.146	0.010340	0.010009	0.010046	0.010040	0.009922	0.009980
295.1	1.298	0.009677	0.009898	0.009940	0.009818	0.009907	0.009837
277.7	1.450	0.010120	0.010072	0.009865	0.009965	0.009869	0.009725
260.6	1.602	0.010024	0.009737	0.009914	0.009806	0.009646	0.009702
244.7	1.756	0.009450	0.009859	0.009733	0.009551	0.009638	
230.6	1.908	0.010267	0.009875	0.009585	0.009685		
216.2	2.060	0.009483	0.009244	0.009491			
203.7	2.212	0.009005	0.009495				
192.5	2.366	0.009984					
180.8	2.518						

Average Damping Ratio = **0.009800** **Average natural frequency = 6.559961**

Data for high amplitude of actively damped vibration

Amplitude (10^{-2} mm)	Time (sec.)	p(j)~p(j+1)	p(j)~p(j+2)	p(j)~p(j+3)	p(j)~p(j+4)	p(j)~p(j+5)	p(j)~p(j+6)
446.8	0.226	0.016506	0.016425	0.016404	0.016808	0.017130	0.017391
402.8	0.380	0.016345	0.016353	0.016909	0.017287	0.017567	0.018000
363.5	0.532	0.016362	0.017191	0.017600	0.017873	0.018331	0.018753
328.0	0.686	0.018020	0.018220	0.018377	0.018824	0.019231	0.019533
292.9	0.840	0.018419	0.018555	0.019092	0.019533	0.019835	
260.9	0.992	0.018691	0.019428	0.019905	0.020189		
232.0	1.148	0.020164	0.020511	0.020689			
204.4	1.298	0.020858	0.020951				
179.3	1.452	0.021043					
157.1	1.606						

Average Damping Ratio = 0.018444 **Average natural frequency = 6.522483**

Data for intermediate amplitude of actively damped vibration

Amplitude (10^{-2} mm)	Time (sec.)	p(j)~p(j+1)	p(j)~p(j+2)	p(j)~p(j+3)	p(j)~p(j+4)	p(j)~p(j+5)	p(j)~p(j+6)
400.1	0.250	0.017790	0.018332	0.018320	0.019005	0.019393	0.019956
357.8	0.404	0.018874	0.018585	0.019409	0.019794	0.020389	0.020959
317.8	0.556	0.018296	0.019677	0.020100	0.020768	0.021376	0.021941
283.3	0.710	0.021058	0.021002	0.021591	0.022146	0.022670	0.023463
248.2	0.864	0.020947	0.021858	0.022509	0.023074	0.023944	
217.6	1.018	0.022770	0.023290	0.023782	0.024693		
188.6	1.168	0.023809	0.024289	0.025334			
162.4	1.324	0.024768	0.026097				
139.0	1.478	0.027426					
117.0	1.638						

Average Damping Ratio = 0.021628 **Average natural frequency = 6.485934**

Data for low amplitude of actively damped vibration

Amplitude (10^{-2} mm)	Time (sec.)	p(j)~p(j+1)	p(j)~p(j+2)	p(j)~p(j+3)	p(j)~p(j+4)	p(j)~p(j+5)	p(j)~p(j+6)
279.9	0.388	0.020877	0.021183	0.021573	0.022010	0.022747	0.023302
245.5	0.540	0.021490	0.021922	0.022388	0.023215	0.023787	0.024719
214.5	0.694	0.022353	0.022837	0.023790	0.024361	0.025364	0.026034
186.4	0.846	0.023320	0.024508	0.025030	0.026117	0.026770	0.027066
161.0	1.002	0.025696	0.025886	0.027049	0.027632	0.027815	
137.0	1.156	0.026075	0.027726	0.028278	0.028345		
116.3	1.310	0.029376	0.029379	0.029101			
96.7	1.464	0.029382	0.028964				
80.4	1.620	0.028546					
67.2	1.778						

Average Damping Ratio = 0.025282 **Average natural frequency = 6.475727**

Experimental Results for Active Vs. Passive Damping for Specimen PF41

Data for high amplitude of passively damped vibration

Amplitude (10^{-2} mm)	Time (sec.)	p(j)~p(j+1)	p(j)~p(j+2)	p(j)~p(j+3)	p(j)~p(j+4)	p(j)~p(j+5)	p(j)~p(j+6)
490.5	2.010	0.007818	0.007038	0.007297	0.007507	0.007433	0.007532
467.0	2.500	0.006259	0.007036	0.007403	0.007336	0.007475	0.007427
449.0	2.978	0.007813	0.007976	0.007695	0.007779	0.007661	0.007528
427.5	3.434	0.008138	0.007637	0.007768	0.007623	0.007472	0.007406
406.2	3.934	0.007135	0.007582	0.007451	0.007305	0.007260	
388.4	4.408	0.008029	0.007609	0.007361	0.007291		
369.3	4.890	0.007188	0.007028	0.007044			
353.0	5.372	0.006867	0.006973				
338.1	5.854	0.007078					
323.4	6.340						

Average Damping Ratio = 0.007417 **Average Natural Frequency =2.079693**

Data for intermediate amplitude of passively damped vibration

Amplitude (10^{-2} mm)	Time (sec.)	p(j)~p(j+1)	p(j)~p(j+2)	p(j)~p(j+3)	p(j)~p(j+4)	p(j)~p(j+5)	p(j)~p(j+6)
337.6	4.910	0.008029	0.007435	0.007141	0.007150	0.006811	0.006891
321.0	5.400	0.006842	0.006698	0.006857	0.006506	0.006663	0.006677
307.5	5.884	0.006554	0.006864	0.006394	0.006618	0.006644	0.006677
295.1	6.352	0.007174	0.006314	0.006640	0.006666	0.006702	0.006800
282.1	6.836	0.005455	0.006373	0.006497	0.006583	0.006725	
272.6	7.381	0.007291	0.007018	0.006960	0.007042		
260.4	7.804	0.006745	0.006794	0.006960			
249.6	8.290	0.006843	0.007067				
239.1	8.762	0.007290					
228.4	9.244						

Average Damping Ratio = 0.006805 **Average Natural Frequency = 2.084408**

Data for low amplitude of passively damped vibration

Amplitude (10^{-2} mm)	Time (sec.)	p(j)~p(j+1)	p(j)~p(j+2)	p(j)~p(j+3)	p(j)~p(j+4)	p(j)~p(j+5)	p(j)~p(j+6)
240.1	4.152	0.006774	0.006420	0.006108	0.006156	0.005963	0.006072
230.1	4.630	0.006065	0.005775	0.005950	0.005761	0.005931	0.006122
221.5	5.128	0.005485	0.005892	0.005659	0.005898	0.006133	0.006087
214.0	5.602	0.006299	0.005746	0.006035	0.006295	0.006208	0.006265
205.7	6.082	0.005193	0.005903	0.006294	0.006185	0.006258	
199.1	6.564	0.006614	0.006844	0.006516	0.006525		
191.0	7.048	0.007074	0.006467	0.006495			
182.7	7.528	0.005859	0.006206				
176.1	8.004	0.006553					
169.0	8.468						

Average Damping Ratio = 0.006156 **Average Natural Frequency = 2.085919**

Data for high amplitude of actively damped vibration

Amplitude (10^{-2} mm)	Time (sec.)	p(j)~p(j+1)	p(j)~p(j+2)	p(j)~p(j+3)	p(j)~p(j+4)	p(j)~p(j+5)	p(j)~p(j+6)
491.7	0.472	0.030325	0.029594	0.029160	0.029175	0.029182	0.028473
406.4	0.996	0.028863	0.028577	0.028792	0.028896	0.028103	0.029079
339.0	1.454	0.028290	0.028756	0.028907	0.027913	0.029122	0.029074
283.8	1.950	0.029222	0.029215	0.027787	0.029330	0.029231	0.027383
236.2	2.448	0.029209	0.027070	0.029366	0.029233	0.027015	
196.6	2.950	0.024930	0.029445	0.029241	0.026466		
168.1	3.424	0.033957	0.031395	0.026978			
135.8	3.922	0.028833	0.023487				
113.3	4.428	0.018139					
101.1	4.900						

Average Damping Ratio = 0.028390 **Average Natural Frequency = 2.035629**

Data for intermediate amplitude of actively damped vibration

Amplitude (10^{-2} mm)	Time (sec.)	p(j)~p(j+1)	p(j)~p(j+2)	p(j)~p(j+3)	p(j)~p(j+4)	p(j)~p(j+5)	p(j)~p(j+6)
306.8	1.710	0.029248	0.029227	0.028499	0.028210	0.027165	0.026592
255.3	2.198	0.029207	0.028124	0.027864	0.026644	0.026061	0.025538
212.5	2.684	0.027041	0.027192	0.025790	0.025275	0.024804	0.025231
179.3	3.196	0.027343	0.025164	0.024686	0.024245	0.024869	0.024024
151.0	3.686	0.022984	0.023357	0.023212	0.024250	0.023360	
130.7	4.180	0.023729	0.023326	0.024672	0.023454		
112.6	4.676	0.022922	0.025144	0.023362			
97.5	5.152	0.027365	0.023581				
82.1	5.668	0.019797					
72.5	6.162						

Average Damping Ratio = 0.025450 **Average Natural Frequency = 2.022697**

Data for low amplitude of actively damped vibration

Amplitude (10^{-2} mm)	Time (sec.)	p(j)~p(j+1)	p(j)~p(j+2)	p(j)~p(j+3)	p(j)~p(j+4)	p(j)~p(j+5)	p(j)~p(j+6)
212.3	2.108	0.026892	0.027117	0.026640	0.026202	0.026346	0.026327
179.3	2.608	0.027343	0.026514	0.025973	0.026210	0.026214	0.025182
151.0	3.108	0.025684	0.025287	0.025832	0.025932	0.024750	0.024443
128.5	3.598	0.024890	0.025905	0.026015	0.024517	0.024194	0.024003
109.9	4.098	0.026921	0.026577	0.024392	0.024020	0.023825	
92.8	4.598	0.026234	0.023128	0.023053	0.023051		
78.7	5.090	0.020021	0.021463	0.021990			
69.4	5.572	0.022904	0.022975				
60.1	6.058	0.023046					
52.0	6.560						

Average Damping Ratio = 0.024923 **Average Natural Frequency = 2.021963**

Experimental Results for Active Vs. Passive Damping for Specimen PF42

Data for high amplitude of passively damped vibration

Amplitude (10^{-2} mm)	Time (sec.)	p(j)~p(j+1)	p(j)~p(j+2)	p(j)~p(j+3)	p(j)~p(j+4)	p(j)~p(j+5)	p(j)~p(j+6)
486.6	1.228	0.007641	0.007816	0.007913	0.007841	0.007808	0.007777
463.8	1.704	0.007990	0.008050	0.007908	0.007849	0.007804	0.007784
441.1	2.176	0.008109	0.007867	0.007802	0.007757	0.007743	0.007741
419.2	2.648	0.007625	0.007649	0.007640	0.007651	0.007668	0.007576
399.6	3.124	0.007673	0.007648	0.007660	0.007678	0.007566	
380.8	3.600	0.007623	0.007653	0.007680	0.007539		
363.0	4.072	0.007683	0.007709	0.007511			
345.9	4.544	0.007734	0.007425				
329.5	5.018	0.007115					
315.1	5.490						

Average Damping Ratio = 0.007716 **Average Natural Frequency = 2.111716**

Data for intermediate amplitude of passively damped vibration

Amplitude (10^{-2} mm)	Time (sec.)	p(j)~p(j+1)	p(j)~p(j+2)	p(j)~p(j+3)	p(j)~p(j+4)	p(j)~p(j+5)	p(j)~p(j+6)
378.8	3.894	0.007973	0.007626	0.007481	0.007418	0.007332	0.007365
360.3	4.368	0.007279	0.007235	0.007233	0.007172	0.007244	0.007237
344.2	4.848	0.007192	0.007210	0.007136	0.007235	0.007229	0.007262
329.0	5.320	0.007228	0.007108	0.007249	0.007238	0.007276	0.007277
314.4	5.792	0.006988	0.007260	0.007242	0.007288	0.007287	
300.9	6.264	0.007531	0.007369	0.007388	0.007361		
287.0	6.740	0.007207	0.007317	0.007305			
274.3	7.210	0.007427	0.007353				
261.8	7.684	0.007280					
250.1	8.158						

Average Damping Ratio = 0.007304 **Average Natural Frequency = 2.110764**

Data for low amplitude of passively damped vibration

Amplitude (10^{-2} mm)	Time (sec.)	p(j)~p(j+1)	p(j)~p(j+2)	p(j)~p(j+3)	p(j)~p(j+4)	p(j)~p(j+5)	p(j)~p(j+6)
293.6	0.842	0.007155	0.007800	0.007732	0.007595	0.007623	0.007623
280.7	1.314	0.008445	0.008020	0.007742	0.007740	0.007716	0.007474
266.2	1.786	0.007596	0.007391	0.007505	0.007534	0.007280	0.007548
253.8	2.262	0.007187	0.007460	0.007513	0.007201	0.007539	0.007378
242.6	2.732	0.007733	0.007677	0.007206	0.007627	0.007416	
231.1	3.204	0.007621	0.006943	0.007592	0.007337		
220.3	3.682	0.006265	0.007577	0.007243			
211.8	4.154	0.008889	0.007731				
200.3	4.626	0.006573					
192.2	5.098						

Average Damping Ratio = 0.007519 **Average Natural Frequency = 2.114713**

Data for high amplitude of actively damped vibration

Amplitude (10^{-2} mm)	Time (sec.)	p(j)~p(j+1)	p(j)~p(j+2)	p(j)~p(j+3)	p(j)~p(j+4)	p(j)~p(j+5)	p(j)~p(j+6)
491.7	0.040	0.030325	0.029594	0.029160	0.029175	0.029182	0.028473
406.4	0.542	0.028863	0.028577	0.028792	0.028896	0.028103	0.029079
339.0	1.030	0.028290	0.028756	0.028907	0.027913	0.029122	
283.8	1.542	0.029222	0.029215	0.027787	0.029330		
236.2	2.066	0.029209	0.027070	0.029366			
196.6	2.678	0.024930	0.029445				
168.1	3.376	0.033957					
135.8	4.060						

Average Damping Ratio = 0.028916 **Average Natural Frequency = 1.775911**

Data for intermediate amplitude of actively damped vibration

Amplitude (10^{-2} mm)	Time (sec.)	p(j)~p(j+1)	p(j)~p(j+2)	p(j)~p(j+3)	p(j)~p(j+4)	p(j)~p(j+5)	p(j)~p(j+6)
472.9	1.466	0.035687	0.039730	0.044349	0.051370	0.062496	0.065677
377.9	1.960	0.043771	0.048677	0.056590	0.069179	0.071656	
287.0	2.458	0.053579	0.062989	0.077621	0.078604		
204.9	2.966	0.072382	0.089594	0.086915			
129.9	3.494	0.106725	0.094161				
66.2	4.088	0.081551					
39.6	4.786						

Average Damping Ratio = 0.066348 **Average Natural Frequency = 1.835156**

Data for low amplitude of actively damped vibration

Amplitude (10^{-2} mm)	Time (sec.)	p(j)~p(j+1)	p(j)~p(j+2)	p(j)~p(j+3)	p(j)~p(j+4)	p(j)~p(j+5)	p(j)~p(j+6)
410.1	1.412	0.040818	0.047670	0.053840	0.073868	0.094982	
317.3	1.914	0.054514	0.060341	0.084836	0.108411		
225.2	2.418	0.066161	0.099914	0.126189			
148.5	2.946	0.133326	0.155733				
63.8	3.544	0.177901					
20.5	4.182						

Average Damping Ratio = 0.091900 **Average Natural Frequency = 1.821947**

Experimental Results for Active Vs. Passive Damping for Specimen PF43

Data for high amplitude of passively damped vibration

Amplitude (10^{-2} mm)	Time (sec.)	p(j)~p(j+1)	p(j)~p(j+2)	p(j)~p(j+3)	p(j)~p(j+4)	p(j)~p(j+5)	p(j)~p(j+6)
477.3	3.084	0.007269	0.007078	0.007080	0.007173	0.007110	0.007090
456.0	3.546	0.006886	0.006985	0.007141	0.007070	0.007054	0.006998
436.7	4.022	0.007083	0.007268	0.007131	0.007096	0.007021	0.007004
417.7	4.484	0.007453	0.007155	0.007100	0.007005	0.006988	0.007013
398.6	4.956	0.006857	0.006924	0.006856	0.006872	0.006925	
381.8	5.414	0.006991	0.006855	0.006877	0.006942		
365.4	5.884	0.006720	0.006821	0.006926			
350.3	6.350	0.006921	0.007029				
335.4	6.824	0.007136					
320.7	7.286						

Average Damping Ratio = 0.007023 **Average Natural Frequency = 2.142187**

Data for intermediate amplitude of passively damped vibration

Amplitude (10^{-2} mm)	Time (sec.)	p(j)~p(j+1)	p(j)~p(j+2)	p(j)~p(j+3)	p(j)~p(j+4)	p(j)~p(j+5)	p(j)~p(j+6)
382.5	2.908	0.005377	0.005963	0.006174	0.006058	0.006396	0.006192
369.8	3.376	0.006549	0.006572	0.006286	0.006651	0.006355	0.006387
354.9	3.842	0.006596	0.006154	0.006685	0.006307	0.006355	0.006395
340.5	4.308	0.005713	0.006730	0.006211	0.006295	0.006355	0.006186
328.5	4.778	0.007747	0.006460	0.006488	0.006516	0.006281	
312.9	5.250	0.005172	0.005859	0.006106	0.005914		
302.9	5.710	0.006546	0.006572	0.006162			
290.7	6.178	0.006598	0.005970				
278.9	6.648	0.005341					
269.7	7.118						

Average Damping Ratio = 0.006274 **Average Natural Frequency = 2.137876**

Data for low amplitude of passively damped vibration

Amplitude (10^{-2} mm)	Time (sec.)	p(j)~p(j+1)	p(j)~p(j+2)	p(j)~p(j+3)	p(j)~p(j+4)	p(j)~p(j+5)	p(j)~p(j+6)
299.2	9.696	0.006241	0.006224	0.006203	0.006285	0.005798	0.005807
287.7	10.162	0.006208	0.006184	0.006300	0.005687	0.005720	0.005734
276.7	10.630	0.006160	0.006346	0.005513	0.005598	0.005639	0.005489
266.2	11.094	0.006533	0.005190	0.005411	0.005508	0.005355	0.005253
255.5	11.562	0.003848	0.004850	0.005167	0.005061	0.004997	
249.4	12.028	0.005852	0.005827	0.005465	0.005284		
240.4	12.492	0.005801	0.005271	0.005094			
231.8	12.962	0.004741	0.004741				
225.0	13.430	0.004741					
218.4	13.902						

Average Damping Ratio = 0.005567 **Average Natural Frequency = 2.139861**

Data for high amplitude of actively damped vibration

Amplitude (10^{-2} mm)	Time (sec.)	p(j)~p(j+1)	p(j)~p(j+2)	p(j)~p(j+3)	p(j)~p(j+4)	p(j)~p(j+5)	p(j)~p(j+6)
489.3	1.888	0.034959	0.037450	0.040989	0.047548	0.056488	0.065660
392.8	2.368	0.039940	0.044003	0.051740	0.061859	0.071780	0.080685
305.6	2.858	0.048063	0.057632	0.069147	0.079710	0.088792	
225.9	3.356	0.067185	0.079656	0.090210	0.098913		
148.0	3.872	0.092089	0.101671	0.109427			
82.8	4.428	0.111225	0.118059				
41.0	5.056	0.124876					
18.6	5.714						

Average Damping Ratio = 0.072954 **Average Natural Frequency = 1.854406**

Data for intermediate amplitude of actively damped vibration

Amplitude (10^{-2} mm)	Time (sec.)	p(j)~p(j+1)	p(j)~p(j+2)	p(j)~p(j+3)	p(j)~p(j+4)	p(j)~p(j+5)	p(j)~p(j+6)
431.9	1.102	0.035795	0.040711	0.045764	0.053265	0.064809	0.079616
344.9	1.590	0.045623	0.050743	0.059078	0.072039	0.088333	
258.9	2.088	0.055858	0.065794	0.080814	0.098944		
182.2	2.584	0.075711	0.093238	0.113195			
113.1	3.102	0.110678	0.131768				
56.2	3.662	0.152681					
21.3	4.246						

Average Damping Ratio = 0.076879 **Average Natural Frequency = 1.916981**

Data for low amplitude of actively damped vibration

Amplitude (10^{-2} mm)	Time (sec.)	p(j)~p(j+1)	p(j)~p(j+2)	p(j)~p(j+3)	p(j)~p(j+4)	p(j)~p(j+5)	p(j)~p(j+6)
490.2	0.044	0.034001	0.038827	0.042947	0.049291	0.059470	0.075473
395.9	0.536	0.043650	0.047415	0.054380	0.065821	0.083727	
300.9	1.014	0.051179	0.059738	0.073192	0.093691		
218.1	1.520	0.068285	0.084161	0.107760			
141.9	2.034	0.099973	0.127320				
75.5	2.566	0.154380					
28.3	3.130						

Average Damping Ratio = 0.072128 **Average Natural Frequency = 1.949855**

Experimental Results for Active Vs. Passive Damping for Specimen PF44

Data for high amplitude of passively damped vibration

Amplitude (10^{-2} mm)	Time (sec.)	p(j)~p(j+1)	p(j)~p(j+2)	p(j)~p(j+3)	p(j)~p(j+4)	p(j)~p(j+5)	p(j)~p(j+6)
480.2	3.084	0.008899	0.008846	0.008974	0.009107	0.008910	0.009508
454.1	4.318	0.008794	0.009012	0.009177	0.008913	0.009630	0.009572
429.7	4.794	0.009230	0.009368	0.008953	0.009839	0.009727	0.009820
405.5	5.266	0.009506	0.008815	0.010042	0.009852	0.009938	0.009837
382.0	5.748	0.008124	0.010310	0.009967	0.010046	0.009904	
363.0	6.224	0.012496	0.010888	0.010686	0.010349		
335.6	6.696	0.009280	0.009781	0.009633			
316.6	7.174	0.010283	0.009809				
296.8	7.652	0.009335					
279.9	8.126						

Average Damping Ratio = 0.009619 **Average Natural Frequency = 1.957537**

Data for intermediate amplitude of passively damped vibration

Amplitude (10^{-2} mm)	Time (sec.)	p(j)~p(j+1)	p(j)~p(j+2)	p(j)~p(j+3)	p(j)~p(j+4)	p(j)~p(j+5)	p(j)~p(j+6)
393.5	4.586	0.010322	0.009714	0.009728	0.009597	0.009457	0.009040
368.8	5.062	0.009106	0.009431	0.009356	0.009241	0.008784	0.008822
348.3	5.542	0.009756	0.009480	0.009285	0.008703	0.008765	0.008843
327.6	6.022	0.009204	0.009050	0.008352	0.008517	0.008660	0.008907
309.2	6.496	0.008895	0.007926	0.008288	0.008524	0.008847	
292.4	6.964	0.006957	0.007984	0.008400	0.008835		
279.9	7.442	0.009011	0.009122	0.009461			
264.5	7.922	0.009232	0.009686				
249.6	8.398	0.010140					
234.2	8.872						

Average Damping Ratio = 0.009011 **Average Natural Frequency = 2.099988**

Data for low amplitude of passively damped vibration

Amplitude (10^{-2} mm)	Time (sec.)	p(j)~p(j+1)	p(j)~p(j+2)	p(j)~p(j+3)	p(j)~p(j+4)	p(j)~p(j+5)	p(j)~p(j+6)
292.9	4.598	0.009752	0.009211	0.009739	0.009606	0.009596	0.009599
275.5	5.074	0.008670	0.009732	0.009558	0.009557	0.009569	0.009445
260.9	5.550	0.010794	0.010001	0.009852	0.009793	0.009600	0.009954
243.8	6.024	0.009209	0.009381	0.009460	0.009301	0.009786	0.009803
230.1	6.502	0.009554	0.009585	0.009332	0.009930	0.009922	
216.7	6.980	0.009616	0.009221	0.010055	0.010015		
204.0	7.452	0.008826	0.010275	0.010147			
193.0	7.930	0.011724	0.010808				
179.3	8.402	0.009892					
168.5	8.876						

Average Damping Ratio = 0.009740 **Average Natural Frequency = 2.103837**

Data for high amplitude of actively damped vibration

Amplitude (10^{-2} mm)	Time (sec.)	p(j)~p(j+1)	p(j)~p(j+2)	p(j)~p(j+3)	p(j)~p(j+4)	p(j)~p(j+5)	p(j)~p(j+6)
446.0	0.482	0.040210	0.044779	0.051440	0.063630	0.093461	
346.4	0.974	0.049344	0.057048	0.071415	0.106667		
254.0	1.476	0.064742	0.082413	0.125569			
169.0	1.982	0.100006	0.155503				
89.9	2.520	0.209566					
23.4	3.114						

Average Damping Ratio = 0.087720 **Average Natural Frequency = 1.908615**

Data for intermediate amplitude of actively damped vibration

Amplitude (10^{-2} mm)	Time (sec.)	p(j)~p(j+1)	p(j)~p(j+2)	p(j)~p(j+3)	p(j)~p(j+4)	p(j)~p(j+5)	p(j)~p(j+6)
468.7	1.388	0.037712	0.041695	0.047125	0.056436	0.077903	
369.8	1.880	0.045675	0.051827	0.062664	0.087899		
277.5	2.376	0.057973	0.071140	0.101881			
192.7	2.882	0.084269	0.123629				
113.3	3.418	0.162414					
40.3	4.018						

Average Damping Ratio = 0.074016 **Average Natural Frequency = 1.911454**

Data for low amplitude of actively damped vibration

Amplitude (10^{-2} mm)	Time (sec.)	p(j)~p(j+1)	p(j)~p(j+2)	p(j)~p(j+3)	p(j)~p(j+4)	p(j)~p(j+5)	p(j)~p(j+6)
435.3	1.706	0.039783	0.044238	0.050596	0.063649	0.090367	
339.0	2.196	0.048691	0.055996	0.071582	0.102920		
249.6	2.702	0.063293	0.082988	0.120818			
167.6	3.214	0.102586	0.149167				
87.7	3.752	0.194776					
25.2	4.438						

Average Damping Ratio = 0.072212 **Average Natural Frequency = 1.857338**

APPENDIX IX

ERROR ANALYSIS FOR THE FINITE ELEMENT RESULTS

Error analysis in the first natural frequency for specimen PF31

Table A10.1 : Real part of the estimated natural frequency ($k_p = 200$)

Mesh size Ω^h	Number of elements	Natural frequency, f_n	Difference Δf_n	Error $e^{h/2}$	Estimated exact f_n
Ω^1	3	6.83860			
Ω^2	4	7.66660	0.8280	0.2760	7.94260
Ω^3	5	7.92610	0.2595	0.0865	8.01260
Ω^4	6	8.03350	0.1074	0.0358	8.06930
Ω^8	10	8.16580	0.1323	0.0441	8.20990
Ω^{12}	14	8.20200	0.0362	0.0121	8.21407
Ω^{16}	18	8.21820	0.0162	0.0054	8.22360

Table A10.2 : Complex part of the estimated natural frequency ($k_p = 200$)

Mesh size Ω^h	Number of elements	Natural frequency, f_n	Difference Δf_n	Error $e^{h/2}$	Estimated exact f_n
Ω^1	3	0.35477			
Ω^2	4	1.41970	1.0649	0.3550	1.77468
Ω^3	5	1.61070	0.1910	0.0637	1.67437
Ω^4	6	1.68900	0.0783	0.0261	1.71510
Ω^8	10	1.78450	0.0955	0.0318	1.81633
Ω^{12}	14	1.81030	0.0258	0.0086	1.81890
Ω^{16}	18	1.82910	0.0188	0.0063	1.83537

Error analysis in the first natural frequency for specimen PF32

Table A10.3 : Real part of the estimated natural frequency ($k_p = 200$)

Mesh size Ω^h	Number of elements	Natural frequency, f_n	Difference Δf_n	Error $e^{h/2}$	Estimated exact f_n
Ω^1	4	7.57070			
Ω^2	6	7.92520	0.3545	0.1182	8.04337
Ω^3	8	8.01500	0.0898	0.0299	8.04493
Ω^4	10	8.05430	0.0393	0.0131	8.06740
Ω^6	14	8.08960	0.0353	0.0118	8.10137
Ω^8	18	8.10600	0.0164	0.0055	8.11147

Table A10.4 : Complex part of the estimated natural frequency ($k_p = 200$)

Mesh size Ω^h	Number of elements	Natural frequency, f_n	Difference Δf_n	Error $e^{h/2}$	Estimated exact f_n
Ω^1	4	1.40780			
Ω^2	6	1.67330	0.2655	0.0885	1.76180
Ω^3	8	1.73850	0.0652	0.0217	1.76023
Ω^4	10	1.76670	0.0282	0.0094	1.77610
Ω^6	14	1.79190	0.0252	0.0084	1.80030
Ω^8	18	1.80320	0.0113	0.0038	1.80697

Error analysis in the first natural frequency for specimen PF33

Table A10.5 : Real part of the estimated natural frequency ($k_p = 200$)

Mesh size Ω^h	Number of elements	Natural frequency, f_n	Difference Δf_n	Error $e^{h/2}$	Estimated exact f_n
Ω^1	5	7.71770			
Ω^2	8	7.90810	0.1904	0.0635	7.97157
Ω^3	11	7.95770	0.0496	0.0165	7.97423
Ω^4	14	7.98020	0.0225	0.0075	7.98770
Ω^5	17	7.99300	0.0128	0.0043	7.99727
Ω^6	20	8.00120	0.0082	0.0027	8.00393

Table A10.6 : Complex part of the estimated natural frequency ($k_p = 200$)

Mesh size Ω^h	Number of elements	Natural frequency, f_n	Difference Δf_n	Error $e^{h/2}$	Estimated exact f_n
Ω^1	5	1.58870			
Ω^2	8	1.72480	0.1361	0.0454	1.77017
Ω^3	11	1.76120	0.0364	0.0121	1.77333
Ω^4	14	1.77740	0.0162	0.0054	1.78280
Ω^5	17	1.78630	0.0089	0.0030	1.78927
Ω^6	20	1.79200	0.0057	0.0019	1.79390

Error analysis in the first natural frequency for specimen PF34

Table A10.7 : Real part of the estimated natural frequency ($k_p = 200$)

Mesh size Ω^h	Number of elements	Natural frequency, f_n	Difference Δf_n	Error $e^{h/2}$	Estimated exact f_n
Ω^1	6	7.71550			
Ω^2	10	7.84020	0.1247	0.0416	7.88177
Ω^3	14	7.87300	0.0328	0.0109	7.88393
Ω^4	18	7.88830	0.0153	0.0051	7.89340
Ω^5	22	7.89720	0.0089	0.0030	7.90017

Table A10.8 : Complex part of the estimated natural frequency ($k_p = 200$)

Mesh size Ω^h	Number of elements	Natural frequency, f_n	Difference Δf_n	Error $e^{h/2}$	Estimated exact f_n
Ω^1	6	1.65250			
Ω^2	10	1.73920	0.0867	0.0289	1.76810
Ω^3	14	1.76340	0.0242	0.0081	1.77147
Ω^4	18	1.77430	0.0109	0.0036	1.77793
Ω^5	22	1.78040	0.0061	0.0020	1.78243

Error analysis in the first natural frequency for specimen PF41

Table A10.9 : Real part of the estimated natural frequency ($k_p = 200$)

Mesh size Ω^h	Number of elements	Natural frequency, f_n	Difference Δf_n	Error $e^{h/2}$	Estimated exact f_n
Ω^1	5	2.78100			
Ω^2	10	2.84910	0.0681	0.0227	2.87180
Ω^3	14	2.86660	0.0175	0.0058	2.87243
Ω^4	18	2.87450	0.0079	0.0026	2.87713
Ω^5	22	2.87900	0.0045	0.0015	2.88050

Table A10.10 : Complex part of the estimated natural frequency ($k_p = 200$)

Mesh size Ω^h	Number of elements	Natural frequency, f_n	Difference Δf_n	Error $e^{h/2}$	Estimated exact f_n
Ω^1	5	0.77192			
Ω^2	10	0.80592	0.0340	0.0113	0.81725
Ω^3	14	0.81451	0.0086	0.0029	0.81737
Ω^4	18	0.81816	0.0037	0.0012	0.81938
Ω^5	22	0.82012	0.0020	0.0007	0.82077

Error analysis in the first natural frequency for specimen PF42

Table A10.11 : Real part of the estimated natural frequency ($k_p = 200$)

Mesh size Ω^h	Number of elements	Natural frequency, f_n	Difference Δf_n	Error $e^{h/2}$	Estimated exact f_n
Ω^1	7	2.79060			
Ω^2	12	2.83930	0.0487	0.0162	2.85553
Ω^3	17	2.85200	0.0127	0.0042	2.85623
Ω^4	22	2.85790	0.0059	0.0020	2.85987
Ω^5	27	2.86120	0.0033	0.0011	2.86230

Table A10.12 : Complex part of the estimated natural frequency ($k_p = 200$)

Mesh size Ω^h	Number of elements	Natural frequency, f_n	Difference Δf_n	Error $e^{h/2}$	Estimated exact f_n
Ω^1	7	0.78370			
Ω^2	12	0.80716	0.0235	0.0078	0.81498
Ω^3	17	0.81327	0.0061	0.0020	0.81531
Ω^4	22	0.81580	0.0025	0.0008	0.81664
Ω^5	27	0.81733	0.0015	0.0005	0.81784

Error analysis in the first natural frequency for specimen PF43

Table A10.13 : Real part of the estimated natural frequency ($k_p = 200$)

Mesh size Ω^h	Number of elements	Natural frequency, f_n	Difference Δf_n	Error $e^{h/2}$	Estimated exact f_n
Ω^1	8	2.78790			
Ω^2	14	2.82530	0.0374	0.0125	2.83777
Ω^3	20	2.83510	0.0098	0.0033	2.83837
Ω^4	26	2.83970	0.0046	0.0015	2.84123

Table A10.14 : Complex part of the estimated natural frequency ($k_p = 200$)

Mesh size Ω^h	Number of elements	Natural frequency, f_n	Difference Δf_n	Error $e^{h/2}$	Estimated exact f_n
Ω^1	8	0.78893			
Ω^2	14	0.80633	0.0174	0.0058	0.81213
Ω^3	20	0.81092	0.0046	0.0015	0.81245
Ω^4	26	0.81292	0.0020	0.0007	0.81359

Error analysis in the first natural frequency for specimen PF44

Table A10.15 : Real part of the estimated natural frequency ($k_p = 200$)

Mesh size Ω^h	Number of elements	Natural frequency, f_n	Difference Δf_n	Error $e^{h/2}$	Estimated exact f_n
Ω^1	9	2.77910			
Ω^2	16	2.80920	0.0301	0.0100	2.81923
Ω^3	21	2.81710	0.0079	0.0026	2.81973
Ω^4	28	2.82090	0.0038	0.0013	2.82217

Table A10.16 : Complex part of the estimated natural frequency ($k_p = 200$)

Mesh size Ω^h	Number of elements	Natural frequency, f_n	Difference Δf_n	Error $e^{h/2}$	Estimated exact f_n
Ω^1	9	0.79086			
Ω^2	16	0.80441	0.0135	0.0045	0.80893
Ω^3	21	0.80797	0.0036	0.0012	0.80916
Ω^4	28	0.80955	0.0016	0.0005	0.81008

VITA

Rajivkumar K. Kapadia was born on July 3, 1971, in Vapi, Gujarat, India. He graduated from T & T. V. Sarvajanik High School, Surat, India in July 1989. The following August he entered the South Gujarat University, Surat, India and graduated in July 1993 with a degree of Bachelor of Engineering in Mechanical Engineering. He worked for a heavy fabrication unit, Larsen & Toubro Ltd., Hazira, India in the Design Department from August 1993 till July 1994. In August 1994 he entered the University of Tennessee, Knoxville as a graduate student where he will receive his Master of Science degree in August 1996.